Control Systems with Friction

Olsson, Henrik

1996

Document Version:
Publisher's PDF, also known as Version of record

Control Systems with Friction

This is a reprocessing, made in October 2006, of the author's original LaTeX text. This means that formatting properties, such as line breaks, page breaks etc. may be different from the printed version. However, no change has been made to the text itself, apart from the inclusion of this statement.

The figure on the cover shows a limit cycle for a control system with friction. The limit cycle is described in Example 4.2.

Control Systems with Friction

Henrik Olsson

Lund 1996

To my parents

Published by
Department of Automatic Control
Lund Institute of Technology
Box 118
S-221 00 LUND
Sweden

ISSN 0280–5316
ISRN LUTFD2/TFRT--1045--SE

Printed in Sweden by Lunds offset ab
Lund 1996

Preface

My interest in friction started in late 1992 with a discussion on friction modeling with Karl Johan Åström and Carlos Canudas de Wit. The discussion lead to substantial work on friction modeling in collaboration with Carlos' group in Grenoble. The final result of my continued work is this thesis which treats friction-related topics in control systems. The work is done from a control engineering point of view but I have tried to always remember that friction is a real physical phenomenon.

Acknowledgments

Many people have helped me in producing this thesis and it is a great pleasure to get this opportunity to thank them.

First and foremost I would like to express my sincere gratitude to my supervisor Karl Johan Åström. He has been a constant source of help, ideas and inspiration. It is a rare privilege to work with someone like him and I have benefited immensely from his vast experience.

Tore Hägglund and Bo Bernhardsson both read early versions of the manuscript and suggested many improvements. Bo has consistently been very helpful during my years at the department and I consider him a true asset.

Ulf Jönsson read Chapter 4 carefully and contributed with many improvements. He is also partly responsible for convincing me to start the doctoral work. Ulf is a good friend with a great taste in music.

Jörgen Malmborg has been a good friend of mine for close to fifteen years. I have had a great number of interesting discussions with him and he has also endured many interrupts as my office neighbor. Karl Henrik Johansson shared office with me for some time. He is also a good friend even though he always beats me in tennis. He helped me, together with Mikael Johansson, to prepare the figure on the cover. Another good friend I would like to mention is Johan Nilsson. Being a natural born computer wizard he has come to my assistance on several occasions.

The excellent computer facilities at the department are maintained by Leif Andersson and Anders Blomdell. Leif, a man of great knowledge, has patiently answered all my questions. Eva Dagnegård worked hard in the final preparations of the manuscript. She is a great TEX-pert with a good sense for layout. Without her assistance the thesis would never have reached its final form.

Most of all I am very grateful to all the people at the department for making it such a fantastic place. In particular, I would like to thank Eva Schildt, Britt-Marie Mårtensson and Agneta Tuszynski for their good spir-

its and friendship which have been important parts of the good working atmosphere.

The work has been partly supported by the Swedish Research Council for Engineering Sciences (TFR), Contract 95-759. The cooperation with the group in Grenoble has partly been made possible through the EU Human Capital and Mobility Network on Nonlinear and Adaptive Control ERBCHRXCT 93-0380.

Finally, I would like to deeply thank my parents and my sister for all their help and support throughout the years.

H.O.

Contents

1

Introduction

Friction is found in almost every mechanism with moving parts. Engineering examples where friction is present abound, e.g., bearings, transmissions, hydraulic and pneumatic cylinders, valves, and brakes. Friction occurs at the physical interface between two surfaces in contact. Lubricants such as grease or oil are often used but the contact may also be dry. Contaminations like dirt and oxides are common. The physics describing the contact interface therefore involves many different areas including both elastic and plastic deformations, fluid mechanics and wave phenomena, as well as material sciences.

Friction is an important aspect of many control systems, both high-precision servo mechanisms and simple pneumatic and hydraulic systems. It may cause large control errors, unwanted oscillations, and excessive wear. Friction-related problems are very often encountered by the practicing control engineer. Other nonlinearities that are common in practice are back-lashes, dead zones, and saturations. They all have very special nonlinear structures and taking these into account can enable design of improved control laws. If friction is dealt with properly it may result in better quality, economy, and safety.

It is important to take the control problem into account already at the hardware design stage. Questions such as sensors and their location, choice of actuators, bearings etc. are important for the success of control. Friction problems can in many cases be solved using, for example, high precision bearings with less friction, or possibly magnetic bearings or air bearings with no friction at all. Another interesting solution was found in early autopilots where vibrators were built in to reduce the friction effects on the gyros, see Oppelt (1976). It is important to have an ongoing discussion between the mechanical design engineer and the control engineer. The drawback with hardware modifications is, of course, higher costs. Another issue showing different objectives is lubrication. Traditionally the main purpose has been to reduce wear. Less attention has been given to

the problem of reducing friction. Certain oil additives are available that reduce static friction.

For a given control system it is the control engineer's task to understand how the system is affected by friction, in what way friction limits the performance and what the difficulties are, and then to find control strategies that makes the best of the situation. This means that it is important to deal with friction in a systematic way in the design of control laws. This thesis treats different aspects of control systems with friction from a control engineering point of view.

Examples

In this section four examples are given that illustrate the wide range of control problems where friction is of interest. They also give a preview of the topics treated in this thesis. The first example describes an application where friction is of utmost importance and where detailed knowledge of friction could improve safety.

EXAMPLE 1.1—ANTI-LOCK BRAKING SYSTEMS

In most cases where control engineers encounter friction it is a drawback. In some cases, however, it is necessary for satisfactory performance. A typical example is in brakes. For a vehicle, friction is present both in the brakes and between wheel and road. In emergency situations it is desirable to perform the best possible braking maneuver. The relative difference between the rotational speed of the wheels and the actual speed of the vehicle is called the slip rate. The maximum braking force normally occurs for a low slip rate before gross skidding occurs. Today's anti-lock braking systems prevent the brakes from locking for longer periods of time by continually monitoring the slip rate. If it is above a threshold the braking force is released until the lock ceases. The design is entirely heuristic. Using more knowledge of the nature of friction for different conditions, such as type of road surface, could perhaps enable better and safer braking systems. Friction behavior and friction modeling for various purposes are discussed in Chapter 2. □

The second example is taken from robotics.

EXAMPLE 1.2—ROBOTICS

A hydraulic robot for nuclear power plant maintenance is used at the research lab of Electricité de France. The robot, which is used to inspect the secondary heating circuit, is required to have high motion precision. It is, therefore, necessary to consider the friction in the joints. Figure 1.1 shows the result of an experimental determination of the friction in the first joint of the robot for constant low-velocity motions. The experiment

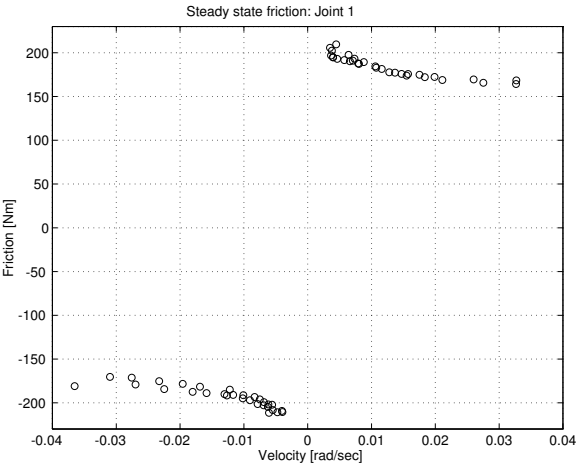

Figure 1.1 Friction as a function of velocity for constant velocity experiments. The hydraulic robot from which the data comes is used at the research lab of Electricité de France. The data have been provided by C. Canudas De Wit and P. Lischinsky at Laboratoire d'Automatique de Grenoble, ENSIEG-INPG, Grenoble, France.

is done under velocity control and each velocity for which the experiment is performed gives one data point. The data shows that friction typically increases with decreasing velocity for low velocities. This phenomenon is called the Stribeck effect. It is reviewed together with other friction characteristics in Chapter 2. The experiment is used to determine the parameters in a friction model which is presented in detail in Chapter 3. □

The third example is taken from Eborn and Olsson (1995) and describes a process control problem.

Example 1.3—Control of Fiber Concentration in Pulp
To produce high quality paper it is necessary to have an even concentration of fibers in the pulp. Figure 1.2 shows a schematic diagram of a control loop for diluting pulp. Pulp flowing through a pipe is diluted with water at the beginning of an enlargement of the pipe. The fiber concentration is measured at the downstream end of the enlargement. The controller in the loop is a PI-controller, which supplies the reference value for the control valve. The control valve consists of a pneumatic positioner, a pneumatic actuator and a valve. Figure 1.3 shows recorded data from such a control loop. The signals, y and v, are normalized. In the control loop there is a problem with concentration fluctuations. The fluctuations appear after a longer period of operation and then increase slowly in am-

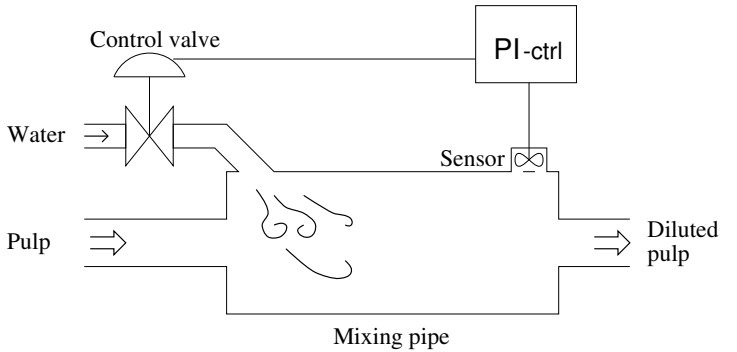

Figure 1.2 A schematic diagram of control of fiber concentration in pulp.

plitude until maintenance on the control valve has to be done. The process flow must be stopped during service and can therefore be costly. In Eborn and Olsson (1995) a complex nonlinear model of the control loop, including friction in the control valve, was developed. The observed fluctuations could be reproduced by the model as seen in Figure 1.4. The oscillations could thus be caused by friction. Another possible cause is backlash. A contributing factor to the problem is the over-dimensioned control valve. Small changes in the valve position give large changes in the water flow

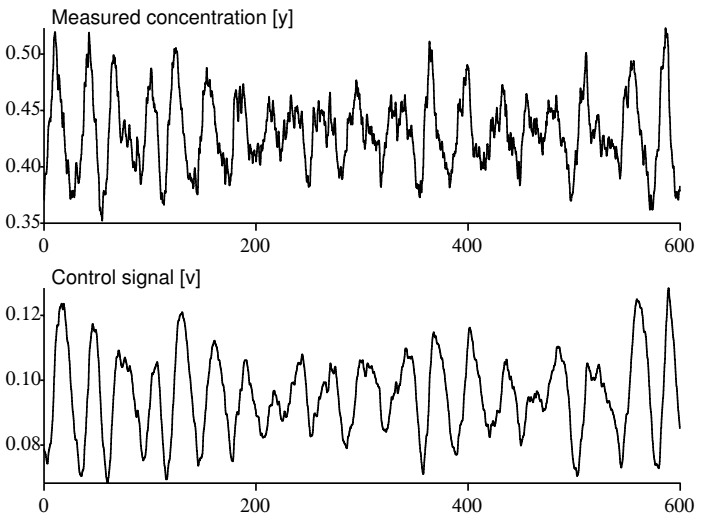

Figure 1.3 Fluctuations during operation of the loop for fiber concentration control. The data have been supplied by Stora Teknik and are collected at a Swedish paper mill.

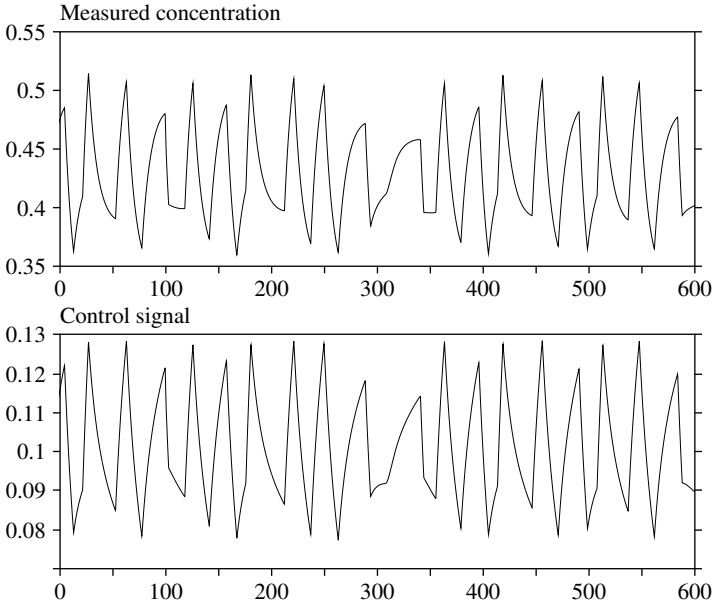

Figure 1.4 Simulation of the control loop model with friction. The same type of oscillations as in Figure 1.3 are obtained. The figure is taken from Eborn and Olsson (1995).

and thus in the concentration. The friction in the valve prohibits small controlled motions. In a survey of Canadian pulp and paper industry, see Bialkowski (1993), it was found that problems of the type described in the example are quite common. Chapter 4 treats oscillations in control systems with friction. □

The fourth and last example is taken from Futami *et al.* (1990) and describes a mechanism for positioning with nanometer accuracy.

EXAMPLE 1.4—NANOMETER POSITIONING

High precision positioning has become more and more important. It is, for example, necessary in machining and processing of semiconductors, optoelectronic components, and high-density magnetic storage devices. A common problem is to combine high precision with a long operating range. Controllers with different structures have been used. A first coarse positioning may be combined with a final fine positioning. This may include different sensors and actuators for the two control tasks. In this example the same actuator is used and the behavior of the actuator is utilized to achieve high accuracy.

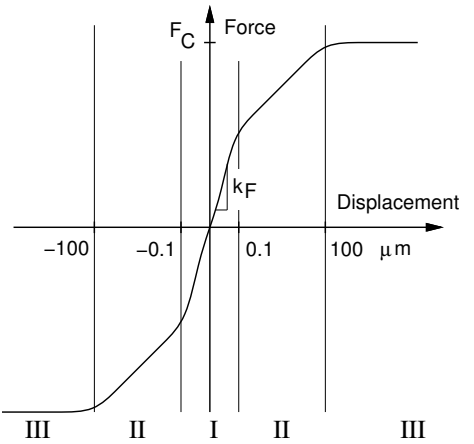

Figure 1.5 Relation between displacement and force for the mechanism. Three different regions of behavior can be observed.

A one-axis stage mechanism is driven by a linear AC motor and supported by a rolling ball guide. The micro-dynamics of the mechanism were studied under position control. The relation shown in Figure 1.5 was found between the displacement and the control force necessary to overcome the friction of the mechanism. The relation holds when starting from an equilibrium position with no applied force (the origin). Three different regions of behavior could be observed. For small displacements, i.e., Region I, the relation is linear and the behavior is the same as that of a linear spring with stiffness k_F. For large displacements in Region III the force saturates at a level F_C. In the mid-region the behavior is somewhere in between. The equations of motion for regions I and III can be described by

$$\text{Region I:} \quad m\frac{d^2x}{dt^2} = u - k_F x \tag{1.1}$$

$$\text{Region III:} \quad m\frac{d^2x}{dt^2} = u - F_C \operatorname{sgn}\left(\frac{dx}{dt}\right) \tag{1.2}$$

where x is the position and u is the control force. (For Region I the position is relative to the equilibrium position obtained when external forces have been removed.) Equation (1.2) is considered for the coarse positioning for which a PID controller is designed. The fine positioning is designed for (1.1) using a pure integrating controller given by

$$u(t) = K_i \int^t (x_r(\tau) - x_f(\tau))d\tau$$

where x_r is the reference position and x_f a low-pass filtered position signal to avoid resonances.

The control strategy is then given by

Step 1: Perform coarse positioning.

Step 2: Release the motor force and pause for 50 ms.

Step 3: Perform fine positioning.

It is necessary to release the applied forces and wait for the system to reach equilibrium, i.e., the origin of the curve in Figure 1.5, before the fine positioning can be done. The reason is that (1.1) only holds when starting from an equilibrium where the applied force is zero.

The necessity of the described control sequence is due to the lack of a unifying friction description of the guide mechanism which covers long coarse motion as well as the short high-precision motion, i.e., all three regions in Figure 1.5. A new friction model, which can capture the behavior of all three regions, is described in Chapter 3 and friction compensation using the model is treated in Chapter 5. □

Goal of the Thesis

Friction related control problems have gained a lot of interest lately. Entire sessions at the major conferences, such as the American Control Conference and the Conference on Decision and Control, have been dedicated to control systems with friction. There are a number of reasons for the interest. First, performance requirements have increased and to comply with the demands it is necessary to deal with limitations caused by friction. The knowledge of friction behavior has also increased and there has been a significant transmission of information from the tribology area to the control community. One such effort is Armstrong-Hélouvry (1991). Finally, computational power is available which makes it possible to implement efficient friction compensating control laws at high sampling rates.

There are three aspects of control systems with friction:

- Modeling
- Analysis
- Compensation

A good model is an essential element of control design. A friction model should be of moderate complexity, work for different engineering contacts and under various operating conditions, yet have built in as much of the friction structure as possible. It should be possible to fit parameters for the particular application by means of standard experiments that highlight the various friction characteristics. It may be necessary to develop

identification methods that are particularly aimed at determining friction parameters.

Engineering systems with friction are often of high order and of course highly nonlinear. Therefore, simulations is the only available analysis tool for many control systems with friction. Describing function analysis is widely used but has been shown to be inaccurate in detecting possible limit cycles, see Amin and Armstrong-Hélouvry (1994) and Olsson (1995). Analysis tools that predict disturbances to motion and give a measure of the performance would be beneficial.

Friction compensation methods are often divided into non-model based techniques, such as dither methods (Bersekerskii (1947)) and "perturb and evaluate" algorithms (Popović *et al.* (1995)), and model-based techniques (Mentzelopoulou and Friedland (1994)). As the knowledge of friction increases model-based friction compensation shows more and more promising. It is, however, necessary to have algorithms that can handle varying friction characteristics and that also work when there are considerable sensor and actuator dynamics.

In Armstrong (1995) some of these challenging research problems were pointed out. The solution of the problems will enable more successful control of systems with friction. The goal of this thesis is to supply some pieces that partly answers the posed problems. A model that is shown to cover many observed friction behaviors is developed and analyzed. The model has received attention from industry (Cubalchini (1996) and Strauch (1996)). An analysis tool suitable for numerical determination of limit cycles in systems with friction is derived. Finally, friction compensation using an observer based on the new model is discussed and investigated.

Outline of the Thesis

Chapter 2 reviews the origins of friction and the factors determining it. It also contains a review and discussion on previous work on friction modeling.

A new dynamic friction model is proposed in Chapter 3. The model attempts to capture most of the different behaviors of friction which have been observed experimentally. Various properties of the model are investigated both analytically and in simulations.

Chapter 4 treats limit cycles that friction may cause. A characterization of friction-generated limit cycle is given and tools for determining and analyzing limit cycles are derived and applied to various examples. Comparisons are made with the describing function method.

Friction compensation is discussed in Chapter 5. A nonlinear observer for the proposed friction model is described and investigated. Velocity control with model-based friction compensation is then thoroughly explored

and the nature of the control error is investigated.

Finally, Chapter 6 contains a summary of the thesis with conclusions. Interesting future research problems are pointed out.

Publications

The thesis is based on the following publications.

Canudas de Wit, C., H. Olsson, K. J. Åström, and P. Lischinsky (1993): "Dynamic friction models and control design." In *Proceedings of the 1993 American Control Conference, San Fransisco, California*, pp. 1920–26.

Canudas de Wit, C., H. Olsson, K. J. Åström, and P. Lischinsky (1995): "A new model for control of systems with friction." *IEEE Trans. Automatic Control*, **40:3**, pp. 419–25.

Eborn, J. and H. Olsson (1995): "Modelling and simulation of an industrial control loop with friction." In *Proceedings of the 4th IEEE Conference on Control Applications, Albany, New York*, pp. 316–322.

Olsson, H. (1995): "On describing function analysis of systems with friction." In *Proceedings of the 4th IEEE Conference on Control Applications, Albany, New York*, pp. 310–15.

Olsson, H. and K. J. Åström (1996): "Friction generated limit cycles." Submitted to the 5th IEEE Conference on Control Applications, Dearborn, Michigan.

Olsson, H. and K. J. Åström (1996): "Observer based friction compensation." Submitted to the 35th IEEE Conference on Decision and Control, Kobe, Japan.

2

Friction Modeling

2.1 Introduction

The desire to understand friction is old. The first concepts date as far back as to the work of Leonardo da Vinci. In this chapter we briefly review some of the various elements of the frictional contact and give a somewhat intuitive picture of the origin of friction. A more thorough description of the mechanisms behind friction can be found in Bowden and Tabor (1973). Various experimental observations of friction behavior are summarized. Most of the chapter is devoted to the issue of friction modeling and models for various purposes are reviewed. The chapter also serves as an introduction to the concepts and the terminology used when discussing friction.

2.2 The Friction Interface

Friction occurs between all surfaces in contact. In engineering applications it is common with lubricated metal to metal contacts such as in ball bearings. The discussion here will mainly relate to such contacts. To get an understanding of the mechanisms behind friction it is necessary to observe the microscopical contact between two surfaces. A simplified picture is shown in Figure 2.1. The surfaces are naturally rough and often covered by a layer of oxide or some other material. If the contact is lubricated there will also be oil or grease present in the interface. The actual contact takes place at a number of asperities and not continuously over the surface. Deformations of the contact points occur due to the load. There may also be adhesion and welding processes. As a tangential force is applied shearing of the contacts take place. This results both in elastic and plastic deformations. As motion occurs between the surfaces more of

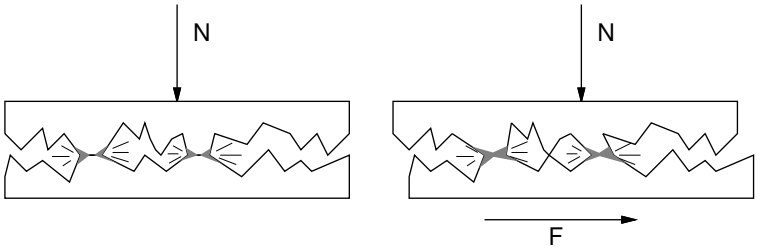

Figure 2.1 The microscopical contact between two surfaces. The contact takes place at a number of asperities which deform under normal and tangential loads.

the lubricant is brought into the interface.

The mechanisms behind friction can roughly be divided into four regions of behavior, see Armstrong-Hélouvry (1991). These depend on the relative velocity between the surfaces. Figure 2.2 shows a relation between friction force and velocity divided into four so called lubrication regimes. The first regime covers the case when no gross motion occurs, i.e., when the surfaces stick. A good mental picture of the behavior is shown in Figure 2.3. The contact can be viewed as formed by a number of springs. As a force is applied the springs are extended which results in the friction force. If the extension becomes too large the springs snap and sliding occurs. Thus, when sticking, the friction force is due to elastic and plastic deformations of the asperity contacts.

For the second regime motion occurs between the surfaces but hardly no lubrication is present in the interface. The friction force in this boundary lubrication regime is due to the shearing resistance of the asperity contacts. Normally the surfaces are covered with oxides or other compounds. The shearing resistance of these are much lower than for the

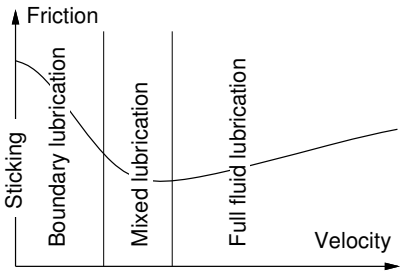

Figure 2.2 A typical relation between velocity and friction force. The relation can be divided into four so called lubrication regimes. The different regions are due to the velocity dependent causes of friction.

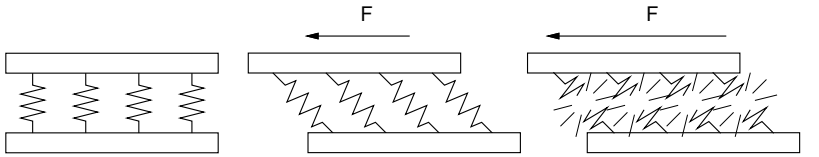

Figure 2.3 In the sticking regime the friction contact can be viewed as consisting of small springs which give rise to the friction force as they are extended. If the displacement becomes too large the springs snap and gross sliding can occur.

metal.

As the sliding speed increases more and more lubricant is brought in, which increases the separation of the surfaces. The transitional region before full fluid lubrication is called the mixed lubrication regime. The friction force is partially due to the lubricant and its viscosity and partially due to asperity contacts.

Finally, as the two surfaces are completely separated by the lubricant, full fluid lubrication occurs. The origin of the friction force for this lubrication regime is, of course, found in the hydrodynamics of the lubricant.

Naturally, dynamics are involved in all the mechanisms like the formation of a lubrication film and the shearing of junctions. The complete behavior of the friction force is therefore very complex. Next we describe some of the rich behavior that friction may exhibit.

2.3 Experimental Observations

The behavior of friction has been extensively examined during the 20th century. Many experiments have, contrary to the conditions for engineering applications, been performed with clean surfaces and for stationary conditions, e.g., constant velocity. Lately the interest in friction dynamics has increased. Some experimental observations of friction are reviewed below. The collection is by no means complete but serves to illustrate the many facets of friction behavior.

Steady Velocity Friction

The friction force as a function of velocity for constant velocity motion typically looks as the curve in Figure 2.2. The relation is called the Stribeck curve after Stribeck (1902). In particular the shape of the force in the boundary lubrication regime and mixed lubrication regime is called the Stribeck effect. No universal function can be given that describes friction as a function of velocity. Instead the relation is application dependent and varies with material properties, temperature, wear etc.

Many friction phenomena do not appear for constant velocity experiments. A number of observations of the dynamic behavior of friction are listed next.

Static Friction and Break-Away Force

The friction when sticking is called static friction and the force necessary to initiate motion, i.e., to overcome the static friction, is called the break-away force. Many experimental investigations were performed in the 50s to study the nature of these two concepts.

Rabinowicz addressed the transition between sticking and sliding in Rabinowicz (1951). He argued that the transition cannot be described satisfactorily as a function of velocity. Instead he investigated friction as a function of displacement. A simple experiment was devised to determine the relationship. A block was placed on an inclined plane and a ball was rolled on the plane and impacted the block. The inclination was such that sliding motion of the block was sustained, but if the block was at rest, it stayed at rest. The distance that the block moved due to the energy transferred by the ball was determined and then used to describe the friction transition in a diagram as in Figure 2.4. The break-away force is given by the peak of the curve. As seen in the figure the maximum friction force occurs at a small displacement from the starting point.

Rabinowicz also investigated the static friction force as a function of dwell-time, i.e., the time spent sticking, see Rabinowicz (1958). This was done using so called stick-slip motion experiments. It was concluded that the static friction increased with the dwell-time. Relations of the form in Figure 2.5 were found.

In Johannes *et al.* (1973) it was pointed out that for stick-slip experiments the dwell-time and the rate of increase of the external force are related and hence the effects of these factors cannot be separated. They therefore redesigned the experiment so that the time sticking and the

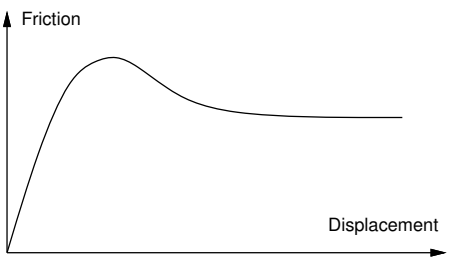

Figure 2.4 The relation between friction and displacement as found by Rabinowicz (1951). The experimental results suggested that friction should be described as a function of displacement and not velocity.

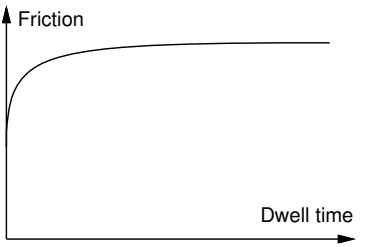

Figure 2.5 Relation between static friction and dwell-time as found by Rabinowicz (1958). The experiment suggested a temporal dependence on the level of static friction.

rate of increase of the applied force could be varied independently. The results showed, contrary to the results of Rabinowicz, that the break-away force did depend on the rate of increase of the external force but not on the dwell-time, see also Richardson and Nolle (1976). A characteristic behavior is seen in Figure 2.6.

Another investigation of the behavior in the sticking regime was done by Courtney-Pratt and Eisner (1957). They studied the spring-like behavior before gross sliding occurs. Their results were presented in diagrams showing force as a function of displacement. A typical relation is seen in Figure 2.7. This should be compared with Figure 2.4.

The experiments examining static friction have shown that even in the sticking regime microscopic motion occurs. This is often called pre-sliding motion. The break-away force which is necessary to cause gross sliding varies with the experimental conditions.

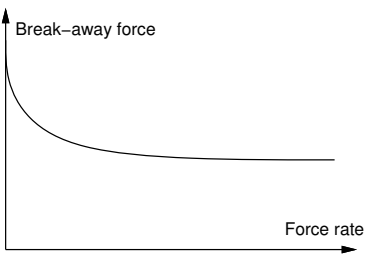

Figure 2.6 Characteristic relation between rate of force application and break-away force as found by Johannes *et al.* (1973). The experiment suggested that the break-away force decreases with increased rate of force application.

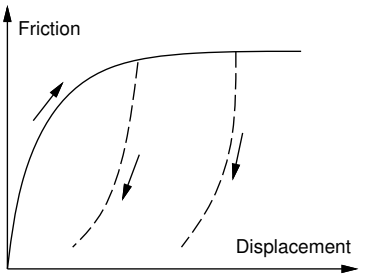

Figure 2.7 Pre-Sliding displacement as found by Courtney-Pratt and Eisner (1957). The result agrees with Figure 2.4 for small displacements. Releasing the applied force results in a permanent displacement as indicated by the dashed lines.

Frictional Lag

Dynamics are not only important in the sticking regime; they also affect the behavior in the other lubrication regimes.

The paper Hess and Soom (1990) has drawn a lot of attention. Hess and Soom chose to perform experiments with a periodic time-varying velocity superimposed on a bias velocity so that the motion becomes unidirectional. The velocity was varied in such a way that all lubrication regimes were covered. Typically the friction–velocity relation appeared as in Figure 2.8. Hysteresis was observed as the velocity varied. The size of the loop increased with normal load, viscosity and frequency of the velocity variation. Hess and Soom explained the hysteresis using a pure time delay in a static relation between velocity and friction force.

The experimental observations have shown that it is necessary to consider the dynamics of friction in order to get a detailed understanding of the friction behavior.

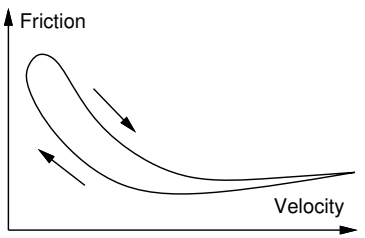

Figure 2.8 The friction–velocity relation observed in Hess and Soom (1990). The friction force is lower for decreasing velocities than for increasing velocities. The hysteresis loop becomes wider as the velocity variations become faster.

2.4 Friction Models

A model of friction is necessary for many purposes. In some cases it is desirable to have a model which provides insight into the physical mechanisms of the friction interface. In others it suffices with a model that can predict the global, qualitative behavior of a system with friction. If the model is to be used for friction compensation there may be limitations on the computational complexity of the model. There are thus many purposes of friction modeling:

- mathematical analysis
- off-line simulations
  - global, qualitative behavior
  - high-fidelity behavior
- physical insight
- friction compensation

It is important to bear the purpose in mind when discussing friction modeling.

This section summarizes previous work on friction modeling and gives a variety of examples of friction models. The intention is not to give a complete review of all existing friction models but to give a glimpse of the wide spectrum that exists. The models have been divided into three categories: static models, dynamic models, and special purpose models. The first category includes models that to a varying extent gives a qualitative understanding of friction. The models in the second category include dynamics in order to more accurately describe the friction phenomena. The final category includes some models that give an understanding of the physical mechanisms behind friction.

Discussion

Figure 2.9 shows a block on a surface. It also introduces some of the notations that are used for the friction contact throughout the thesis. Motion is considered only in the horizontal direction and friction occurs at the contact interface. The variables shown in the figure are: the friction force arising at the interface F, the relative velocity between the surfaces v, the relative position x, an external applied force F_e, and the normal force N. Furthermore, the contact area between the surfaces is denoted A. The early work on friction modeling tried to determine how these variables were related, e.g., Amontons (1699) and Coulomb (1785). It was, for example, investigated if the contact area affected the friction force. As a

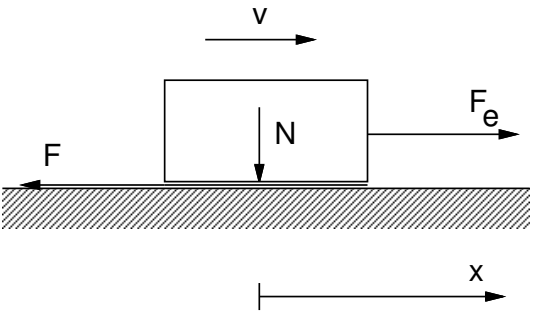

Figure 2.9 Notation for the variables affecting the friction force at the contact between two surfaces. The friction force is denoted F and any external tangential force F_e. Velocity and position are always denoted v and x, respectively. Motion is only considered in the horizontal direction.

result friction became known as force which opposes motion and which magnitude is given by a coefficient of friction times the normal force. The relation thus looks like

$$F = \mu N \tag{2.1}$$

It is still very common to discuss friction in terms of the friction coefficient μ. Typical variations in the friction force which are handled using μ are variations caused by material properties and contact geometries. The description (2.1) is too simplistic for many purposes. The dependence on normal load is more complicated than described by (2.1), see SKF (1970). Another complication is that the normal force may change. Slow changes can be accounted for by scaling or adapting parameters of the friction model. Rapid variations may, however, effect the friction force significantly. This effect is not considered in the work in this thesis. We have chosen to model the entire friction force and not just the friction coefficient. However, if so desired, the models can also be thought of as modeling μ instead of F.

For certain applications, such as gears, friction may depend on rotational position and also on the direction of motion. This can be handled for example, by letting the coefficients of the models be position dependent. Such variations have not been taken into account in the model discussion.

Static Friction Models

The friction models from past centuries regard friction as a static function of velocity. Therefore, they are called static friction models and are described next. The category includes the classical descriptions of friction but also refinements that have been made in order to adapt these models

to simulation demands.

Classical Models: The classical models of friction consist of different components, which each take care of a certain part of the friction force. The purpose of these models was to give a rough understanding of the behavior of friction, which agreed with simple experiments that could be performed.

The work on friction of da Vinci was rediscovered by Amonton in the late 17th century and then developed by Coulomb in the 18th century. The main idea is that friction opposes motion and that the friction force is independent of velocity and contact area. It can therefore be described as

$$F = F_C \operatorname{sgn}(v) \tag{2.2}$$

This description of friction is termed *Coulomb friction*, see Figure 2.10 a). Other names include kinetic friction, dynamic friction, sliding friction and relay-type friction. The Coulomb friction model does not specify the friction force for zero velocity. Depending on how the sign function is defined it may either be zero or it can take on any value in the interval between $-F_C$ and F_C. The Coulomb friction model has, because of its simplicity, often been used for friction compensation, see for example Friedland and Park (1991) and Baril (1993). Some confusion in the terminology exists and sometimes Coulomb friction denotes also velocity-dependent sliding friction as in Brandenburg and Schäfer (1991).

In the 19th century the theory of hydrodynamics was developed leading to expressions for the friction force caused by the viscosity of lubricants, see Reynolds (1886). The term *viscous friction* is used for this force component, which is normally described as

$$F = F_v v \tag{2.3}$$

Viscous friction together with Coulomb friction is shown in Figure 2.10 b). It is not always correct to let the viscous friction be linear in velocity. A more general relation is

$$F = F_v |v|^{\delta_v} \operatorname{sgn}(v) \tag{2.4}$$

where δ_v depends on the geometry of the application, see SKF (1970) and Andersson (1993).

Stiction is short for static friction as opposed to dynamic friction. It describes the friction force at rest. Morin (1833) introduced the idea of a friction force at rest that is higher than the Coulomb friction level. Static friction counteracts external forces below a certain level and thus keeps an object from moving. However, if the external force is too large then

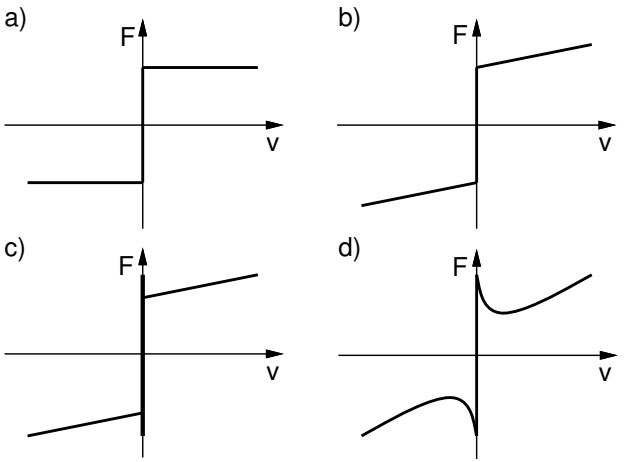

Figure 2.10 Examples of static friction models. The friction force is given by a static function except possibly for zero velocity. Figure **a)** shows Coulomb friction and Figure **b)** Coulomb plus viscous friction. Stiction plus Coulomb and viscous friction is shown in Figure **c)** and Figure **d)** shows how the friction force may decrease continuously from the static friction level.

the friction force cannot prevent motion. It is hence clear that friction at rest cannot be described as a function of only velocity. Instead it has to be modeled using the external force in the following manner.

$$F = \begin{cases} F_e & \text{if } v = 0 \text{ and } |F_e| < F_S \\ F_S \operatorname{sgn}(F_e) & \text{if } v = 0 \text{ and } |F_e| \geq F_S \end{cases} \tag{2.5}$$

The friction force for zero velocity is a function of the external force and not the velocity. The traditional way of depicting friction in block diagrams with velocity as the input and force as the output is therefore incorrect. If doing so, stiction must be expressed as a multi-valued function that can take on any value between the two extremes $-F_S$ and F_S. Specifying stiction in this way leads to non-uniqueness of the solutions to the equations of motion for the system, see Bliman and Sorine (1995).

The classical friction components can be combined in different ways, see Figure 2.10 c), and any such combination will be referred to as a classical model.

The classical models include components that are either linear in velocity or constant. If accurate measurements of friction for steady velocity motion is performed these may reveal different dependencies. Stribeck

(1902) observed that for low velocities the friction force is normally decreasing continuously with increasing velocities, not in a discontinuous manner. The phenomenon is termed Stribeck effect and the extra low-velocity friction force above the constant Coulomb level is called Stribeck friction. A more general description of friction than the classical models is, therefore,

$$F = \begin{cases} F(v) & \text{if } v \neq 0 \\ F_e & \text{if } v = 0 \text{ and } |F_e| < F_S \\ F_S \operatorname{sgn}(F_e) & \text{otherwise} \end{cases} \tag{2.6}$$

where $F(v)$ is an arbitrary function, which may look as in Figure 2.10 d). It can be given either as a look-up table or as a parameterized curve that fits experimental data. A number of parameterizations of $F(v)$ have been proposed, see Armstrong-Hélouvry (1991). The most common is of the form

$$F(v) = F_C + (F_S - F_C)e^{-|v/v_S|^{\delta_S}} + F_v v \tag{2.7}$$

where v_S is called the Stribeck velocity. Such models have been used for a long time. Tustin (1947) used the parameterization with $\delta_S = 1$ and Bo and Pavelescu (1982) suggested δ_S in the range of 0.5 to 1. Armstrong-Hélouvry (1991) used a Gaussian parameterization with $\delta_S = 2$ and also proposed to use the sum of two exponentials to match experimental data better. Other parameterizations can of course also be used such as

$$F(v) = F_C + (F_S - F_C)\frac{1}{1 + (v/v_S)^{\delta_S}} + F_v v$$

and a parameterization used by Canudas de Wit (1993)

$$F(v) = F_S - F_d|v|^{1/2}$$

This parameterization has the advantage that it is linear in the parameters but it is only valid in a limited velocity range because of the term $-F_d|v|^{1/2}$, which should account for the Stribeck effect. Outside this interval the friction force may have the wrong sign.

Friction depends on many factors. No particular parameterization can yet be theoretically motivated. Which parameterization to choose depends on the specific application and can be determined from simple experiments.

The main disadvantage when using a model such as (2.6), either in simulations or for control purposes, is the problem of detecting or determining when the velocity is zero. A remedy for this is found in the model described next.

The Karnopp Model: Karnopp proposed the model in Figure 2.11 for simulation purposes, see Karnopp (1985). The model in the figure is drawn for the system

$$m\frac{dv}{dt} = F_e - F \tag{2.8}$$

The Karnopp model was developed to overcome the problems with zero velocity detection and to avoid switching between different state equations for sticking and sliding. The model defines a zero velocity interval, $|v| < DV$. For velocities within this interval the internal state of the system (the velocity) may change and be non-zero but the output of the block is maintained at zero by a dead-zone. Depending on if $|v| < DV$ or not, the friction force is either a saturated version of the external force or an arbitrary static function of velocity. The interval $\pm DV$ can be quite coarse and still promote so called stick-slip behavior.

The drawback with the model is that it forms an integrated part with the rest of the system. The external force is an input to the model and this force is not always explicitly given. This is, for example, the case for the system in Figure 2.12. The model equations therefore have to be tailor-made for each configuration. Variations of the Karnopp model are widely used since they allow efficient simulations. The zero velocity interval does, however, not agree with real friction.

The friction models presented so far have considered friction only for steady velocities. No attention is paid to the behavior of friction as the velocity is varied. Experimental investigations have pointed out a num-

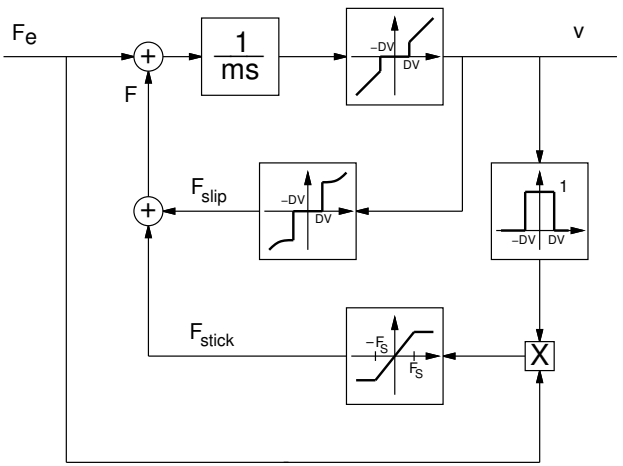

Figure 2.11 Block diagram for the Karnopp model.

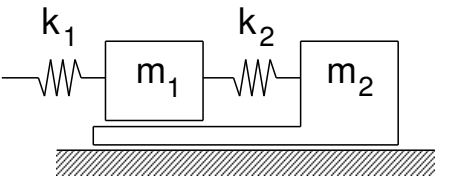

Figure 2.12 Example of a system with two friction interfaces which complicates the use of the Karnopp model.

ber of phenomena that cannot be described by static models. Some of these were described in Section 2.3. Attention has lately been drawn to the dynamics of friction as the demands on control precision have increased and new hardware has enabled implementation of more advanced controllers. Following are a number of models which to a varying extent capture the dynamics of friction. They have all been developed from the 1960s and onwards with increased interest in the 1990s.

Dynamic Friction Models

A dynamic model can be obtained by slightly modifying the static models in the previous section. This is done for Armstrong's seven parameter model. Because of the relation to the static models it is described first of the dynamic friction models.

Armstrong's Seven Parameter Model: To account for some of the observed dynamic friction phenomena a classical model can be modified as in Armstrong-Hélouvry *et al.* (1994). This model introduces temporal dependencies for stiction and Stribeck effect. The modifications, however, do not handle pre-sliding displacement. This is instead done by describing the sticking behavior by a separate equation. Some mechanism must then govern the switching between the model for sticking and the model for sliding. The friction is described by

$$F(x) = \sigma_0 x \tag{2.9}$$

when sticking and by

$$F(v,t) = \left(F_C + F_S(\gamma, t_d) \frac{1}{1 + (v(t-\tau_l)/v_S)^2} \right) \operatorname{sgn}(v) + F_v v \tag{2.10}$$

when sliding, where

$$F_S(\gamma, t_d) = F_{S,a} + (F_{S,\infty} - F_{S,a}) \frac{t_d}{t_d + \gamma} \tag{2.11}$$

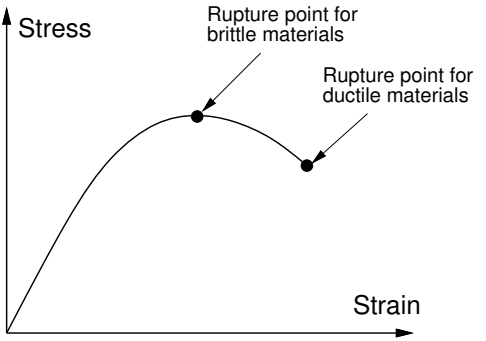

Figure 2.13 Classical stress–strain relation for brittle and ductile materials.

$F_{S,a}$ is the Stribeck friction at the end of the previous sliding period and t_d the dwell time, i.e., the time since becoming stuck. The sliding friction (2.10) is equivalent to a static model where the momentary value of the velocity in the Stribeck friction has been replaced by a delayed version and where it has a time dependent coefficient. As the name states, the model requires seven parameters. These are: the pre-sliding stiffness σ_0; the Coulomb friction F_C; the steady-state stiction force $F_{S,\infty}$; the viscous friction F_v; the Stribeck velocity v_S; the frictional lag τ_l; and finally the parameter determining the temporal behavior of the static friction γ. Since the model consists of two separate models, one for sticking and one for sliding, a logical statement—probably requiring an eighth parameter—determines the switching. Furthermore, the model states have to be initialized appropriately every time a switch occurs.

Another approach, which leads to dynamic friction models, is to use the simplified pictures of the physical contact in Figures 2.1 and 2.3 as the starting point. The result is models that naturally include dynamics and can be called true dynamic friction models.

The Dahl Model: In Dahl (1968) two friction models are introduced. The first model uses as its starting point the relation between strain and stress for shearing processes, as seen in Figure 2.13. The friction interface is modeled as a junction at which shearing takes place. The resulting friction force depends on the strain caused by the external force. This corresponds to pre-sliding displacement. If the strain is large enough the junction breaks and the friction force remains constant at the level at which rupture took place. When the external force is removed the result is a permanent deformation. The model includes static friction if the stress–strain characteristic is as typical for ductile materials. It considers only

friction due to contact between solids but the friction model for brittle materials is believed to work well both for rolling friction and for sliding friction between lubricated surfaces.

The second model introduced in Dahl (1968) is based on the assumption that the friction force can be described by

$$\frac{dF}{dt} = \frac{dF}{dx}\frac{dx}{dt}$$

This implies that the friction force is only position dependent. This so called rate independence is an important property of the model for analysis especially when studying it as a hysteresis operator, see Bliman (1992). Results from simulations were compared with experimental results for ball bearings. A good agreement between the model and true friction was observed. The model exhibits hysteresis between velocity and friction force. The hysteresis depends on the rate of change of the velocity. Dahl also noted that the model is a generalization of ordinary Coulomb friction.

The second model is further studied in Dahl (1975) and Dahl (1976) where it is used to describe frictional damping of a wire pendulum. The damping of the pendulum is due to the bending of the wire and thus not from relative motion between surfaces. The model is, however, applied even to this internal friction. The position dependency of the friction force is further explored and Dahl proposes the relation

$$\frac{dF}{dx} = \sigma_0 \left| 1 - \frac{F}{F_C} \operatorname{sgn}\left(\frac{dx}{dt}\right) \right|^i \operatorname{sgn}\left(1 - \frac{F}{F_C} \operatorname{sgn}\left(\frac{dx}{dt}\right)\right) \tag{2.12}$$

where σ_0 is the stiffness and the exponent i a model parameter. The second factor is present to stabilize the differential equation for simulation purposes. The model (2.12) is the general Dahl model. Using the friction model and the linearized pendulum equations the damping ratio and energy dissipation of the pendulum are determined. It is concluded that for large amplitudes of oscillation the model resembles Coulomb friction, but as the amplitude decays the hysteresis and dynamics become more and more important for the damping.

The Dahl model (2.12) leads to a friction displacement relation that bears much resemblance with stress–strain relations proposed in classical solid mechanics, see Ramberg and Osgood (1943) and Sargin (1971).

In Dahl (1977) the model is used when experimentally studying friction in ball bearings. A force–deflection test is done on a ball bearing and parameters of the model are fitted to agree with the experiments. Three types of fittings are done. In the first, the exponent i in (2.12) is estimated together with $x_c = F_C/\sigma_0$ while F_C is determined as the friction

force asymptote for unidirectional motion. In the other two fittings the exponent i is fixed to 1 and 2, respectively. For the first type of fitting i is estimated to 1.5 quite consistently. It is observed that the rest stiffness σ_0 is important for the fit. The cases with fixed exponents do not agree with the measured data over an as large friction force range.

When referred to in the literature the Dahl model is often simplified, using $i = 1$, to

$$\frac{dF}{dt} = \sigma_0 \left(1 - \frac{F}{F_C} \operatorname{sgn}(dx/dt)\right) \frac{dx}{dt} \tag{2.13}$$

The Dahl model has been used for adaptive friction compensation (see Walrath (1984) and Ehrich Leonard and Krishnaprasad (1992)) with improved performance as the result.

When summarizing Dahl's papers two sentences from Dahl (1968) are worth citing, firstly:

> "The origin of friction is in quasi static bonds that are continuously formed and subsequently broken."

and, secondly:

> "The resulting functions behave as a brush whose bristles must bend as the brush moves in one direction and then flop or bend in the opposite direction if the motion is reversed."

This view of the origins of friction has been the starting point for several models and is, as we will see, also the inspiration for a new model in Chapter 3.

The Bristle Model: In Haessig and Friedland (1991) a friction model is introduced, which also is based on the microscopical contact points between two surfaces. Due to irregularities in the surfaces the number of contact points and their location are random. Each point of contact is thought of as a bond between flexible bristles. As the surfaces move relative to each other the strain in the bond increases and the bristles act as springs giving rise to a friction force. The force is given by

$$F = \sum_{i=1}^{N} \sigma_0 (x_i - b_i) \tag{2.14}$$

where N is the number of bristles, σ_0 the stiffness of the bristles, x_i the relative position of the bristles, and b_i the location where the bond was formed. As $|x_i - b_i|$ becomes equal to δ_s the bond snaps and a new one is formed at a random location relative to the previous location. The new location is determined by

$$b_i^{k+1} = b_i^k + \text{uniform}(\Delta) \operatorname{sgn}(x_i - b_i^k)$$

where Δ determines the uniform distribution. A suitable number of bristles is 20–25 according to the authors but even a single bristle will work, although giving rise to larger variations in the friction force. The stiffness of the bristles, σ_0, can be made velocity dependent. The model is inefficient in simulations due to the many actions that has to be taken. The deflection of each bristle has to be checked to see if it has snapped, and if so, a new location has to be determined. The resulting behavior when sticking may be oscillatory since no damping of the bristles is present in the model.

The Reset Integrator Model: A second model also proposed in Haessig and Friedland (1991) is the reset integrator model. This model is similar to the bristle model and can be seen as representing a single bond. Instead of snapping the strain in the bond is kept constant by a logical statement, which shuts off the strain increase at the point of rupture. The model utilizes an extra state to determine the strain in the bond, which is modeled by

$$\frac{dz}{dt} = \begin{cases} 0 & \text{if } (v > 0 \text{ and } z \geq z_0) \text{ or } (v < 0 \text{ and } z \leq -z_0) \\ v & \text{otherwise} \end{cases}$$

The friction force is given by

$$F = (1 + a(z))z\sigma_0(v) + \sigma_1 \frac{dz}{dt} \tag{2.15}$$

where $\sigma_1 dz/dt$ is a damping term that is active only when sticking. The damping coefficient can be chosen to give a desired relative damping of the resulting spring-mass-damper system. Stiction is achieved by the function $a(z)$, which is given by

$$a(z) = \begin{cases} a & \text{if } |z| < z_0 \\ 0 & \text{otherwise} \end{cases}$$

If $|z| < z_0$ the model describes sticking where the friction force is a function of z. As the artificial deflection reaches the maximum value z_0 the variable z remains constant and the friction force drops since $a(z)$ becomes zero. The friction force when slipping is an arbitrary function of the velocity given by $\sigma_0(v)$. The reset integrator model is far more efficient to simulate than the bristle model but, still, a test is necessary to check whether $|z| > z_0$ or not.

The Models by Bliman and Sorine: Bliman and Sorine have developed a family of dynamic models in a series of papers: Bliman and Sorine (1991), (1993) and (1995). The starting point for the models is the experimental investigations by Rabinowicz in the 1950s, see Rabinowicz (1951). Results as in Figure 2.4 were obtained when studying the breakaway behavior. It is seen in Figure 2.4 that the maximum friction force is reached after a small distance. After some further motion the Coulomb friction level has been reached. Bliman and Sorine stresses velocity independence, i.e., that the curve will be the same no matter how fast the distances are covered. The rate independence makes it possible to express the models with distance instead of time as the independent variable. They hence replace the time variable t by a space variable s through the transformation

$$s = \int_0^t |v(\tau)| d\tau$$

The models are now expressed as

$$\begin{aligned} \frac{dZ_s}{ds} &= AZ_s + Bv_s \\ F &= CZ_s \end{aligned} \tag{2.16}$$

where $v_s = \text{sgn}(v)$. The models are linear systems when expressed in the new space variable. A first-order model is given by

$$A = -\sigma_0/F_C, \quad B = \sigma_0/F_C \quad \text{and} \quad C = F_C. \tag{2.17}$$

Expressed with time as the independent variable this becomes

$$\frac{dF}{dt} = \sigma_0 \left(v - |v| \frac{F}{F_C} \right)$$

which coincides with the Dahl model, see (2.13). The first-order model does not yield a friction peak as in Figure 2.4. This can, however, be achieved by a second-order model with

$$\begin{aligned} A &= \begin{pmatrix} -\sigma_0/(\eta(F_C + \Delta F)) & 0 \\ 0 & -\sigma_0/\Delta F \end{pmatrix} \quad B = \begin{pmatrix} \sigma_0/\eta(F_C + \Delta F) \\ -\sigma_0/\Delta F \end{pmatrix} \\ \text{and} \quad C &= \begin{pmatrix} F_C + \Delta F & \Delta F \end{pmatrix} \end{aligned} \tag{2.18}$$

and with $0 < \eta < \Delta F/(F_C + \Delta F)$, see Bliman and Sorine (1995). The second-order model actually consists of two first-order models in parallel. The fastest model has the highest steady-state friction. The friction force

from the slower model is subtracted from the faster model, which gives the resulting friction force. Both the first- and second-order models can be shown to be dissipative. The velocity or rate independence also makes them attractive, since hysteresis theory can be applied. Bliman and Sorine also show that, as σ_0 goes to infinity, the models behave as a classical Coulomb friction model (first-order model) or as a classical model with Coulomb friction and stiction (second-order model). It should be noted that the Stribeck effect of the second-order model claimed by the authors is not the same as observed in Stribeck (1902). The emulated effect by the second-order model is only present at a certain distance after motion starts. This means that it will not appear when slowing down, as the true Stribeck effect would. The friction peak is instead the equivalent of stiction for a dynamic model.

The models described so far have all been applicable to the general contact shown in Figure 2.9. They have also, without exceptions, been considered for control purposes. Advanced friction models have, of course, also been derived outside the control area. These models often have different purposes and aim to explain, for example, phenomena for idealized contacts, dynamics of lubricants, and even earthquakes. Some of these modeling efforts are now shortly described in order to highlight the various aspects of friction modeling.

Special Purpose Models

The special purpose models we describe include a category of models that describes contact forces using continuum mechanics. Another is based on the hydrodynamics of lubricated contacts. There are also special purpose models for road–tire friction and rock mechanics.

Continuum Mechanics: The relation between stress and strain for various materials is treated in classical solid mechanics. If friction is seen as a one-dimensional shearing process such relations could form the basis for friction models. This was the case for the Dahl model (2.12). Another approach to friction modeling is to describe the friction interface using continuum mechanics. This is done in Oden and Martins (1985). The method combines a simple friction relation, which holds locally, with a complicated model of the contact. In particular, the model includes motion in the normal direction of the interface.

A typical friction interface is shown in Figure 2.14. Empirically the local normal stress can be described as a power function of the compression of the surface, i.e.,

$$\sigma_N = c_N a^\gamma$$

where $a = t_0 - t$. The friction force per area unit is then given by the

classical relation

$$\sigma_F = \mu \sigma_N \operatorname{sgn}(v)$$

The total friction force is achieved by integrating over the contact area. The continuum problem can be formulated using variational methods and be solved by, for example, finite element methods. The variational formulation requires a regularization of the sign function. The approach should be compared with the combination of an elaborate friction model with a simple model of the interface. The difference is illustrated with a simple example taken from Oden and Martins (1985).

The set-up of the example is shown in Figure 2.15. Assuming motion with one degree of freedom the system can be described by

$$\frac{d^2x}{dt^2} = F - kx$$

where F is the friction force and x the horizontal position. To account for various friction phenomena an elaborate friction model may be required, which introduces additional states. The continuum mechanics approach is instead to model the deformation between the block and the belt. With the block assumed rigid we get the situation shown in Figure 2.16. Three degrees of freedom are necessary for the two dimensional motion. With the coordinates introduced in Figure 2.16 the system is described by

$$M\frac{d^2\xi}{dt^2} + K\xi + P(\xi) + J\left(\xi, \frac{d\xi}{dt}\right) = F_e$$

where

$$\xi = \begin{pmatrix} x \\ y \\ \theta \end{pmatrix} \quad M = \begin{pmatrix} m & 0 & 0 \\ 0 & m & 0 \\ 0 & 0 & 1 \end{pmatrix} \quad K = \begin{pmatrix} k & 0 & 0 \\ 0 & 0 & 0 \\ 0 & 0 & 0 \end{pmatrix} \quad F_e = \begin{pmatrix} 0 \\ mg \\ 0 \end{pmatrix}$$

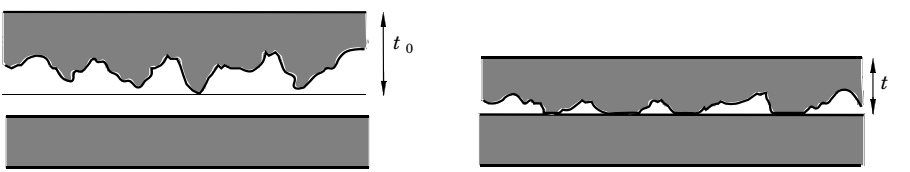

Figure 2.14 Microscopical picture of the friction interface. The asperities deform as contact is made. The compression is given by $t - t_0$. For simplicity the lower surface is shown as being rigid.

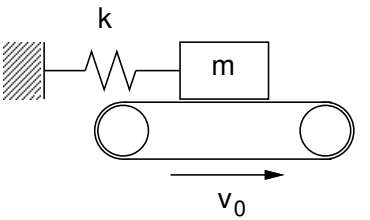

Figure 2.15 Set-up of the example in Oden and Martins (1985).

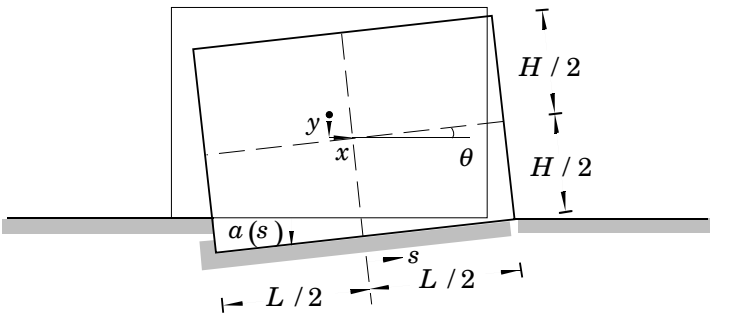

Figure 2.16 Deformation model for the contact between the rigid block and the belt.

and

$$P = \begin{pmatrix} 0 \\ P_y \\ P_\theta \end{pmatrix} = Bc_N \int_{-L/2}^{L/2} (y - s\theta)^\gamma(s) \begin{pmatrix} 0 \\ 1 \\ -s \end{pmatrix} ds$$

$$J = \begin{pmatrix} J_x \\ 0 \\ J_\theta \end{pmatrix} = B\mu c_N \operatorname{sgn}\left(\frac{dx}{dt} + \frac{H}{2}\frac{d\theta}{dt} - v_0\right) \begin{pmatrix} 1 \\ 0 \\ H/2 \end{pmatrix} \int_{-L/2}^{L/2} (y - s\theta)^\gamma(s) ds$$

where B is the breadth of the block. The term $P(\xi)$ includes the force and torque caused by the deformation of the belt. The friction force is given by the term $J(\xi, d\xi/dt)$. The system description is of order six.

Lubricated Contacts: For most engineering applications lubrication is present in the friction interface. Friction models have therefore been derived using hydrodynamics. A simple example is viscous friction as given by (2.3). Other models also exist. Hess and Soom (1990) used the following

model to describe the friction coefficient for steady sliding:

$$\mu = \frac{\mu_b}{1 + c_1(\eta v/\sqrt{WE})^2} + c_2 \frac{\eta v L}{W} \tag{2.19}$$

where μ_b is the coefficient of friction in the boundary lubrication regime, η the viscosity coefficient, W the normal load, E Young's modulus, and L the contact length. The second term is equivalent to linear viscous friction and the first term accounts for friction due to boundary lubrication. The model thus covers all lubrication regimes except sticking. Dynamics are introduced by substituting the velocity in (2.19) with $v(t - \Delta t)$. Comparisons with experimental data show that a constant time lag gives good agreement.

In Harnoy and Friedland (1993) a model based on the hydrodynamics of a lubricated journal bearing is introduced. The model covers both the boundary, mixed and hydrodynamic lubrication regimes. It stresses the dynamics of the friction force. The eccentricity ε of the bearing is an important variable in determining the friction force which, with some simplification, is given by

$$F = K_1(\varepsilon - \varepsilon_{tr})^2 \Delta + \frac{K_2}{\sqrt{1 - \varepsilon^2}} v. \tag{2.20}$$

The first term is due to the shearing of asperity contacts and the second term is due to the viscosity of the lubricant. The function Δ is an indicator function that is one for $\varepsilon > \varepsilon_{tr}$ and zero otherwise. This implies that for small eccentricities there is no friction due to asperity contacts. The eccentricity is given by a fourth-order differential equation, which determines the pressure distribution in the lubricant. The model requires five parameters. Simulations show a behavior very similar to the observations in Hess and Soom (1990). An extension including sleeve compliance is given in Harnoy and Friedland (1994). The model then becomes more complicated and requires determination of initial values when switching between slipping and sticking. The paper shows that a low sleeve compliance may be advantageous in precise motion control.

Rock Mechanics: The desire to predict earthquakes has inspired research that aims to model the friction between the crustal plates of Earth. This is described in Dieterich (1972). The stability of tectonic sliding has been analyzed using a special friction model in Ruina (1983). The model has also been used in connection with control, see Dupont (1994).

The "Magic Formula Tire Model": When simulating the behavior of road vehicles it is important to know the contact force between the

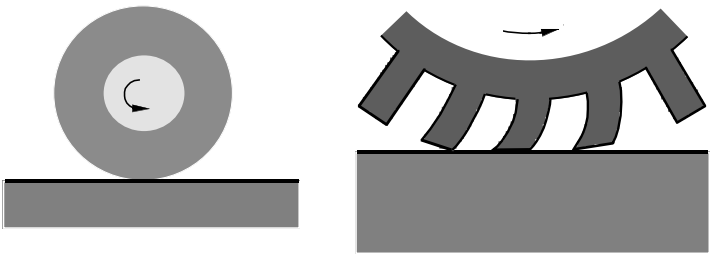

Figure 2.17 A simplified picture of a road–tire contact. The tread deflects when a force is transferred by the contact between tire and road surface.

road surface and the tires of the vehicle, see Bakker *et al.* (1987) and Pacejka (1991). This is also of considerable interest when designing anti-lock braking systems, compare with Example 1.1 in Chapter 1. Since the wheels rotate, we get a slightly unfamiliar way of describing friction. A simplified picture of a tire on a surface is shown in Figure 2.17. The rubber of the tire is elastic and therefore the tread deforms as a force is transmitted over the contact. The deformation starts as the tread comes into contact with the ground and ceases as it loses contact. This results in a reduction in the effective circumference of the tire, which implies that the ground velocity will not equal $v = \omega r$, where ω is the rotational speed of the wheel and r the wheel radius. Instead we have an effective radius r_e. The slip rate is defined as

$$s = \frac{\omega(r - r_e)}{\omega r}$$

The contact force is modeled as a function of the slip. The slip can be measured and hence it is possible to know how much contact force that can be transferred. The relation depends, of course, on the tire and the type of road surface. A characteristic shape of the relation is shown in Figure 2.18 which is closely related to Figure 2.4. The behavior can be explained using Figure 2.17. Small values of the slip corresponds to a small deflection or displacement of the tread. Larger values implies that there is also gross sliding. This is the same behavior as noted in Figure 2.4. In Bakker *et al.* (1987) curves of the form

$$F(s) = D \sin(C \arctan(Bs - E(Bs - \arctan(Bs)))) \tag{2.21}$$

are suggested to fit experimental data. Equation (2.21) is called the "Magic Formula Tire Model".

In Bliman *et al.* (1995) the authors propose to use the second-order model by Bliman and Sorine, i.e., (2.16) and (2.18), to model the friction between tire and road. They model the contact area as a rectangle and let ξ denote the longitudinal position along the contact area. The friction is then model by means of $Z(\xi)$, which is the friction state along the contact. The model becomes

$$\frac{d}{dt}Z(\xi) = \frac{dZ}{d\xi}\frac{d\xi}{dt} = AZ|\omega(r-r_e)| + B(\omega(r-r_e))$$
$$F = C\int_0^L Z(\xi)d\xi$$

where L is the length of the contact zone. Since the wheel is rotating, it holds that $d\xi/dt = \omega r$ and the model equations can then be written as

$$\frac{dZ}{d\xi} = AZ|s| + Bs$$
$$F = C\int_0^L Z(\xi)d\xi$$

For constant slip s we can integrate along the contact area to achieve the friction force. The first-order model (2.17) gives a monotonously increasing friction–slip relation, but for the second-order model (2.18) with

$$C = \begin{pmatrix} (F_C + \Delta F)/L & \Delta F/L \end{pmatrix}$$

we get

$$F(s) = (F_C + \Delta F)\left[1 - \frac{\eta(F_C+\Delta F)}{\sigma_0 Ls}\left(1 - e^{-(\sigma_0 Ls/\eta(F_C+\Delta F))}\right)\right] - \Delta F\left[1 - \frac{F_C}{\sigma_0 Ls}\left(1 - e^{-(\sigma_0 Ls/F_C)}\right)\right] \quad (2.22)$$

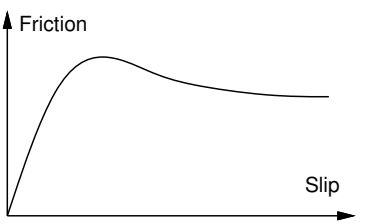

Figure 2.18 Typical relation between slip rate and contact force for a tire.

for $s > 0$. This function can model the desired behavior and fit experimental data as shown in Bliman *et al.* (1995). The parameters also have a physical interpretation, which they lack in (2.21).

Simulation Efficiency and Accuracy

One of the purposes with a friction model is to use it in simulations. It is necessary that these simulations can be performed efficiently. The reviewed friction models show various difficulties when simulated.

Discontinuities are notoriously difficult to simulate, since it is necessary to find the time where the events of discontinuity occur, see Hairer *et al.* (1987). Simulation software must have a structured way of finding zero crossings, otherwise the step size of the integration routine must be decreased. The problem of detecting zero velocity is present for all the static models except for the Karnopp model. The Karnopp model avoids this problem by defining an interval as zero velocity. By doing so it is not necessary to detect exactly when the interval is entered. A coarse estimate of the first time inside the interval suffices, which implies that a larger step size can be used without event handling. The problem of zero velocity detection occurs also for some of the dynamic models such as Armstrong's seven parameter model, which further uses a time delay. This requires that the history of the velocity is stored.

Some models consists of two sub-models, one for sticking and one for sliding. It is then necessary to have a mechanism that determines when to switch between the sub-models. It is also necessary to initialize the models appropriately after a switch. This holds for Armstrong's seven parameter model and for the bristle model.

The Dahl model, the models by Bliman and Sorine, and the reset integrator model are all efficient to simulate. The differential equations, however, may be stiff depending on the choice of parameters. A stiff solver may therefore be advantageous for the simulations.

Some of the models derived from continuum mechanics and hydrodynamics include partial differential equations that require special solvers.

2.5 Summary

This chapter has given a short introduction to the mechanisms behind friction and to some of the many experimental observations of friction. The observations show that friction exhibits a very rich and dynamic behavior.

The main emphasis in the chapter lies on friction modeling. A small survey of existing friction models for various purposes is presented. The two main categories include friction models that all have been considered

	1	2	3	4	5	6	7
Arbitrary Steady-State Char.	yes	yes	yes	–	yes	yes	–
Stiction	yes	yes	yes	–	yes	yes	yes
Varying Break-Away Force	–	–	yes	–	–	–	–
Pre-Sliding Displacement	–	–	yes	yes	yes	yes	yes
Frictional Lag	–	–	yes	–	–	–	–
Simulation Efficiency	–	yes	–	yes	–	yes	yes

Table 2.1 A summary of the friction characteristics for the reviewed models: Classical models (1), Karnopp model (2), Armstrong's seven parameter model (3), Dahl model (4), Bristle model (5), reset integrator model (6), and models by Bliman & Sorine (7).

for control purposes. The models are categorized depending on if they include dynamics or not. The emphasis is made on a number of dynamic friction models that have been proposed for control purposes since the end of the 1960s. A third category describes special purpose models from a wide range of application fields. Many connections between the different models are pointed out.

Table 2.1 gives a summary of the different characteristics of the models. For the special purpose models most of the characterizations are not applicable. These models have therefore been excluded from the table.

3

A New Model

3.1 Introduction

In this chapter a new friction model is developed. Many friction models have been proposed and the motivation for developing yet another one is twofold; firstly the need for a model that facilitates design of improved controllers for high-precision motion and for low-velocity tracking and secondly the desire to have a model that more accurately describes friction in the analysis and simulation of control systems. The models used for control today are often very simple and they do not describe all of the various friction phenomena that have been observed. This is particularly true for low velocity motion and during velocity reversals.

Few attempts have been made to unify, into a single model, the results from the experimental observations of friction that are widely scattered in the literature, e.g., Hess and Soom (1990); Courtney-Pratt and Eisner (1957), and Richardson and Nolle (1976). Some of these observations were reviewed in Chapter 2. One problem has been the desire to derive the models from first principles. Friction, e.g., in a machine tool, is such a complicated phenomenon and involves theory from so many different areas that it is almost impossible to develop a "complete" friction model.

The aim in this chapter is to derive a model that qualitatively captures most of the complex nonlinear behavior of friction and is fairly simple with as few parameters as possible to tune. There is, of course, a trade-off between model complexity and its ability to describe intricate friction behavior. It is not necessary that the model explains the friction behavior physically from first principles. Therefore, it is not based on mechanics for contacts between solid bodies or on hydrodynamics for lubricants as done in Oden and Martins (1985) and in Harnoy and Friedland (1993), see also Chapter 2. The reasoning behind the model is instead intuitive. It is

influenced by the description of friction behavior found in experimental investigations of machine tools and frictional contacts; and derived from a dynamical systems point of view.

The new model was first introduced in Canudas de Wit *et al.* (1993) and (1995). The material in this chapter is partly based on those publications.

3.2 Model Derivation

The qualitative mechanisms of friction are fairly well understood as described in Chapter 2, see also Armstrong-Hélouvry (1991). The friction force between two lubricated surfaces in contact is caused by two factors; the solid-to-solid contact between the surfaces and the viscous resistance of the lubricant. The relative velocity between the surfaces determines the relative contribution of each factor, i.e., it determines the lubrication regime, see Chapter 2.

The starting point for the new model derivation is the force caused by the solid-to-solid contact. This is visualized in Figure 3.1. Surfaces are very irregular at the microscopic level and they make contact at a number of asperities. This is pictured as a contact through elastic bristles. When a tangential force is applied, the bristles deflect like springs and give rise to the friction force. If the force is sufficiently large some of the bristles deflect so much that they slip off each other. New contacts are then formed and as the two surfaces continue to move the process goes on. The relative velocity between the surfaces determines the amount of lubricant that is forced in between them and hence how far they are pushed apart. The contact phenomenon is highly random due to the irregular forms of the surfaces.

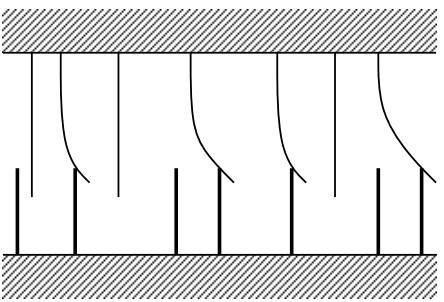

Figure 3.1 The friction interface between two surfaces is thought of as a contact between bristles. For simplicity the bristles on the lower part are shown as being rigid.

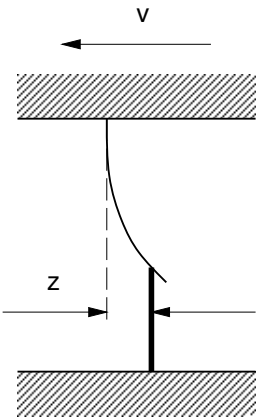

Figure 3.2 A single bristle represents the average deflection of the bristles in Figure 3.1.

The proposed model is based on the average behavior of the bristles that make up the contact. Figure 3.2 shows the contact interface with a single bristle representing the average behavior. Since this bristle should capture the aggregated behavior, it can never slip off. For a motion with constant velocity the deflection should reach a steady-state value. If the velocity is high, much lubricant is forced into the interface forcing the surfaces apart, and thus the bristles do not deflect as much before they slip. This means that the average bristle should reach a lower steady-state deflection than if the velocity is low and hardly no lubricant makes its way into the interface. This corresponds to the Stribeck effect and to different lubrication regimes. The average deflection of the bristles is denoted by z, as in Figure 3.2, and modeled by

$$\frac{dz}{dt} = v - \frac{|v|}{g(v)}z \tag{3.1}$$

where v is the relative velocity between the two surfaces and $g(v)$ a function which is discussed later. The first term gives a deflection that is proportional to the integral of the relative velocity and the second term asserts that the deflection z approaches the value

$$z_{ss} = \frac{v}{|v|}g(v) = g(v)\,\mathrm{sgn}(v)$$

in steady state, i.e., when v is constant. The function g is always positive and, furthermore, $g(v) > \varepsilon > 0$ for bounded velocities. The effect

of the lubricant on the solid-to-solid contact, as discussed above, should be included in g and it is, therefore, normally larger for smaller magnitudes of the velocity than for larger. It depends, however, on many factors such as material properties, lubrication, and temperature. It need not be symmetrical and direction-dependent behavior can therefore be captured.

The friction force is generated by the bending of the bristles that act as springs. It is proportional to the average deflection and the rate of change of the deflection. The friction force from the solid-to-solid contact is thus given by

$$F = \sigma_0 z + \sigma_1(v)\frac{dz}{dt}$$

where $\sigma_0 > 0$ is the stiffness and $\sigma_1(v) > 0$ a velocity dependent damping coefficient.

The second factor that makes up the friction force is caused by the viscosity of the lubricant. It is a function of the relative velocity and depends on the type of friction interface, e.g., if it is a roller or sliding bearing. The viscous friction force is added to the friction force caused by the solid-to-solid contact in order to get the total friction force which becomes

$$F = \sigma_0 z + \sigma_1(v)\frac{dz}{dt} + f(v) \tag{3.2}$$

A common case is that f is linear in velocity, i.e.,

$$f(v) = F_v v$$

where F_v is the coefficient of viscous friction. The steady-state relation between velocity and friction force for the proposed friction model is given by (3.1) and (3.2) when $dz/dt = 0$, i.e.,

$$F_{ss}(v) = \sigma_0 g(v)\,\mathrm{sgn}(v) + f(v) \tag{3.3}$$

The model given by (3.1) and (3.2) is characterized by the parameter σ_0, and the functions $g(v)$, $\sigma_1(v)$ and $f(v)$. The parameterization of these functions is treated next.

3.3 The Functions $g(v)$, $\sigma_1(v)$, and $f(v)$

The friction model (3.1) and (3.2) has been stated in a general form. It is specified by the parameter σ_0, and the functions $g(v)$, $\sigma_1(v)$, and $f(v)$. In this section different ways to parameterize these functions are discussed.

Determining the parameters of the model is a matter of nonlinear system identification and is done in Canudas de Wit and Lischinsky (1996).

Parameterization of $g(v)$

The function $g(v)$, which appears in (3.1), affects how the average deflection depends on the relative velocity between the moving surfaces. It influences both the steady-state and the dynamic behavior. The classical way to describe friction has been as a static function of velocity as done in (3.3). Experiments to determine friction has typically been done for constant velocity motions, see Chapter 2. It is thus natural that the friction model agrees with these simple experiments and descriptions for steady motion. The steady-state friction from the solid-to-solid contact is given by $\sigma_0 g(v)$, and since σ_0 is a constant the shape of $g(v)$ should agree with the shape of the experimentally observed variations with velocity. It assumes, however, that the viscous friction can be separated. Another possibility to take care of the variations with velocity would be to allow σ_0 to depend on velocity. This will, however, not be discussed. The parameter σ_0 hence acts as a scaling factor, which multiplied by $g(v)$ gives the steady state friction force. In order to have the same friction force, a decrease of σ_0 implies an increase of $g(v)$ and vice versa. If we rewrite (3.1) as

$$dz/dt = -\frac{1}{\tau(v)}z + v$$

we see that the relation between v and z is given by a first order equation with the "time constant"

$$\tau(v) = \frac{g(v)}{|v|} \tag{3.4}$$

In this way, it is clear how the speed with which the steady-state of (3.1) is reached can be affected. Decreasing $g(v)$ (and thus increasing σ_0) yields a shorter "time constant," which implies that the dynamics of (3.1) are faster. For an experimentally determined steady-state friction, the problem is to find a parameterized function that fits the data and then to determine the stiffness σ_0 to obtain the desired speed of the dynamics.

To agree in notation with existing static friction models the parameter σ_0 is used in the parameterization of $g(v)$ to scale friction forces. The function $g(v)$ then becomes

$$g(v) = \frac{F(v)}{\sigma_0}$$

where some expressions for the steady-state friction $F(v)$ were given in Chapter 2. In the simulations in Section 3.6 we use the following parameterization.

$$g(v) = \frac{1}{\sigma_0}\left(F_C + (F_S - F_C)e^{-(v/v_S)^2}\right) \tag{3.5}$$

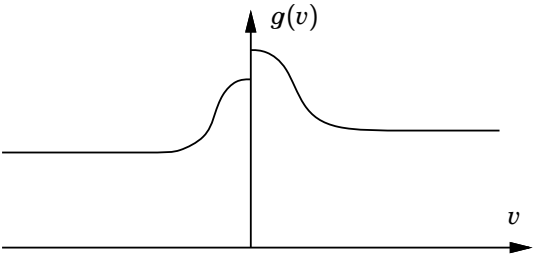

Figure 3.3 The function $g(v)$ is positive but may be asymmetric. It may also be discontinuous at zero velocity.

The friction force may be different for different directions of motion and it is possible to have an asymmetric $g(v)$ of the type shown in Figure 3.3. In that case different sets of parameters can be used for positive and negative velocities, respectively.

Parameterization of the Damping Coefficient $\sigma_1(v)$

The damping force is essential to make the system well behaved in transitions between sticking and sliding, as is seen in the simulations in Section 3.6. To avoid undamped oscillations in the bristle deflection the term $\sigma_1(v)dz/dt$ is added to the friction force. Most of the evaluation of the damping is done in Section 3.6, where the model behavior is studied in simulations. There are no experimental investigations of the damping reported. It is also seen in Section 3.5 that the damping affects the dissipativity properties of the model

The most common description of damping in dynamical systems is a term linear in the rate of change of the variable. For linear damping $\sigma_1(v)$ is a constant. This is the simplest parameterization of the damping but it limits the ability to reproduce some of the friction phenomena as will be seen in Section 3.6. A parameterization we suggest here is

$$\sigma_1(v) = \sigma_1 e^{-(v/v_d)^{\delta_d}}$$

which is characterized by the parameters, σ_1, v_d and δ_d. For this parameterization the damping force vanishes as the velocity increases. This is similar to Haessig and Friedland (1991), where it was suggested to include linear damping for the sticking behavior of the reset integrator model.

It is also interesting to observe some other parameterizations that relates the new model to the static models explained in Chapter 2. A static friction model is obtained with the following parameterization, which

leads to an unbounded damping for zero velocity.

$$\sigma_1(v) = \frac{\sigma_0 g(v)}{|v|} \tag{3.6}$$

Inserting (3.1) in (3.2) with (3.6) yields

$$F = \sigma_0 g(v)\,\mathrm{sgn}(v) + f(v)$$

which is a static model with no dynamics. For $\sigma_1(v) = \sigma_1/|v|$ the friction force becomes

$$F = (\sigma_0 - \frac{\sigma_1}{g(v)})z + \sigma_1\,\mathrm{sgn}(v) + f(v)$$

which is classical Coulomb friction superimposed on the dynamic friction model with reduced and velocity-dependent stiffness and no damping.

The behaviors of the different dampings are further studied in Section 3.6, where we use both

$$\sigma_1(v) = \sigma_1 \tag{3.7}$$

and

$$\sigma_1(v) = \sigma_1 e^{-(v/v_d)^2} \tag{3.8}$$

Parameterization of the Viscous Friction $f(v)$

Viscous friction is normally included in the classical friction models together with Coulomb friction and stiction, see Chapter 2. In the new model it is described by the function $f(v)$ in (3.2). It does not involve any dynamics. Instead it is a static, but possibly, nonlinear function of the velocity. Thus it can be parameterized as done in the classical static models. Suitable parameterizations for the viscous friction depend on the application. A general expression is given by

$$f(v) = F_v|v|^{\delta_v}\,\mathrm{sgn}(v)$$

where the parameters depend on the application. In Section 3.6 we use linear viscous friction

$$f(v) = F_v v. \tag{3.9}$$

The Standard Models

The following parameterizations thus represent a standard model.

$$\boxed{\begin{aligned} \frac{dz}{dt} &= v - \frac{|v|}{g(v)}z \\ g(v) &= \frac{1}{\sigma_0}\left(F_C + (F_S - F_C)e^{-(v/v_S)^2}\right) \\ F &= \sigma_0 z + \sigma_1(v)\frac{dz}{dt} + F_v v \\ \sigma_1(v) &= \sigma_1 e^{-(v/v_d)^2} \end{aligned}} \tag{3.10}$$

A simplified version of the standard model is obtained using (3.8).

$$\boxed{\begin{aligned} \frac{dz}{dt} &= v - \frac{|v|}{g(v)}z \\ g(v) &= \frac{1}{\sigma_0}\left(F_C + (F_S - F_C)e^{-(v/v_S)^2}\right) \\ F &= \sigma_0 z + \sigma_1\frac{dz}{dt} + F_v v \end{aligned}} \tag{3.11}$$

These models will be extensively simulated in Section 3.6.

3.4 Comparisons with Other Models

The proposed model can be related to many existing friction models. Some of these can be obtained by special choices of the parameterizations in the new model.

Static Models: As described in Chapter 2, simple friction models are static functions between relative velocity and friction force. No dynamics are considered. The new model gives the following relation between relative velocity and friction force for constant velocity motion.

$$F_{ss}(v) = \sigma_0 g(v)\,\mathrm{sgn}(v) + f(v)$$

It is therefore possible through the choice of the functions g and f to get any desired steady-state relationship. It should be noted, however, that when the velocity is not constant, the dynamics of the model are very

important in determining the friction force and they give rise to different types of phenomena. For the particular choice of damping

$$\sigma_1(v) = \frac{\sigma_0 g(v)}{|v|}$$

the model reduces to a classical static model determined by

$$F(v) = \sigma_0 g(v)\,\mathrm{sgn}(v) + f(v)$$

and with no dynamics.

The Dahl Model: The dynamics of the new model are closely related to the Dahl model described in Chapter 2. The proposed model can be seen as an extension, since, for the particular choice $g(v) = F_C/\sigma_0$, $\sigma_1(v) = 0$ and $f(v) = 0$, (3.1) and (3.2) reduce to

$$\frac{dF}{dt} = \sigma_0 \frac{dz}{dt} = \sigma_0 v \left(1 - \frac{F}{F_C}\,\mathrm{sgn}(v)\right)$$

which is the Dahl model in (2.13).

The Models by Bliman and Sorine: The models of Bliman and Sorine described in Chapter 2 can also be seen as extensions of the Dahl model. They, however, stress the rate independence of friction, i.e., that friction only depends on the distance moved since a velocity reversal, not on the velocity used to cover the distance. This property makes their model more tractable when regarded as a mathematical hysteresis operator, see Bliman and Sorine (1991). In Chapter 2 it was shown how a model by Bliman and Sorine could be used to describe friction between road and tire. The rate independence implied that for steady slip rates the friction could be described as a function of the slip rate only. The difference between wheel velocity and vehicle velocity was not included in the expression. The model developed in this chapter can also be used to describe tire–road friction giving similar relations. The friction will depend, however, both on the slip rate and the sliding speed, i.e., $F(s, \omega(r - r_e))$, see Chapter 2 for notation. The measurements in the literature, e.g., Bakker *et al.* (1987), are made for a single constant value of ωr. Thus, it cannot be determined if the friction force depends only on the slip rate or also on the actual speed.

The Bristle Model and the Reset Integrator Model: The intuitive picture of the frictional contact, as shown in Figure 3.1, is the same as that used for the two models in Haessig and Friedland (1990). The bristle

model was proposed to capture the random behavior of friction. The contact was, therefore, viewed as consisting of a number of minute bristles that deflect and at a certain deflection slip off and form a new contact at a randomly determined site. The resulting friction force from the model gets a non-deterministic behavior. The simpler reset integrator model, in a sense, can be said to describe the aggregated behavior of the bristles as is done in the model developed here. The reset integrator model, however, involves a logical statement to shut off the integration as discussed in Chapter 2.

3.5 Mathematical Properties

Some mathematical properties of the model given by (3.1) and (3.2) will now be explored. In particular, some fundamental properties of the differential equation describing the model are studied. The differential equation will also be linearized around an operating point to gain further insight.

It is important that the model is a well-defined differential equation so that a solution exists to the equations describing the system with friction. Friction is frequently used as an example of a discontinuous nonlinearity in control systems. Introducing discontinuities in differential equations implies that care has to be taken in order to get well-posed problems so that existence and uniqueness of solutions are assured. For the new model this is not a problem.

Existence and Uniqueness

The average deflection is described by (3.1). Let the velocity v be at least piece-wise continuous and bounded and regard the right-hand side of (3.1) as a function of t and z, i.e.,

$$\frac{dz}{dt} = v(t) - \frac{|v(t)|}{g(v(t))}z = f(z,t)$$

The right-hand side is continuous even for a $g(v)$ of the form shown in Figure 3.3 and it is differentiable except at $v = 0$. It also satisfies a Lipschitz condition in z and hence (3.1) has a unique solution. This is stated as a property.

PROPERTY 3.1
Let $v(t)$ be piece-wise continuous and bounded and let $g(v)$ be bounded away from zero. A unique solution to (3.1) then exists.

Proof.

$$|f(z_1,t) - f(z_2,t)| = \left| \left(v(t) - \frac{|v(t)|}{g(v(t))} z_1 \right) - \left(v(t) - \frac{|v(t)|}{g(v(t))} z_2 \right) \right|$$
$$= \left| \frac{v(t)}{g(v(t))} \right| |z_1 - z_2| \leq L |z_1 - z_2|$$

since $v(t)$ is bounded and $g(v) > \varepsilon > 0$. This Lipschitz condition guarantees the existence and uniqueness of a solution to (3.1), see Coddington and Levinson (1955). □

Next we note an intrinsic property of (3.1).

Boundedness

The deflection z should be bounded to agree with the intuitive properties of the bristle model in Figure 3.2. This is indeed the case as seen by the following property.

PROPERTY 3.2
Assume that $0 < g(v) \leq a$. If $|z(0)| \leq a$ then $|z(t)| \leq a$ for $t \geq 0$.

Proof. Let $V = z^2/2$. The time derivative of V evaluated along the solution of (3.1) becomes

$$\frac{dV}{dt} = z(v - \frac{|v|}{g(v)} z) = -|v||z| \left(\frac{|z|}{g(v)} - \operatorname{sgn}(v) \operatorname{sgn}(z) \right)$$

The derivative dV/dt is negative when $|z| > g(v)$. Since $g(v)$ is strictly positive and bounded by a, we see that the set $\Omega = \{z : |z| \leq a\}$ is an invariant set for the solutions of (3.1), i.e., all the solutions of $z(t)$ starting in Ω remain there. □

It follows from (3.1) that, since z is bounded and since $g(v) > \varepsilon > 0$, dz/dt is bounded for bounded v. The friction force F given by (3.2) is then well-defined and bounded unless the damping is unbounded.

Dissipativity

Intuitively it may be expected that friction dissipates energy. Since the model given by (3.1) and (3.2) is dynamic, there may be phases where friction stores energy and others where it gives energy back. The energy consumed by the friction is given by

$$\int F dx = \int F v d\tau$$

It is, therefore, interesting to see if it is possible to find a nonnegative function $V(z(t))$ such that

$$\int_0^t F v d\tau \geq V(z(t)) - V(z(0))$$

This implies that energy is dissipated by the friction, see Willems (1972). If we restrict the damping this is indeed the case. For simplicity we omit the viscous friction $f(v)$.

PROPERTY 3.3
If $0 \leq \sigma_1(v) \leq 4\sigma_0 g(v)/|v|$ then $\int_0^t F v dt \geq V(z(t)) - V(z(0))$ with $V(z(t)) = \sigma_0 z(t)^2/2$. This implies that the friction model is dissipative.

Proof. We have

$$\begin{aligned}
Fv &= \sigma_0 z \frac{dz}{dt} + \sigma_1(v)\left(\frac{dz}{dt}\right)^2 + \sigma_0 \frac{|v|}{g(v)} z^2 + \sigma_1(v)\frac{|v|}{g(v)}\frac{dz}{dt} z \\
&= \sigma_0 z \frac{dz}{dt} + \sigma_1(v)\left(\left(\frac{dz}{dt}\right)^2 + \frac{\sigma_0|v|}{\sigma_1(v)g(v)} z^2 + \frac{|v|}{g(v)}\frac{dz}{dt} z\right) \\
&= \sigma_0 z \frac{dz}{dt} + \sigma_1(v)\left(\left(\frac{dz}{dt} + \frac{|v|z}{2g(v)}\right)^2 + \frac{|v|}{g(v)}\left(\frac{\sigma_0}{\sigma_1(v)} - \frac{|v|}{4g(v)}\right) z^2\right) \\
&\geq \sigma_0 z \frac{dz}{dt} + \sigma_1(v)\frac{|v|}{g(v)}\left(\frac{\sigma_0}{\sigma_1(v)} - \frac{|v|}{4g(v)}\right) z^2
\end{aligned}$$

Hence

$$Fv \geq \sigma_0 z \frac{dz}{dt}$$

if $\sigma_1(v) \leq 4\sigma_0 g(v)/|v|$, which means that

$$\int_0^t F v d\tau \geq \sigma_0 \frac{z(t)^2}{2} - \sigma_0 \frac{z(0)^2}{2}$$

□

Dissipativity is not only related to physical energy. It can also be used as a mathematical property in order to prove stability for feedback systems, see Willems (1972) and Hill and Moylan (1977). The systems are then considered as operators that map the input to the output. For the friction model the velocity v is the input and the friction force F the output. We can, however, also study (3.1) as an input–output operator. For this system it can be proven that the map $\varphi : v \to z$ is dissipative.

PROPERTY 3.4
The map $\varphi : v \mapsto z$, as defined by (3.1) is dissipative with respect to the function $V(z(t)) = z^2(t)/2$, i.e.,

$$\int_0^t z(\tau)v(\tau)\, d\tau \geq V(z(t)) - V(z(0)).$$

Proof. It follows from (3.1) that

$$zv = z\frac{dz}{dt} + \frac{|v|}{g(v)}z^2 \geq z\frac{dz}{dt}$$

Hence

$$\int_0^t z(\tau)v(\tau)\, d\tau \geq \int_0^t z(\tau)\frac{dz(\tau)}{d\tau}d\tau \geq V(z(t)) - V(z(0))$$

□

Linearization

We will now study the differential equation when linearized around an arbitrary equilibrium point. The friction model is specified by the three functions $g(v)$, $\sigma_1(v)$, and $f(v)$. The linearization, of course, involves these functions and their derivatives. As has been seen in Section 3.3, the functions need not be differentiable everywhere and at zero velocity they may not even be continuous. The linearization, however, is done assuming differentiability of the functions and the other cases have to be discussed accordingly. Here we list the assumptions and potential problems.

- The function $g(v)$ is assumed continuous and differentiable everywhere except possibly at $v = 0$.
- The function $\sigma_1(v)$ is assumed continuous and differentiable except at $v = 0$.
- The function $f(v)$ may, for some applications, not be differentiable at $v = 0$.
- The right-hand side of (3.1) involves the absolute value of the velocity, which is not differentiable at $v = 0$.

We see that care has to be taken when linearizing around zero velocity, where we may have discontinuities. However, even with a discontinuous $g(v)$ the right-hand side of (3.1) is continuous at zero velocity. An example of how (3.1) looks with such a $g(v)$ is shown in Figure 3.4. The surface is differentiable except in the v-direction at zero velocity. The linearized

behavior of the differential equation for zero velocity, however, can be described using two different sets of parameters. The problems with (3.1) are thus resolved easily.

The relation (3.2) is the second equation to linearize. This is a nonlinear map relating v and z to the friction force. The parameterizations that have been proposed for damping and viscous friction include some that are not differentiable at zero velocity. These are not considered here when linearizing around $v_0 = 0$.

We now show the linearized equations around $v = v_0$ and $z = z_0$. Letting $d|v(t)|/dt = \mathrm{sgn}(v(t))$, where the sign function is undetermined for zero argument, we get in a straightforward way

$$\begin{aligned}
\frac{d(\delta z)}{dt} &= -\frac{|v|}{g(v)}\bigg|_{\substack{v=v_0\\z=z_0}} \delta z + H(v,z)\bigg|_{\substack{v=v_0\\z=z_0}} \delta v \\
\delta F &= \left(\sigma_0 - \sigma_1(v)\frac{|v|}{g(v)}\right)\bigg|_{\substack{v=v_0\\z=z_0}} \delta z \\
&\quad + \left(\sigma_1'(v)\left(v - \frac{|v|}{g(v)}z\right) + \sigma_1(v)H(v,z) + f'(v)\right)\bigg|_{\substack{v=v_0\\z=z_0}} \delta v
\end{aligned} \tag{3.12}$$

where

$$H(v,z) = \left(1 - \frac{z}{g(v)}\,\mathrm{sgn}(v) + \frac{g'(v)}{g^2(v)}|v|z\right)$$

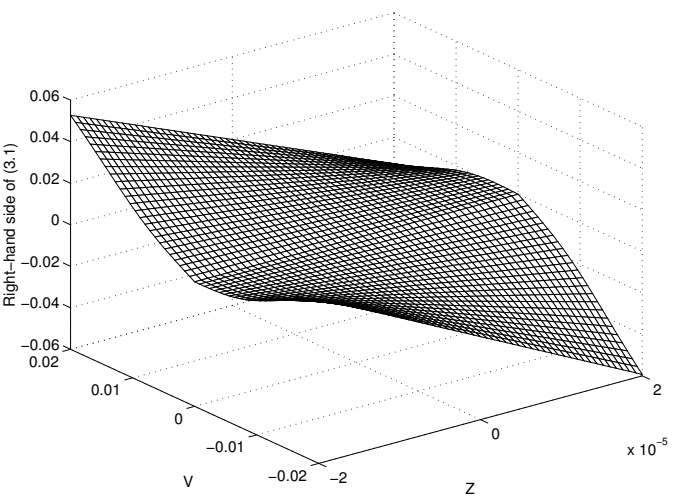

Figure 3.4 A mesh plot of the right-hand side of (3.1) for a discontinuous $g(v)$.

and the prime denotes derivatives with respect to v. The linearization is valid for all equilibrium points except $v_0 = 0$ due to the assumptions made. For $v_0 = 0$ we first look at the special case when $z_0 = 0$. The linearized equations can then be simplified to

$$\frac{d(\delta z)}{dt} = \delta v$$
$$\delta F = \sigma_0 \delta z + (\sigma_1(0) + f'(0))\delta v$$

where we have assumed that $\sigma_1(0)$ is bounded and that $f'(0)$ exists. The friction model thus acts as a linear spring with stiffness σ_0 and damping $\sigma_1(0) + f'(0)$. For the simple equation of motion

$$\frac{d^2x}{dt^2} = -F$$

this corresponds to a relative damping

$$\zeta = (\sigma_1(0) + f'(0))/2\sqrt{\sigma_0} \tag{3.13}$$

and natural frequency

$$\omega_0 = \sqrt{\sigma_0} \tag{3.14}$$

Normally $\sigma_1(0)$ is much larger than $f'(0)$ in (3.13).

If $v_0 = 0$ but $z_0 \neq 0$ we must have different equations for positive and negative velocities. This can be described as

$$\frac{d(\delta z)}{dt} = G(\delta v, z_0)\delta v$$
$$\delta F = \sigma_0 \delta z + (\sigma_1(0)G(\delta v, z_0) + f'(0))\,\delta v$$

where

$$G(\delta v, z_0) = \begin{cases} \left(1 - \dfrac{z_0}{g(0^+)}\right) & \text{for } \delta v > 0 \\ \left(1 + \dfrac{z_0}{g(0^-)}\right) & \text{for } \delta v < 0 \end{cases}$$

We allow $g(v)$ to be discontinuous at zero velocity and, therefore, $g(0^+)$ denotes the value of $g(v)$ for values of v slightly larger than zero. $g(0^-)$ is defined in the same manner. The effect of $z_0 \neq 0$ is that both the stiffness and the damping (not the viscous) is changed by the factor $G(v, z_0)$. The spring characteristics of the friction model are thus different for different directions of motion. The linearization holds under the assumptions that $\sigma_1(0)$ is bounded and that $f'(0)$ exists.

Parameter	F_C	F_S	σ_0	v_S	σ_1	F_v
Value	1	2	10^5	0.01	$2\sqrt{10^5}$	0.4

Table 3.1 Default parameter values for the simplified standard model used in the simulations.

3.6 Dynamic Behavior

Some mathematical properties of the model introduced in Section 3.2 were shown in Section 3.5. Here we illustrate the rich dynamic behavior that this simple model exhibits. The model is assessed through simulations and the results are studied with respect to parameter changes. At the same time it is shown that the model qualitatively captures the experimental behaviors described in Chapter 2. It is natural that a fair amount of prejudices will bias the discussions in this section. The intuitive conceptions of friction behavior are probably based on real life experiences but also on the belief that friction should behave as if described by a static model including stiction.

Different ways to parameterize the functions describing the new friction model were introduced in Section 3.3. In this section we mainly use the simplified standard model (3.11). If nothing else is specified, the default values of the parameters have been used. These values are found in Table 3.1. In some simulations, however, the parameters are changed in order to high-light certain characteristics. The default values are to some extent based on experimental results, see Armstrong-Hélouvry (1991). The stiffness σ_0 is chosen to give a pre-sliding displacement of the same magnitude as reported in various experiments. The value of the damping coefficient σ_1 is chosen to give a relative damping of $\zeta = 1$, see (3.13). The Coulomb friction level F_C corresponds to a friction coefficient $\mu \approx 0.1$ for a unit mass and F_S gives hundred percent higher friction for very low velocities. The viscous friction F_v and the Stribeck velocity v_S are also of the same order of magnitude as given in Armstrong-Hélouvry (1991).

First we study the two most intriguing behaviors due to friction, i.e., getting stuck and breaking away. They both involve the complexity of friction for low or even zero velocity. Transition from solid-to-solid contact to full fluid lubrication and vice versa, which is the underlying phenomenon, has not yet been described accurately physically and is only partly understood. The behavior is therefore judged qualitatively.

Sticking

The behavior around the time where an object gets stuck due to friction can be expected to be quite complicated. The setup for the simulations is

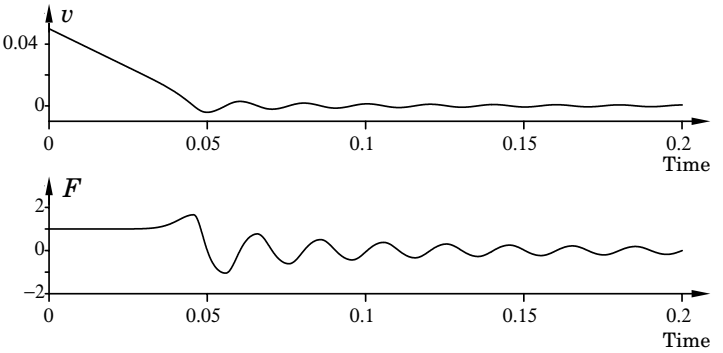

Figure 3.5 The sticking behavior for the simplified standard model without damping ($\sigma_1 = 0$). The sticking behavior is very oscillatory.

the simplest possible and agrees with Figure 2.9. A unit mass with initial velocity different from zero is subjected to friction and hence decelerates. No other force than the friction force affects the mass so the equation of motion is given by

$$\frac{d^2x}{dt^2} = -F \tag{3.15}$$

where F is the friction force and x the position of the mass. The resulting motion of (3.15) is studied with respect to different parameterizations and parameter values. Particular attention is given to the behavior close to when the mass stops.

We start by studying solid-to-solid friction without damping and viscous friction, i.e., the simplified standard model (3.11) with $F_v = 0$ and $\sigma_1 = 0$. The mass has an initial velocity $v(0) = 0.05$ and $z(0) = 0.00001$, which means that the deflection equation (3.1) is close to equilibrium. Figure 3.5 shows the velocity and the friction force. As can be seen, the friction force increases due to the Stribeck effect when the velocity approaches zero. This leads to a pronounced deceleration. The motion becomes oscillatory, however, and the mass does not come to an immediate rest. The behavior of the system is poorly damped.

We next see what happens if we reduce the stiffness with a factor of 100 to $\sigma_0 = 1000$. This implies that the dynamics of the differential equation (3.1) are much slower. For this case the initial value of the deflection was changed to $z(0) = 0.001$ to agree with the new stiffness. The results are shown in Figure 3.6. The motion starts to decelerate at the same rate as before. The dynamics are, however, so slow that even though $g(v)$ increases as the velocity decreases, the friction force is not increased to the same extent. The Stribeck effect is therefore less pronounced. It also takes a very long time for the friction force to react to the change of direction of

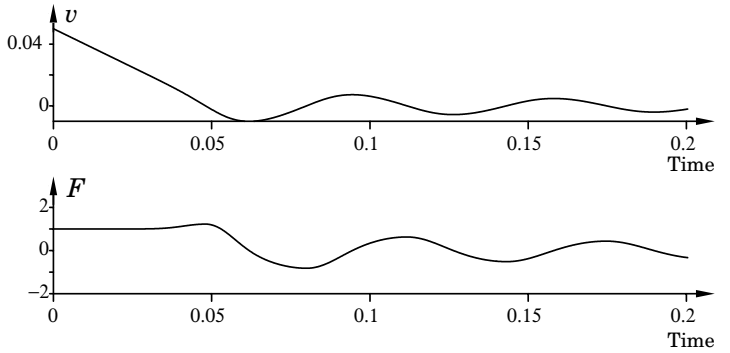

Figure 3.6 The sticking behavior for the simplified standard model without damping ($\sigma_1 = 0$) and with slow dynamics ($\sigma_0 = 1000$). The friction response to velocity changes is sluggish and the behavior is also oscillatory. Compare with Figure 3.5.

the motion, i.e., before it changes its sign. The oscillations become larger and slower as expected.

In the previous two simulations the friction force did not include any damping and, therefore, the resulting motion became oscillatory. Damping is essential for the behavior for low velocities as we see next.

We first let the damping coefficient be constant as in the simplified standard model. The parameters agree with Table 3.1. The chosen damping coefficient gives a relative damping of $\zeta = 1$, see (3.13). Figure 3.7 shows the results. The oscillations have disappeared but the friction force

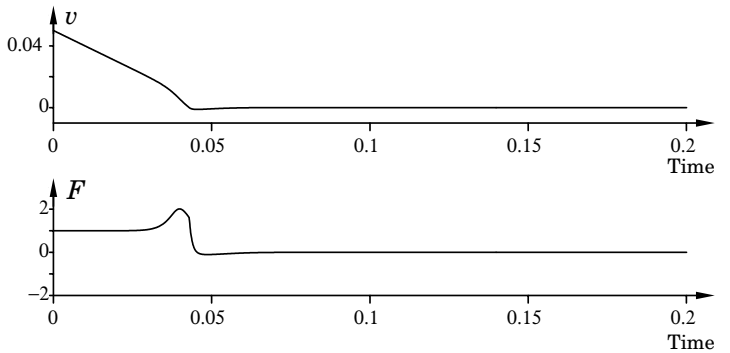

Figure 3.7 The sticking behavior for the simplified standard model with damping ($\sigma_1 = 2\sqrt{10^5}$). The behavior becomes well damped. A small undershoot can be noticed in the velocity and the friction force drops slightly before zero velocity is reached for the first time. Compare with Figure 3.5.

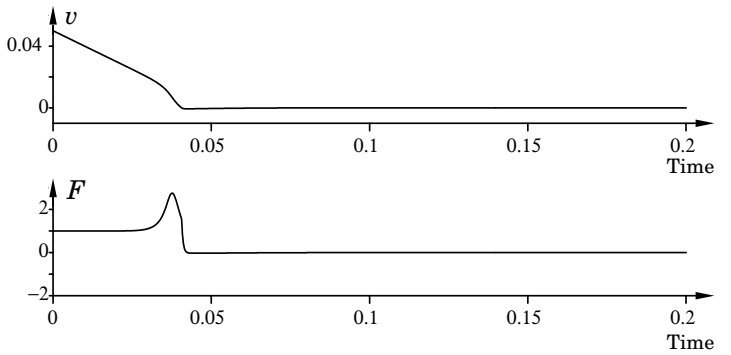

Figure 3.8 The sticking behavior for the simplified standard model with damping ($\sigma_1 = 4\sqrt{10^5}$). The undershoot in the velocity is smaller than in Figure 3.7. The peak friction force exceeds $F_S = 2$.

decreases shortly before the motion stops. It is also noted that there is still a small undershoot in the velocity. These observations contradict, to some extent, the intuition of what should happen just before the full stop.

Figure 3.8 shows the behavior if the damping is doubled to $\sigma_1 = 4\sqrt{10^5}$. The undershoot in the velocity is slightly reduced but there is still a clear drop in the friction force before the mass stops. Note also that the peak friction force is higher than $F_S = 2$.

In Figure 3.9 the two components $\sigma_0 z$ and $\sigma_1 dz/dt$ of the friction have been plotted. It is seen that, as $\sigma_0 z$ approaches its maximum, dz/dt decreases and hence the damping force. This results in the decreasing friction force. To avoid this problem the damping coefficient $\sigma_1(v)$ may

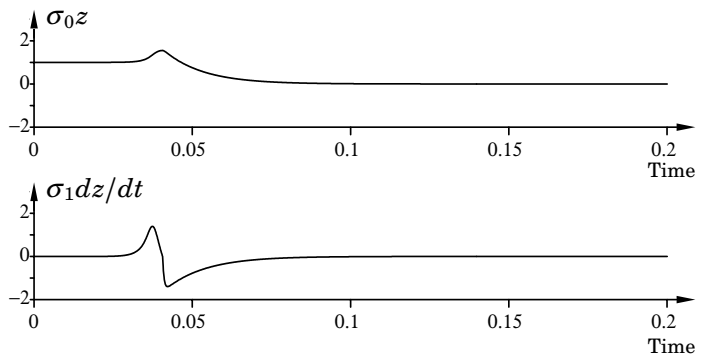

Figure 3.9 The friction force components $\sigma_0 z$ and $\sigma_1 dz/dt$ corresponding to the simulations in Figure 3.8.

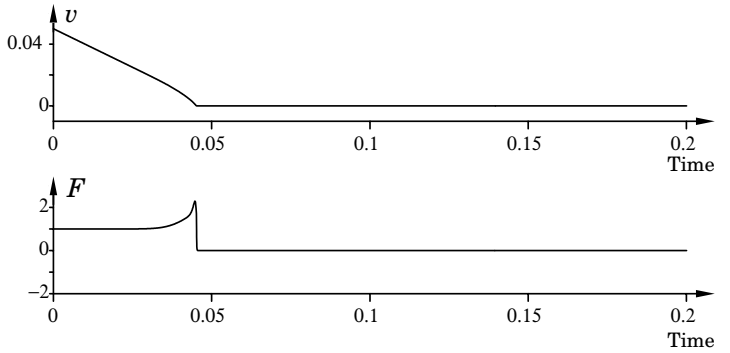

Figure 3.10 The sticking behavior for the standard model with velocity dependent damping coefficient given by $\sigma_1 = 10000$ and $v_d = 0.001$. The friction increases until zero velocity is reached when it drops abruptly to zero.

increase with the decreasing velocity so that the decrease in dz/dt is compensated by an increase in $\sigma_1(v)$. Thus, the damping is modified according to (3.8) with $\sigma_1 = 10000$ and $v_d = 0.001$. The resulting simulation is shown in Figure 3.10 and the terms $\sigma_0 z$ and $\sigma_1(v)dz/dt$ are shown in Figure 3.11. The friction force now continues to increase almost until the motion stops and then it drops sharply to zero. This behavior of the motion and the friction force is the most credible, so far, in the sense that we get an abrupt stop.

It is very important that v_d is not too small for this type of nonlinear damping. The parameter v_d determines the velocity interval around zero for which the damping is active. If this interval is too small, the motion

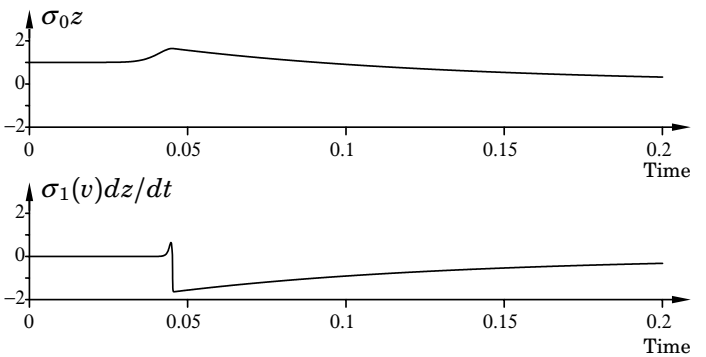

Figure 3.11 The friction force components $\sigma_0 z$ and $\sigma_1(v)dz/dt$ corresponding to the simulation in Figure 3.10.

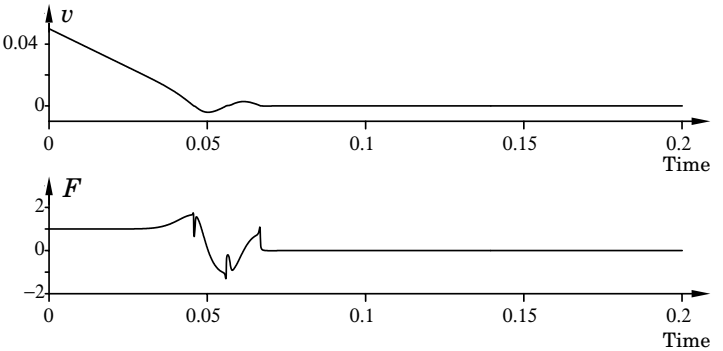

Figure 3.12 The sticking behavior for the standard model with velocity dependent damping coefficient given by $\sigma_1 = 10000$ and $v_d = 0.00015$. The damping is active only for a small region around zero velocity. Therefore, the motion comes to rest first at the third time that zero velocity is approached.

may pass through zero without slowing down enough to stop completely. This is illustrated in Figure 3.12 where $v_d = 0.00015$. The motion is not stopped until the third time the velocity approaches zero.

The simulations have so far not included any viscous friction. This friction type mainly affects the behavior for higher velocities and does therefore not influence the simulations presented to any larger degree.

It has been seen that the model with nonlinear parameterization of the damping agrees best with the intuitive and traditional understandings of friction. If the damping coefficient grows large as the velocity goes to zero this leads to the most abrupt drop in the friction force when zero velocity is reached. A velocity-dependent damping coefficient may also give a friction model that is dissipative as discussed in Section 3.5. No experimental investigation of this damping have been found and it is, therefore, hard to discuss correctness. A few questions should be borne in mind regarding the damping:

- How well damped is a real physical system when motion stops? Can microscopical oscillations be found and if so at what frequency?
- In what velocity interval around zero is there damping?

Breaking Away

The behavior when breaking away is studied next. The effect of the dynamics of the friction model will be clear in the study. We consider the same set-up as for sticking but with an external force affecting the mass in addition to the friction force, see Figure 2.9. The equation of motion is

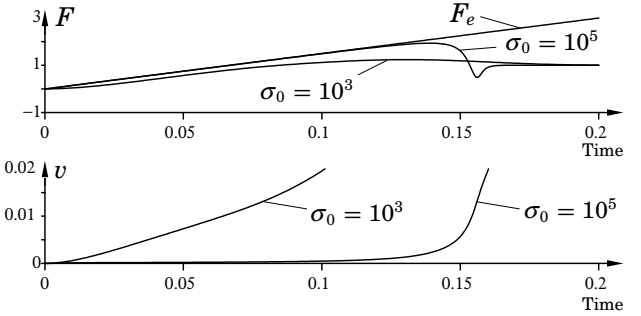

Figure 3.13 The break-away behavior for the simplified standard model with $\sigma_0 = 10^5$, $\sigma_1 = 2\sqrt{10^5}$ and $\sigma_0 = 10^3$, $\sigma_1 = 2\sqrt{10^3}$. The higher stiffness gives a characteristic break-away behavior at $t \approx 0.15$. For the lower stiffness it is questionable to talk about break-away.

given by

$$\frac{d^2x}{dt^2} = F_e - F \tag{3.16}$$

where F_e is the external force and F the friction force. Equation (3.16) will be studied when F_e is linearly ramped up from zero. All initial conditions are set to zero.

We start with the simplified standard model (3.11) without viscous friction, i.e., $F_v = 0$. Viscous friction would not affect the simulation to any larger extent. We compare the simplified standard model with a simulation with lower stiffness and damping coefficient, i.e., $\sigma_0 = 10^3$ and $\sigma_1 = 2\sqrt{10^3}$. Note that the steady-state friction force and the relative damping (3.13) are the same for both cases. Figure 3.13 shows the results. The simplified standard model shows a typical break-away behavior. The velocity is almost zero until the friction force no longer can follow the applied force. This happens when the friction force approaches the value $F_S = 2$. There is then an increase in the velocity and due to the Stribeck effect the friction force drops. An undershoot can also be noted before the friction force approaches its steady-state value $F = 1$. For the lower stiffness it is questionable to talk about break-away. The mass starts to move almost instantly at quite a high speed so that it is outside the velocity region of the Stribeck effect. No sharp drop can then occur in the friction force and, thus, we do not get any characteristic break-away.

Figure 3.14 shows the result if the damping of the simplified standard model is changed to $\sigma_1 = 4\sqrt{10^5}$ and $\sigma_1 = \sqrt{10^5}$, i.e., doubled and halved, respectively. The behaviors are similar to that in Figure 3.13 except for the undershoot in the friction force, which occurs after break away. This is pronounced if the damping is increased but has almost vanished for the

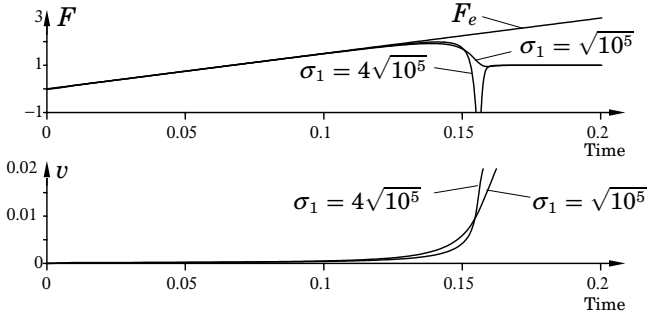

Figure 3.14 Break-away behavior for the simplified standard model with $\sigma_1 = 4\sqrt{10^5}$ and $\sigma_1 = \sqrt{10^5}$. For the higher stiffness there is a pronounced undershoot in the friction force as break-away occurs.

case when the damping is halved.

Three simulations where the damping is modified according to (3.8) have also been performed. With this model the parameter σ_1 determines the damping for zero velocity and v_d determines the velocity interval around zero where there is damping. The result of these simulations are shown in Figure 3.15. In the first case the parameters are $\sigma_1 = 2000$ and $v_d = 0.001$ (Case 1). This implies that the damping is high for very low velocities but that it has almost vanished at the Stribeck velocity $v_S = 0.01$. The break-away behavior has no undershoot in the friction force, since the damping is almost zero at this point. If the velocity interval is increased with $v_d = 0.01$ (Case 2), we see a large undershoot that was also present in Figures 3.13 and 3.14. Finally, Figure 3.15 also shows the case when $\sigma_1 = 10000$ and $v_d = 0.001$ (Case 3). In this case the break-away takes place later due to the higher damping. The drop in the friction force occurs

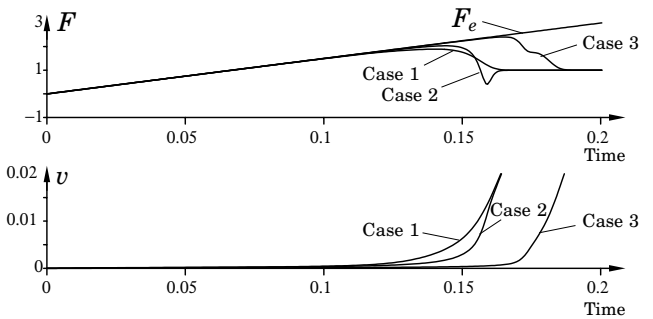

Figure 3.15 Break-away behavior for three cases of velocity-dependent damping coefficient.

in two phases. The first drop is due to the vanishing damping, which is determined by $v_d = 0.001$. The second drop is due to the Stribeck effect, which is determined by $v_S = 0.01$. This suggests that if high damping for zero velocity is desired by using (3.8) then v_d must be chosen in relation to v_S.

Varying Break-Away Force

The break-away force is the force required to initiate motion of a mass at rest. Classically, the concept is defined by reasoning in static terms. The break-away force is then often a parameter of the friction model as for the static model (2.6) where F_S is the break-away force. This means that the break-away force is unique and well-defined. For a dynamic model this is not the case. In order to compare with experiments in the literature we must define the break-away force in other terms. As discussed in Chapter 2 and this chapter, the model gives rise to microscopic displacements in order to build up the friction force. Therefore, the detection of non-zero velocity cannot be used to define break-away. Instead we define the break-away force using a linearly increased external force. If the external force, after being increased, is held constant and motion is continued in steady-state then break-away has occurred. The value at which the external force is held constant is then larger than the break-away force. The smallest such force giving rise to sustained motion is defined as the break-away force. Notice that the definition includes the experimental condition, i.e., that the externally applied force is increased linearly and also the rate at which it is increased. This means that a force increased in another way may or may not cause break-away even if it is kept constant at the same level.

Experimental studies have shown that the break-away force varies with the experimental conditions. In Johannes *et al.* (1973) and Richard-

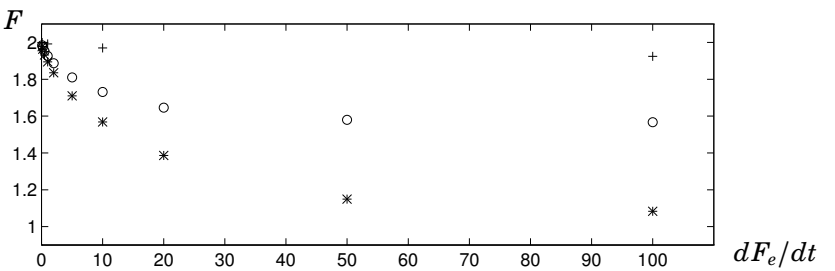

Figure 3.16 The varying break-away force as a function of the rate of increase of the applied force: for default parameters (+); $v_S = 0.001$ (∗); and $\sigma_0 = 10000$, $\sigma_1 = 200$ (∘).

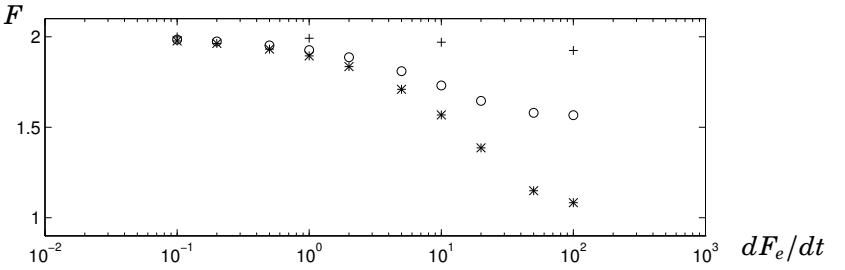

Figure 3.17 The dependence of the break-away force on the rate of force application with logarithmic x-axis for: default parameters (+); $v_S = 0.001$ (∗); and $\sigma_0 = 10000$, $\sigma_1 = 200$ (∘).

son and Nolle (1976) it is pointed out that the break-away force depends on the rate of increase of the external force. A series of simulations have been performed using the new model to determine the break-away force for different rates of force application. Figure 3.16 shows the results for the simplified standard model: with default parameters (+), with $v_S = 0.001$ (∗), and, finally, with stiffness and damping decreased to $\sigma_0 = 10000$ and $\sigma_1 = 200$ (∘). The break-away force is shown as a function of the rate of increase of the applied force. The same relation but with logarithmic x-axis is shown in Figure 3.17. For the simplified standard model with default parameters there is only a slight decrease in the break-away force as the rate of force application is increased. The decrease in break-away force is more pronounced if either the Stribeck velocity v_S or the stiffness σ_0 is decreased. The behavior of the break-away force as a function of rate of force application agrees qualitatively with the experimental results in Johannes *et al.* (1973) and Richardson and Nolle (1976). Increasing the damping $\sigma_1(v)$ at low velocities would prevent early break-away as was seen in Figure 3.15.

Pre-Sliding Displacement

Microscopical motion occurs in order to build up the reactive friction force before break-away occurs. This is called pre-sliding displacement. Courtney-Pratt and Eisner (1957) showed that friction behaves like a nonlinear spring if the external force is less than the break-away force. A simulation was performed to investigate if the new model captures this phenomenon. The simplified standard model was used with default parameter values. An external force was applied to a unit mass subjected to friction. The force was slowly ramped up to 1.98, which is 99% of $F_S = 2$, and then ramped down to the value -1.98. Finally, it was ramped up to 1.98 again. The result of the simulation is shown in Figure 3.18, where the

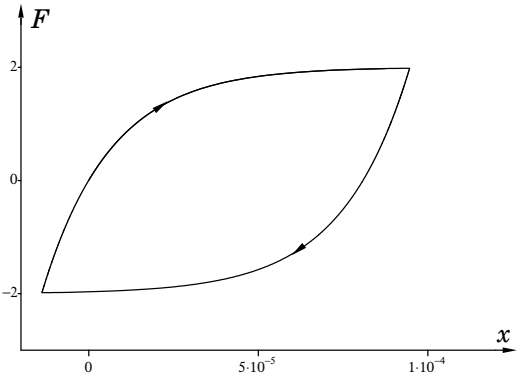

Figure 3.18 Pre-Sliding displacement as described by the simplified standard model. The simulation was started with zero initial conditions. The result agrees qualitatively with the experimental results given in Courtney-Pratt and Eisner (1957).

friction force is shown as a function of displacement. The behavior in Figure 3.18 agrees qualitatively with the experimental results in Courtney-Pratt and Eisner (1957).

Frictional Lag

Hess and Soom (1990) studied the dynamic behavior of friction when velocity is varied during unidirectional motion. They found that there is hysteresis in the relation between friction force and velocity. The friction force is lower for decreasing velocities than for increasing velocities. The hysteresis loop becomes wider at higher rates of the velocity changes. This cannot be explained with the classical friction models, where the friction force is unique for every nonzero velocity. We now study the behavior of the new model for the same type of experiment. The input to the friction model is the velocity, which is changed sinusoidally. The resulting friction force is presented as a function of velocity. Note that the motion never changes direction in this experiment.

In the first simulation we use the simplified standard model without damping and viscous friction, i.e., $\sigma_1 = 0$ and $F_v = 0$. We have seen previously that damping is essential in order to get good behavior for motion close to sticking, but it is despite this fact interesting to start without damping. In Figure 3.19 we see the results of the first simulations with three different frequencies of the sinusoidal velocity, $\omega = 20$, $\omega = 50$, and $\omega = 100$. The hysteresis loop increases with ω. The model clearly exhibits hysteresis as described in the experimental investigations of Hess and Soom.

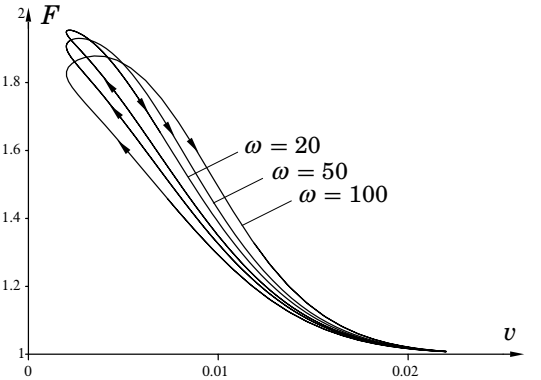

Figure 3.19 Hysteresis exhibited by the simplified standard model without damping ($\sigma_1 = 0$). The frequencies of the velocity variations are $\omega = 20$, 50 and 100. The results agree with the experimental results in Hess and Soom (1990).

Next we add linear damping. We let $\omega = 20$ and compare with the previous simulation. The constant damping coefficient is $\sigma_1 = 2\sqrt{10^5}$. The result is shown in Figure 3.20 together with the result for $\sigma_1 = 0$. The hysteresis loop with damping has been reversed except for the lowest velocities. The reason for this is seen if we plot the contributions to the friction force, i.e., $\sigma_0 z$ and $\sigma_1 dz/dt$, separately as in Figure 3.21. When the velocity is reduced $g(v)$ increases and then the deflection z increases. This implies that dz/dt is positive for decreasing velocities. The damping force will, therefore, show hysteresis that opposes the desired one. How

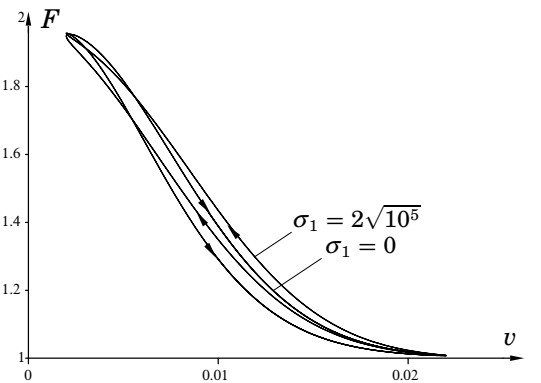

Figure 3.20 The hysteretic behavior of the simplified standard model for $\omega = 20$ with damping $\sigma_1 = 0$ and $\sigma_1 = 2\sqrt{10^5}$. The hysteresis loop is reversed when damping is introduced.

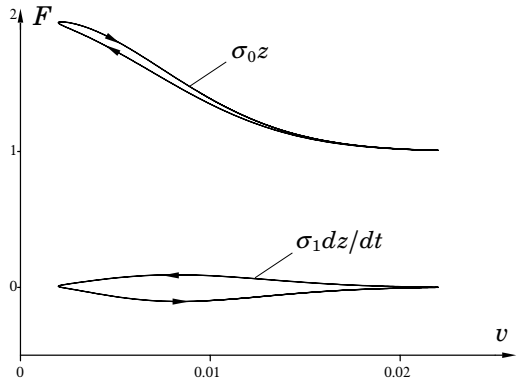

Figure 3.21 The two components of the friction force in Figure 3.20 for $\omega = 20$ and $\sigma_1 = 2\sqrt{10^5}$.

much it will affect the resulting friction force depends on the velocity. The "time constant" (3.4) for the dynamics of the model is higher for higher velocities. Thus, dz/dt is likely to assume larger values for higher velocities and the damping force may dominate and reverse the hysteresis loop. If the Stribeck velocity was lower so that dz/dt started to increase at lower velocities then the hysteresis loop could still assume a normal shape. In order to get a correct hysteretic behavior, the Stribeck velocity must be relatively low. For Figure 3.20 it would have to be approximately $v_S = 0.001$.

The velocity dependent damping coefficient (3.8) gives better hysteretic

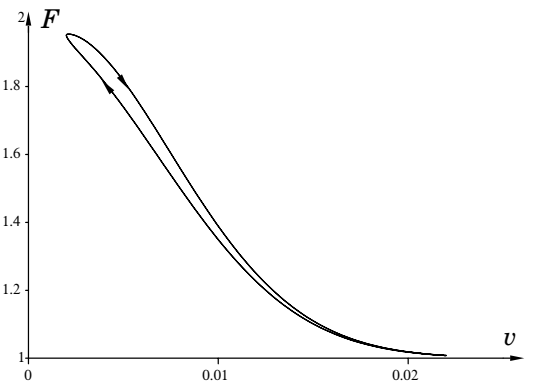

Figure 3.22 Hysteresis for the model with velocity dependent damping coefficient given by $\sigma_1 = 10000$ and $v_d = 0.001$. The frequency of the velocity variation is $\omega = 20$.

behavior. However, if it is made very large for small velocities, the problem can still be observed. In Figure 3.22 the same simulation as in Figure 3.20 was performed with damping given by $\sigma_1 = 10000$ and $v_d = 0.001$. The behavior is now the same as the desired one in Figure 3.19. If the velocity variations would be in the region where the damping is large, then this model, however, would also show undesired behavior.

The conclusion drawn from the simulations of sticking and hysteresis is that high damping is required but only for low velocities. It is very hard to control motions with such low velocities and, therefore, experimental results are difficult to obtain. The damping for zero velocity should exceed the value for critical damping as given by (3.13) but vanish for those velocities where hysteresis behavior is interesting.

The simulations in this section have shown that the new friction model is able to capture many of the experimentally observed friction phenomena.

3.7 Summary

A new model for friction has been presented. It attempts to describe the average behavior of friction, not the randomness due to surface irregularities. The model is described by a first-order nonlinear differential equation. The model is simple yet exhibits a very rich behavior, which has been shown in the different simulations. The results agreed with experimental observations. In its standard form the model is given by

$$\begin{aligned} \frac{dz}{dt} &= v - \frac{|v|}{g(v)}z \\ g(v) &= \frac{1}{\sigma_0}\left(F_C + (F_S - F_C)e^{-(v/v_S)^2}\right) \\ F &= \sigma_0 z + \sigma_1 \frac{dz}{dt} + F_v v \\ \sigma_1(v) &= \sigma_1 e^{-(v/v_d)^2} \end{aligned}$$

A simplified form is given by $\sigma_1(v) = \sigma_1$.

The parameters are, of course, application dependent. The friction levels F_C, F_S and F_v can therefore not be given any nominal values. Reasonable choices for the other parameters can, however, be given. These are $\sigma_0 = 10^3$–10^5, $v_S = 0.01$ and $\sigma_1 = 2\sqrt{\sigma_0 m}$, where m is the inertia of the body subjected to friction.

The study of the model has indicated the need for validation experiments. In particular the following experiments would be revealing:

- Accurate sticking and break-away experiments
- Unidirectional low-velocity motion with velocity variations

The experimental requirements are hard to specify a priori. If friction would behave as the simplified standard model with default parameters the following approximate accuracies are needed:

- Position resolution: 10^{-7} m
- Velocity resolution: 10^{-4} m/s
- Sampling rate: 10 kHz

In addition to this, accurate measurements of externally applied forces are necessary.

4

Limit Cycles Caused by Friction

4.1 Introduction

Friction affects control systems in different ways. It may cause steady-state control errors but also unwanted oscillations. In this chapter we will study such oscillations. Stick-slip motion is a classical example, which has been observed and studied for a long time.

In this chapter we only consider systems with a single friction interface. It has an associated relative velocity v, relative position x, friction force F, and external force F_e, as seen in Figure 2.9. The motion at the friction interface has one degree of freedom. The friction model we will use is

$$F = \begin{cases} F_C \operatorname{sgn}(v) & \text{if } v \neq 0 \\ F_e & \text{if } v = 0 \text{ and } |F_e| < F_S \\ F_S \operatorname{sgn}(F_e) & \text{otherwise} \end{cases} \tag{4.1}$$

Viscous friction can be included in the process models and is therefore omitted. The model suffices to analyze most limit cycles qualitatively. The results will also be compared with those obtained with the friction model in Chapter 3.

Section 4.2 presents some examples where friction causes unwanted oscillations. The limit cycles are characterized in Section 4.3 and theory to compute and analyze them are given in Section 4.4. The theory is applied to the examples in Section 4.5. The results are compared with describing function analysis in Section 4.6 and the dependence of the limit cycles on the friction model is investigated in Section 4.7. Finally, Section 4.8 contains a summary of the results.

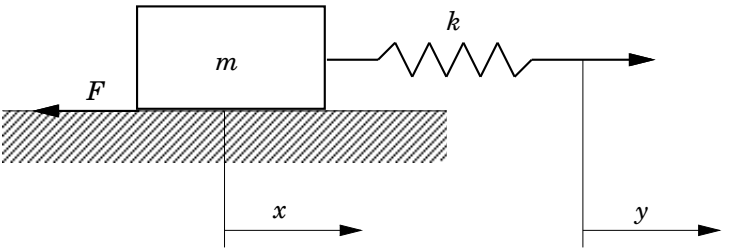

Figure 4.1 A simple set-up for stick-slip motion as described in Example 4.1.

4.2 Examples

In this section we present some simple examples where friction causes oscillations.

EXAMPLE 4.1—STICK-SLIP MOTION
Stick-slip motion is a common problem occuring for low velocity motion. The resulting motion is jerky and switches between periods of sticking and slipping. Stick-slip motion is often highly undesirable in applications such as machine tools. Apart from poor control performance, the motion can also give vibrations and noise. It is, therefore, interesting to understand the nature of stick-slip motion and how to avoid it. Stick-slip motion is caused by the friction force at zero velocity, which is higher than at a small nonzero velocity. When motion starts, the friction force decreases rapidly and the accelerating force is therefore large. A simple set-up, which generates stick-slip motion, is shown in Figure 4.1. The external force is applied by moving the free end of the spring with constant velocity. The equations of motion are given by

$$\begin{aligned} m\frac{d^2x}{dt^2} &= k(y-x) - F \\ \frac{dy}{dt} &= v_{ref} \end{aligned} \tag{4.2}$$

The problem is illustrated in the block diagram in Figure 4.2. It is equivalent to velocity control using a purely integrating controller with a nonzero reference. The reference is the velocity v_{ref} of the free end of the spring. Figure 4.3 shows the result of a simulation. In this particular case $v_{ref} = 0.1$, $m = 1$, and $k = 2$. The friction force is given by (4.1) with $F_S = 1.5$ and $F_C = 1$. Linear viscous friction with $F_v = 0.4$ is added to the linear process model. To begin with, the mass is at rest and the force from the spring increases linearly as y increases. During this phase the friction

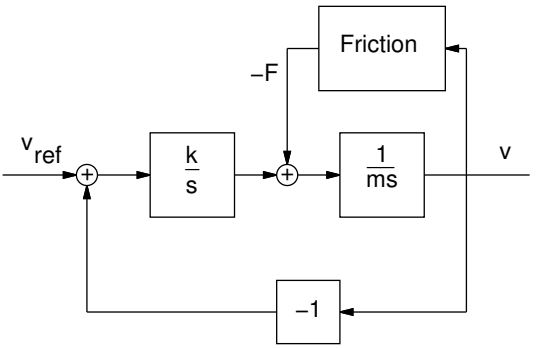

Figure 4.2 Block diagram for the stick-slip motion set-up in Example 4.1.

force counteracts the spring force to keep the mass at rest. When the applied force reaches F_S the mass starts to slide and the friction force drops to the Coulomb level F_C. The mass accelerates but as it moves the spring contracts and the spring force decreases. The mass slows down and finally the motion stops. The phenomenon then repeats itself in another cycle. There would be no limit cycle if $F_S = F_C$. □

Next we give an example of an oscillation, that occurs for position control with a controller having integral action. The controlled position will often

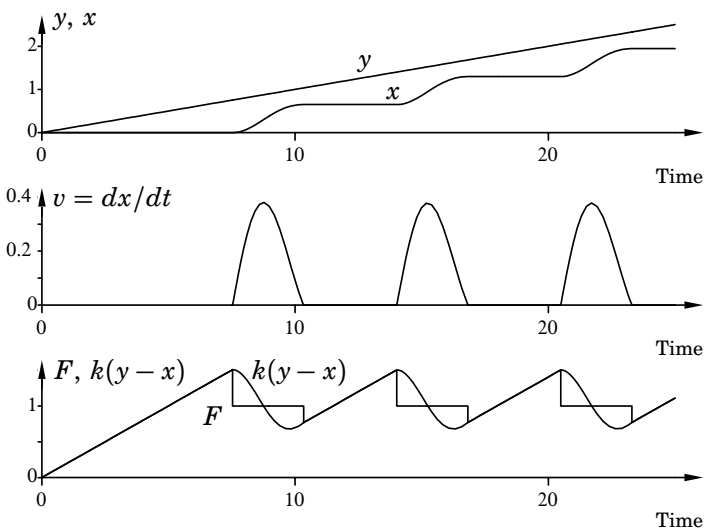

Figure 4.3 Simulation of stick-slip motion in Example 4.1.

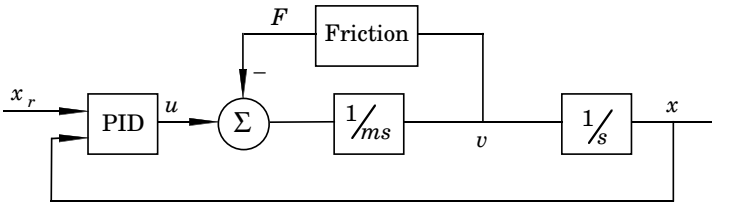

Figure 4.4 Block diagram for PID position control as described in Example 4.2.

"jump" from one side of the constant reference value to the other without ever reaching the desired one. This phenomenon is called hunting, see Newton *et al.* (1957).

EXAMPLE 4.2—HUNTING
Consider PID position control. The equation of motion is given by

$$m\frac{d^2x}{dt^2} = u - F \tag{4.3}$$

where the control force u is given by

$$u(t) = -K_v v(t) - K_p x(t) - K_i \int^t (x(\tau) - x_r(\tau))d\tau \tag{4.4}$$

A block diagram of the system is shown in Figure 4.4. The controller parameters $K_v = 2$, $K_p = 2$, and $K_i = 1$ give good performance when no friction is present. The reference position is chosen as $x_r = 1$ and $m = 1$. If friction is present, the behavior of the control loop deteriorates and limit cycles may occur. This is shown in Figure 4.5. The friction is given by (4.1) with parameters $F_S = 1$ and $F_C = 0.5$. There is no viscous friction. The mass starts to move almost immediately but passes the desired position and gets stuck after slowing down. The integral action in the controller then decreases the control force until it reaches $-F_S$. The mass starts to move towards the desired position and the friction force goes from $-F_S$ to $-F_C$ at the same time. The motion, therefore, passes the desired position once again and gets stuck, this time on "the other side." The period when the mass is stuck is longer if the position error is small because it then takes a longer time for the integral action to overcome the static friction. The behavior shown in the simulation is qualitatively similar to what has been observed experimentally. A common way to overcome hunting is to introduce a dead zone so that no integral action is obtained for small control errors. The oscillation is then avoided at the cost of a small position error. The limit cycle is also extinguished if $F_S = F_C$. □

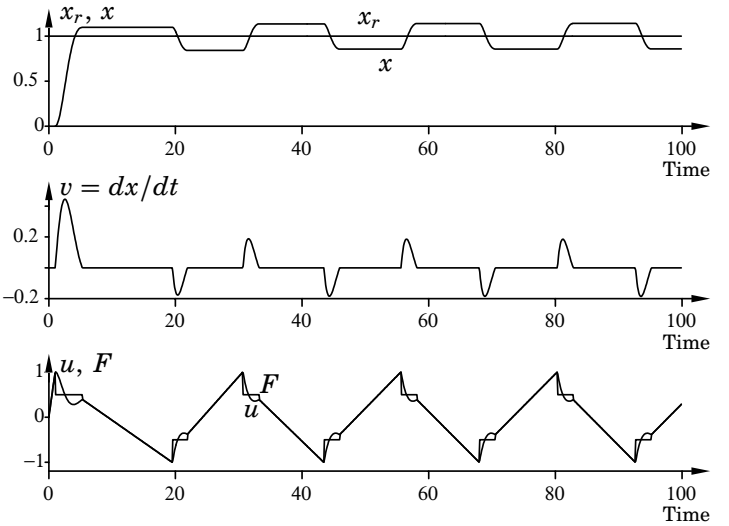

Figure 4.5 Simulation of PID position control as discussed in Example 4.2.

Next we describe two examples where a limit cycle may occur even if $F_S = F_C$.

EXAMPLE 4.3—INVERTED PENDULUM ON A CART

An inverted pendulum on a cart is a popular example of an unstable process. A simple linearized model of the pendulum in Figure 4.6 is given by

$$\begin{aligned} \frac{d^2\theta}{dt^2} &= \theta + u - F = F_e - F \\ \frac{d^2x}{dt^2} &= u - F \end{aligned} \tag{4.5}$$

where θ denotes the angle of the pendulum and x the position of the cart. The control signal u is the control force at the pivot. The friction force F between cart and ground is given by (4.1) with parameters $F_S = 1$ and $F_C = 1$. The static friction is thus equal to the sliding friction. There is no viscous friction. The rotational friction at the pivot is neglected. The model is valid for small deflections from the upright position $\theta = 0$. In this region linear feedback suffices to stabilize the pendulum. The control law

$$u = -L \begin{pmatrix} d\theta/dt & \theta & dx/dt & x \end{pmatrix}^T \tag{4.6}$$

with $L = \begin{pmatrix} 1.05 & 0.25 & -3.15 & -3.48 \end{pmatrix}$ gives the characteristic polynomial $(s^2 + 2\zeta\omega_1 + \omega_1^2)(s^2 + 2\zeta\omega_2 s + \omega_2^2)$ with $\zeta = 0.7$, $\omega_1 = 1$ and $\omega_2 = 0.5$.

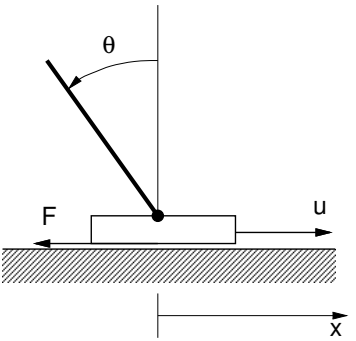

Figure 4.6 The inverted pendulum on a cart in Example 4.3.

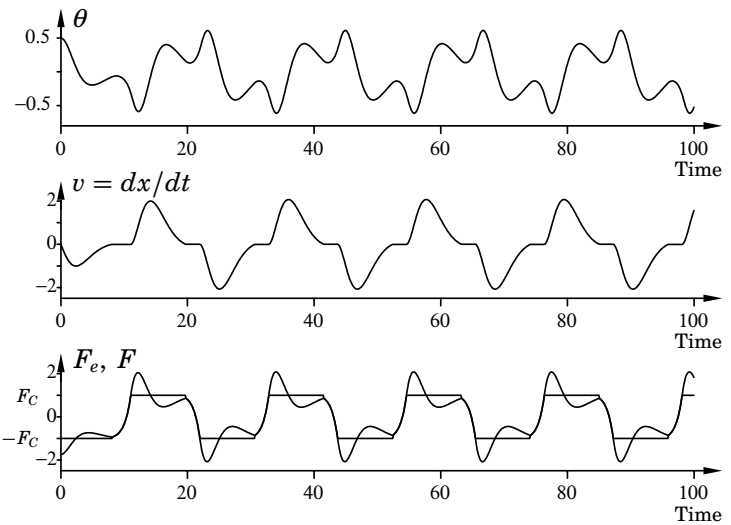

Figure 4.7 Simulation of an inverted pendulum on a cart as described in Example 4.3. The figure shows the pendulum angle, the cart velocity, and the external force and friction force.

Figure 4.7 shows the behavior of the control loop. In this example there is also a periodic solution. A detailed investigation shows that the motion actually stops, but only for a very short time. In this respect the limit cycle differs from the previous examples, where the motion is stopped during the major part of the period. □

EXAMPLE 4.4—FLEXIBLE SERVO

A servo consisting of a motor, a flexible shaft and a load is shown in

Figure 4.8. The angular velocity of the motor is denoted ω_1 and the velocity of the load ω_2. The equations of motion for the system are given by

$$\begin{aligned} J_1\frac{d\omega_1}{dt} &= -k(\varphi_1-\varphi_2)-d_1\omega_1+u-F=F_e-F \\ J_2\frac{d\omega_2}{dt} &= k(\varphi_1-\varphi_2)-d_2\omega_2 \\ \frac{d(\varphi_1-\varphi_2)}{dt} &= \omega_1-\omega_2 \end{aligned} \tag{4.7}$$

where $J_1 = 2.2\cdot 10^{-5}$ and $J_2 = 6.0\cdot 10^{-5}$ are the moments of inertia, $d_1 = 3\cdot 10^{-5}$ and $d_2 = 3\cdot 10^{-5}$ viscous damping coefficients, and $k = 4\cdot 10^{-4}$ the stiffness of the shaft. The friction is given by (4.1) with $F_S = F_C = 5\cdot 10^{-4}$. We assume that there is friction only on the motor side. The objective is to control the velocity on the load side, i.e., ω_2. The only available measurement is the velocity of the motor $y_1 = k_\omega\omega_1$. The system can be controlled with state feedback and integral action using an observer. The control law therefore is

$$u = -L\hat{x}_e \tag{4.8}$$

where

$$\hat{x}_e = \begin{pmatrix} \hat{x} \\ x_i \end{pmatrix} \tag{4.9}$$

The variables $\hat{x}$ and x_i are given by

$$\frac{d\hat{x}}{dt} = A\hat{x}+Bu+K(y_1-C\hat{x}) \tag{4.10}$$

and

$$\frac{dx_i}{dt} = y_r-y_1 \tag{4.11}$$

The vectors L and K are chosen to get the desired closed-loop poles. They are placed in a Butterworth pattern with the observer poles twice as fast as the other poles. The design is specified by the variable ρ, which

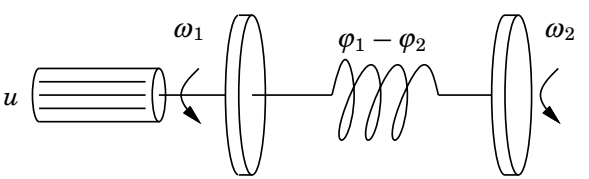

Figure 4.8 A schematic picture of the flexible servo in Example 4.4.

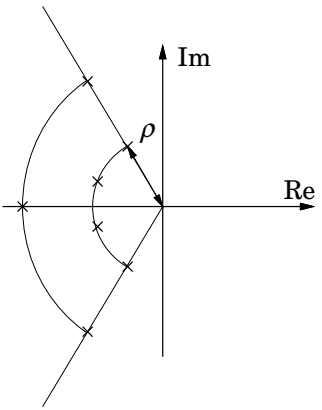

Figure 4.9 The closed-loop pole locations for Example 4.4.

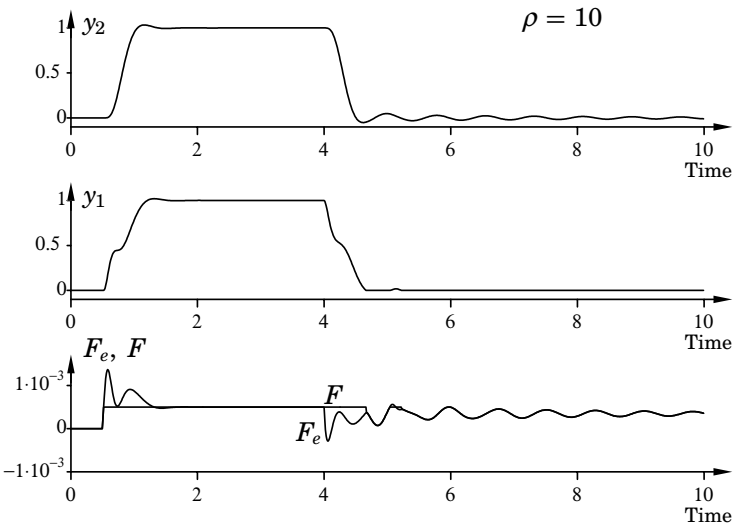

Figure 4.10 Simulation of the flexible servo for $\rho = 10$. No limit cycle occurs for this design.

determines the radius of the Butterworth pattern, see Figure 4.9. We will now see how the behavior of the system changes with the design parameter ρ. The values of ρ have been 10, 11, 12, and 15 and the corresponding simulations are shown in Figures 4.10, 4.11, 4.12, and 4.13. The diagrams show $y_2 = k_\omega \omega_2$, $y_1 = k_\omega \omega_1$, and F_e and F, respectively. The reference velocity is $y_r = 1$ between $t = 0.5$ and $t = 4$ and zero otherwise. The

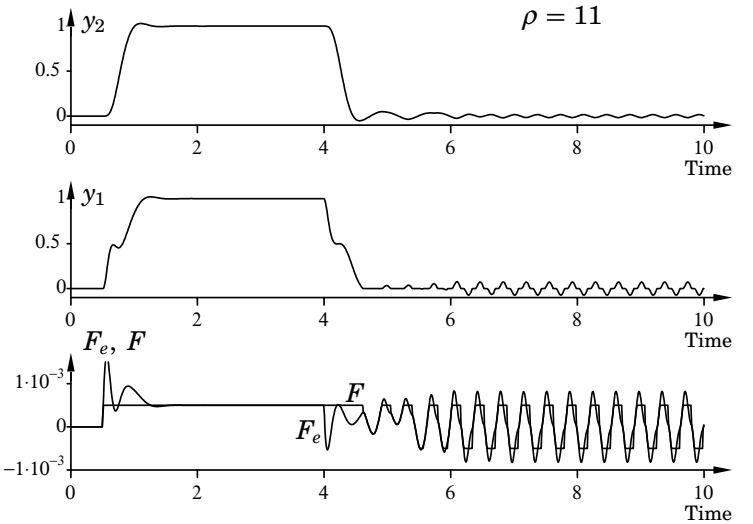

Figure 4.11 Simulation of the flexible servo for $\rho = 11$. A limit cycle with periods of sticking occurs.

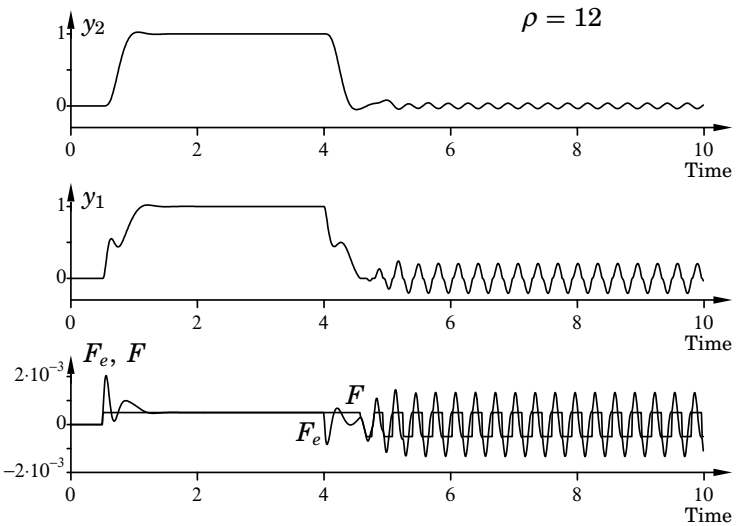

Figure 4.12 Simulation of the flexible servo for $\rho = 12$. The limit cycle is a pure relay oscillation with no sticking, i.e., the friction force switches instantly between the levels $\pm F_C$.

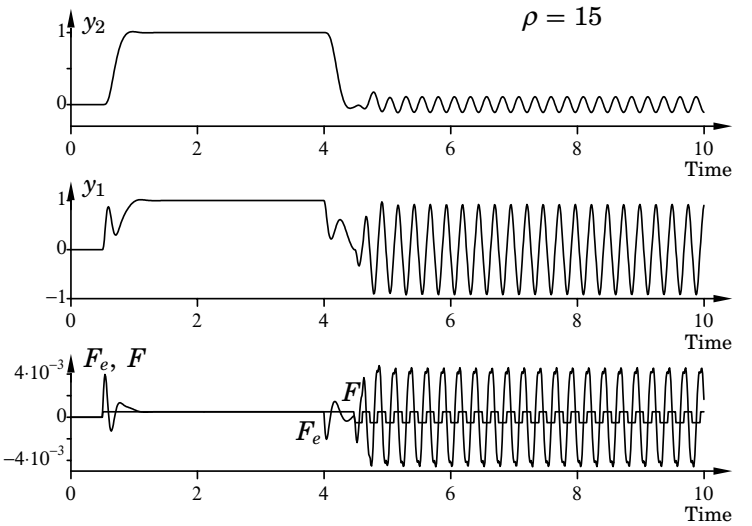

Figure 4.13 Simulation of the flexible servo for $\rho = 15$. The limit cycle is a pure relay oscillation, i.e., the friction force switches instantly between the levels $\pm F_C$. The velocity $y_1 = k_\omega \omega_1$ is almost sinusoidal.

controller works properly in all cases until the reference is brought back to zero at $t = 4$. Various limit cycles are then initiated. Close-ups of y_1, i.e., the measurement of the velocity associated with the friction, for $9 \leq t \leq 10$ are shown in Figure 4.14. The behavior obtained in the different cases can be summarized as follows:

For $\rho = 10$, the motion of the motor stops soon after $t = 4$. The velocity of the load is then a decaying oscillation. There are no limit cycles.

With $\rho = 11$, a limit cycle with quite small amplitude is slowly built up after $t = 4$. The close-up reveals that motion stops completely during parts of the limit cycle period.

If $\rho = 12$, the limit cycle becomes a pure relay oscillation in the sense that the friction force switches instantly between the levels $\pm F_C$. The external force at the times when the velocity becomes zero is sufficiently large to overcome the stiction. The acceleration is, however, quite low immediately after the zero crossings.

When $\rho = 15$, the shape of the velocity $y_1 = k_\omega \omega_1$ is almost sinusoidal. The external force is in this case much larger than the friction at the times when the velocity is zero.

The behavior of the flexible servo is thus very different for the differ-

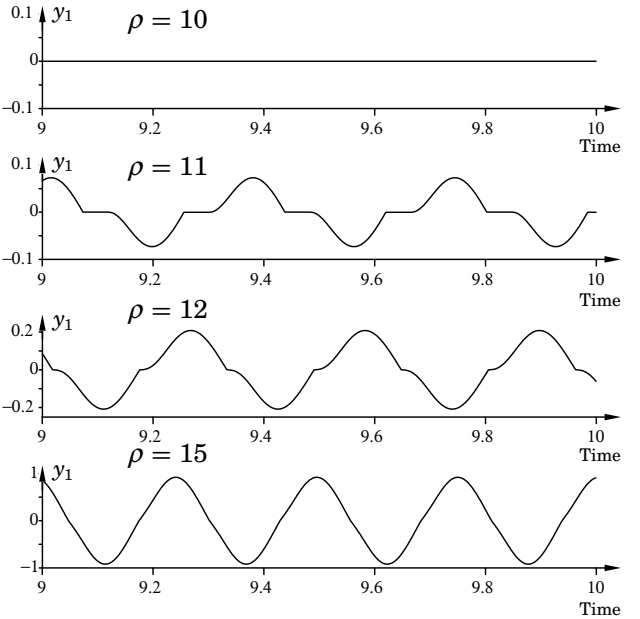

Figure 4.14 Close-ups of the oscillatory behavior of the flexible servo for different values of the design parameter ρ. For $\rho = 10$ there is no limit cycle. If $\rho = 11$ we get a limit cycle that includes periods of sticking. For $\rho = 12$ and 15 the velocity is zero only for single time instants.

ent values of ρ. No sustained oscillation is obtained when $\rho = 10$. For $\rho = 11$ the limit cycle period includes sticking and is, therefore, of the same character as in the previous three examples. For $\rho = 12$ and 15 the oscillations are of relay type, i.e., there is no sticking and in this respect differs from the previous three examples. □

The results of the simulations in the examples depend on the friction model. The presence of limit cycles, which has been indicated by the classical model (4.1), may not agree with the results from simulations using other models like the dynamic model from the previous chapter. Since that model can be seen as a generalization of several other models and also captures many of the experimentally observed features of friction, it is interesting to see how the appearance of the limit cycles changes with that model. This is done in Section 4.7.

4.3 Characteristics of the Limit Cycles

The examples in the previous section showed different limit cycles caused by friction. In this section these limit cycles will be characterized.

We will make a distinction between limit cycles with and without sticking. For limit cycles with sticking the velocity at the friction interface is kept at zero for a period of time by the friction force. For limit cycles without sticking the friction behaves as described by a pure relay $F = F_C \operatorname{sgn}(v)$, since the crossing of zero velocity is instantaneous. The limit cycles in examples 4.1, 4.2, and 4.3 all include periods of sticking. In Example 4.4 sticking occurs for $\rho = 11$ but not for $\rho = 12$ and 15.

The variable that determines if sticking occurs is the size of the external force (all forces excluding friction) acting on the friction interface at the time when the velocity becomes zero. If the magnitude of the external force is larger than F_S, then the limit cycle will not have sticking. When there is sticking the velocity will be zero until some mechanism has made the external force become larger than the static friction.

The difference between the two types of limit cycles can also be illustrated using a switching plane, in the phase space, given by $v = 0$. For pure relay oscillations the solution passes through the switching plane momentarily, whereas for limit cycles with sticking the solution lies in the switching plane during a period of time. The friction force during this period is a function of the external force as seen in (4.1). In general, it is therefore necessary to specify the behavior for $v = 0$ in the friction model. As expected, different friction models will thus give drastically different behavior in the case of sticking. For example, it has been observed that a simple relay model may cause chattering.

Intuitively friction counteracts motion. Different mechanisms are, therefore, necessary to sustain the oscillation. The external force must either directly, as velocity becomes zero, or after a period of sticking be larger than the stiction to initiate a new period of the oscillation. The examples in the previous section showed different ways in which this may occur. For Example 4.1 the position y is constantly increasing. This implies that if sticking occurs the spring extension (and thus the external force) increases linearly until it overcomes the static friction. In Example 4.2 the integral action of the controller increases the control signal until motion is initiated. The inverted pendulum in Example 4.3 is in itself unstable and, as it falls, the control signal increases until the cart moves. Finally, in Example 4.4 the controller is unstable for $\rho = 11$, 12, and 15 but not for $\rho = 10$, in which case no limit cycle was observed.

Three different instability mechanisms has thus been pointed out. These are:

- unstable position reference
- unstable controller
- unstable process.

It is also possible to distinguish between limit cycles that requires $F_S > F_C$ and those that exist also for $F_S = F_C$. Examples 4.1 and 4.2 both require that $F_S = F_C$.

4.4 Theory

In this section we develop theory that permits exact calculation of the shape and the stability of the limit cycles with sticking in Section 4.2. The problem is similar to analysis of limit cycles in systems with relay feedback. Tools for that problem were developed in Åström (1995). These are now generalized to deal with the problem of sticking. The new tools will then be applied to the examples in Section 4.2. The tools developed in Åström (1995) will be used for the examples with limit cycles of relay type.

We consider a general linear system with a single friction interface. The motion at the friction interface is given by

$$\frac{d^2x}{dt^2} = u - F \tag{4.12}$$

where u is the sum of all external forces acting at the interface. The system can be written on the following form

$$\begin{aligned} \frac{d\xi}{dt} &= A\xi + B(u - F) + B_r y_r \\ v &= C_v \xi \\ u &= -L\xi \end{aligned} \tag{4.13}$$

which has the special structure

$$\begin{aligned} \frac{d\xi}{dt} = \frac{d}{dt}\begin{pmatrix} v \\ x \\ \eta \end{pmatrix} &= \begin{pmatrix} 0 & 0 & 0\cdots 0 \\ 1 & 0 & 0\cdots 0 \\ A_{\eta v} & A_{\eta x} & A_{\eta\eta} \end{pmatrix}\begin{pmatrix} v \\ x \\ \eta \end{pmatrix} \\ &\quad + \begin{pmatrix} 1 \\ 0 \\ B_\eta \end{pmatrix}(u - F) + \begin{pmatrix} 0 \\ 0 \\ B_{r_\eta} \end{pmatrix} y_r \\ v = C_v\xi &= \begin{pmatrix} 1 & 0 & 0\cdots 0 \end{pmatrix}\xi \\ u &= -L\xi \end{aligned} \tag{4.14}$$

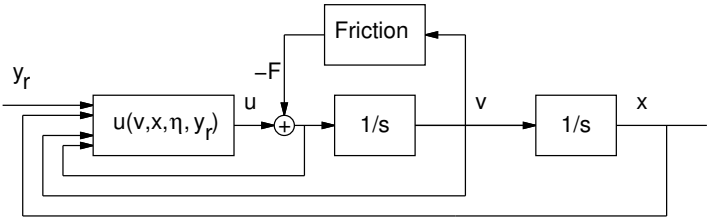

Figure 4.15 A block diagram showing the structure of (4.14).

The state vector ξ may include both process states and controller states. This means that u contains both control force and forces from the process itself. The reference y_r is assumed to be constant and the friction model is given by (4.1). A block diagram of the system is shown in Figure 4.15.

For limit cycles with sticking the velocity at the friction interface behaves as either of the two curves in Figure 4.16. In Example 4.1 the motion is unidirectional and the velocity is as shown in the lower part of Figure 4.16. This type of limit cycle is called an even oscillation. In examples 4.2, 4.3, and 4.4 there were oscillations around an equilibrium position and the velocity, therefore, behaved as in the upper curve of Figure 4.16. This type of limit cycle is called an odd oscillation. The period in the case of an odd oscillation includes the four phases slip-stick-slip-stick, whereas for the even it includes only two. The duration of a slipping phase is denoted by h_1 and the length of the sticking period by h_2 in both cases.

Odd Limit Cycles

We start by investigating odd limit cycles. Figure 4.17 shows how the velocity and the signal u may behave for an odd limit cycle. The velocity is zero at the beginning of the periodic solution. The signal u overcomes the friction force at $t = 0$ and motion begins. It continues until time $t = h_1$ when the velocity becomes zero. At this point motion stops and the velocity then remains zero until the signal u exceeds the static friction force again. This time motion starts in the opposite direction. A complete period consists of four phases, two periods of sliding and two of sticking. By symmetry it is sufficient to study half a period. Between $t = 0$ and $t = h_1$ the velocity is positive and the motion is given by

$$\begin{aligned} \frac{d\xi}{dt} &= (A - BL)\xi - BF_C + B_r y_r \\ v &= C_v \xi \end{aligned} \tag{4.15}$$

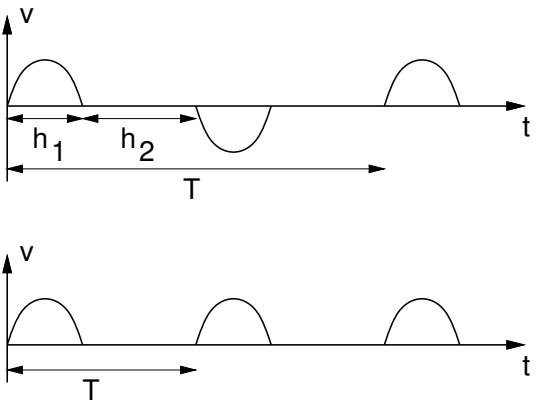

Figure 4.16 The characteristics of the velocity for friction limit cycles with sticking. The upper curve shows an odd (bidirectional) limit cycle and the lower curve an even (unidirectional) limit cycle.

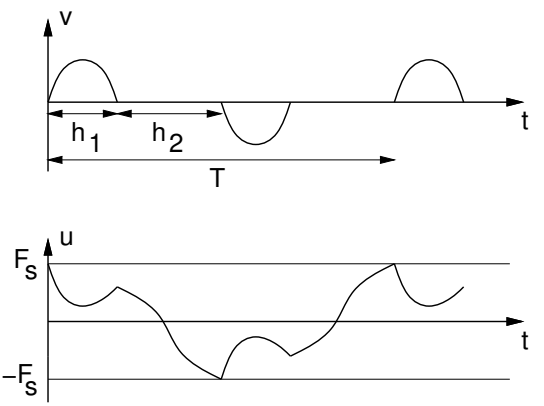

Figure 4.17 Velocity and control signal for an odd limit cycle as shown, for example, in Figure 4.5.

The following boundary conditions hold

$$C_v\xi(0) = C_v\xi(h_1) = 0$$

Furthermore it must be required that $C_v\xi(t) > 0$ for $0 < t < h_1$. If this condition is not fulfilled, the velocity becomes zero before $t = h_1$.

In the time interval $h_1 \leq t \leq h_1 + h_2$ the motion is constrained by the static friction force, which cancels the signal u such that the velocity is

retained at zero and the position at some constant value. The equation governing this motion is

$$\frac{d\xi}{dt} = A\xi + B_r y_r \tag{4.16}$$

with the boundary condition

$$-L\xi(h_1 + h_2) = -F_S$$

The condition $|L\xi(t)| < F_S$ must also hold for $h_1 \leq t < h_1 + h_2$; otherwise motion would be initiated before $t = h_1 + h_2$. For an odd limit cycle we also require that $\xi(h_1 + h_2) = -\xi(0)$ because of the symmetry. Necessary conditions for a limit cycle can be given. The next theorem states conditions in terms of h_1 and h_2 that are necessary for the existence of an odd limit cycle. Candidate values of h_1 and h_2 can be found by solving a nonlinear equation system. Two further constraints on the system solution $\xi(t)$ must also hold. A procedure for applying the theory is given later. We need to define the following variables

$$A_c = A - BL \qquad \Phi_c = e^{A_c h_1} \qquad \Phi = e^{Ah_2}$$

$$\Gamma_c = \int_0^{h_1} e^{A_c s} ds B \qquad \Gamma_{cr} = \int_0^{h_1} e^{A_c s} ds B_r \qquad \Gamma_r = \int_0^{h_2} e^{As} ds B_r$$

Note that Φ_c, Γ_c, Γ_{cr} are functions of h_1 and that Φ and Γ_r are functions of h_2.

THEOREM 4.1
Consider the system (4.14) and friction force (4.1). Assume that there exists an odd periodic solution with period $T = 2(h_1 + h_2)$ and that the matrix $I + \Phi\Phi_c$ is nonsingular. Assume further that the motion is unconstrained in the interval $0 < t < h_1$, but in the interval $h_1 \leq t \leq h_1 + h_2$ the friction force keeps the velocity at zero as in Figure 4.17. The following nonlinear equations then hold

$$f_1(h_1, h_2) = C_v(I + \Phi_c\Phi)^{-1}(-\Phi_c\Gamma_r y_r - \Gamma_c F_C + \Gamma_{cr} y_r) = 0 \tag{4.17}$$

$$f_2(h_1, h_2) = -L(I + \Phi\Phi_c)^{-1}(-\Phi\Gamma_c F_C + \Phi\Gamma_{cr} y_r + \Gamma_r y_r) = -F_S \tag{4.18}$$

The solution $\xi(t)$ must also satisfy

$$v(t) = C_v\xi(t) > 0 \quad \text{for} \quad 0 < t < h_1 \tag{4.19}$$

$$|u(t)| = |L\xi(t)| < F_S \quad \text{for} \quad h_1 \leq t < h_1 + h_2 \tag{4.20}$$

The state vector $\xi(t)$ is for $0 \leq t \leq h_1$ given by

$$\xi(t) = -e^{A_c t}a - \int_0^t e^{A_c(t-s)}dsBF_C + \int_0^t e^{A_c(t-s)}dsB_r y_r$$

and for $h_1 \leq t \leq h_2$ by

$$\xi(t) = e^{A_c t}b + \int_0^t e^{A(t-s)}dsB_r y_r$$

where

$$a = (I + \Phi\Phi_c)^{-1}(-\Phi\Gamma_c F_C + \Phi\Gamma_{cr}y_r + \Gamma_r y_r)$$
$$b = (I + \Phi_c\Phi)^{-1}(-\Phi_c\Gamma_r y_r - \Gamma_c F_C + \Gamma_{cr}y_r)$$

The periodic solution is obtained with the initial condition

$$\xi(0) = -a = -(I + \Phi\Phi_c)^{-1}(-\Phi\Gamma_c F_C + \Phi\Gamma_{cr}y_r + \Gamma_r y_r) \tag{4.21}$$

and further the state at time h_1 is given by

$$\xi(h_1) = b = (I + \Phi_c\Phi)^{-1}(-\Phi_c\Gamma_r y_r - \Gamma_c F_C + \Gamma_{cr}y_r) \tag{4.22}$$

Proof. Integrating the system equation (4.15) during the slipping phase with the initial condition $\xi(0) = -a$ gives

$$\xi(h_1) = -\Phi_c a - \Gamma_c F_C + \Gamma_{cr}y_r \tag{4.23}$$

At time h_1 the velocity should be zero, i.e., $v(h_1) = C_v\xi(h_1) = 0$. The constrained motion with zero velocity then continues until time $t = h_1 + h_2$ when the control signal overcomes the friction force. Integrating equation (4.16) we get

$$\xi(h_1 + h_2) = \Phi\xi(h_1) + \Gamma_r y_r = -\xi(0) = a \tag{4.24}$$

since the periodic solution is odd. Solving the equations yields the initial condition (4.21). The conditions $v(h_1) = 0$ and $u(h_1 + h_2) = -F_S$ are equivalent to (4.17) and (4.18). It is further required that $v(t) > 0$ for $0 < t < h_1$, and $|u(t)| < F_S$ for $h_1 \leq t < h_1 + h_2$, which gives (4.19) and (4.20). □

Remark 1. Conditions (4.17) and (4.19) imply that the derivative of the velocity at $t = h_1^-$ is negative, i.e,

$$\frac{dv}{dt}(h_1^-) = C_v\left(A_c b - BF_C + B_r y_r\right) = C_v z < 0$$

and conditions (4.18) and (4.20) imply that the derivative of the control signal at $t = h_1 + h_2^-$ is negative, i.e,

$$\frac{du}{dt}(h_1 + h_2^-) = -L(Aa + B_r y_r) = -Lw < 0$$

This is also clear from Figure 4.17. If these conditions are not satisfied, then (4.19) and (4.20) cannot be fulfilled.

Remark 2. Note that if $I+\Phi\Phi_c$ is nonsingular then $I+\Phi_c\Phi$ is also nonsingular. The assumption on regularity is necessary when solving equations (4.23) and (4.24). There may be more than one solution if the condition is not satisfied. The desired solution is such that the velocity is zero at both $t = h_1$ and $t = h_1 + h_2$, and the position at $t = h_1 + h_2$ equals that at $t = h_1$.

There may be problems when solving (4.23) and (4.24) as indicated in Remark 2. Although Example 4.1 shows an even limit cycle, we can explain the problem using that example. The equilibrium solution $dx/dt = v_{ref}$ and $y-x = F_C/k$ satisfies equations corresponding to (4.23) and (4.24) for all values of h_1 and h_2. For the particular values of h_1 and h_2, which agree with the limit cycle, there are infinitely many solutions as the matrix $I + \Phi_c\Phi$ then becomes singular. For the equilibrium solution both $C_v\xi(t)$ and $-L\xi(t)$ are constant but $v = C_v\xi(t) \neq 0$. It is thus not simple to find the desired solution. In order to overcome the problem it is necessary to include the constraint $v(0) = v(h_1) = 0$ in the solution procedure. For problems where the position is part of the state we must in the same manner include $x(h_1) = -x(0)$. This is described next.

Reduction of Velocity and Position Equations

Inserting $v(0) = v(h_1) = 0$ and $x(h_1) = -x(0)$ in the equations (4.23) and (4.24) and using the knowledge of the structure of A, B, and B_r, as seen

in (4.14), we get

$$\begin{pmatrix} 0 \\ -x(0) \\ \eta(h_1) \end{pmatrix} = \begin{pmatrix} \Phi_{cvv} & \Phi_{cvx} & \Phi_{cv\eta} \\ \Phi_{cxv} & \Phi_{cxx} & \Phi_{cx\eta} \\ \Phi_{c\eta v} & \Phi_{c\eta x} & \Phi_{c\eta\eta} \end{pmatrix} \begin{pmatrix} 0 \\ x(0) \\ \eta(0) \end{pmatrix} - \begin{pmatrix} \Gamma_{cv} \\ \Gamma_{cx} \\ \Gamma_{c\eta} \end{pmatrix} F_C + \begin{pmatrix} \Gamma_{crv} \\ \Gamma_{crx} \\ \Gamma_{cr\eta} \end{pmatrix} y_r \tag{4.25}$$

$$\begin{pmatrix} 0 \\ -x(0) \\ -\eta(0) \end{pmatrix} = \begin{pmatrix} 1 & 0 & 0 \\ h_2 & 1 & 0 \\ \Phi_{\eta v} & \Phi_{\eta x} & \Phi_{\eta\eta} \end{pmatrix} \begin{pmatrix} 0 \\ -x(0) \\ \eta(h_1) \end{pmatrix} + \begin{pmatrix} 0 \\ 0 \\ \Gamma_{r\eta} \end{pmatrix} y_r \tag{4.26}$$

The matrices have been partitioned according to the system structure. There are thus two sets of equations with the single constraint

$$-L \begin{pmatrix} 0 \\ -x(0) \\ -\eta(0) \end{pmatrix} = -F_S$$

which corresponds to (4.18) in Theorem 4.1. The velocity constraint $v(h_1) = C_v\xi(h_1) = 0$, i.e., (4.17), has been included in the equations. The first two equations of (4.26) are trivially fulfilled and the first two equations of (4.25) can be seen as new constraints on the velocity and the position. We thus obtain two matrix equations for $\eta(0)$ and $\eta(h_1)$, namely the last equation of both (4.25) and (4.26). Notice that if $\xi \in R^n$ then $\eta \in R^{n-2}$. The unknowns, $\eta(0)$ and $\eta(h_1)$ are functions of the three variables h_1, h_2, and $x(0)$, i.e.,

$$\begin{aligned} \eta(h_1) &= \Phi_{c\eta x}x(0) + \Phi_{c\eta\eta}\eta(0) - \Gamma_{c\eta}F_C + \Gamma_{cr\eta}y_r \\ -\eta(0) &= -\Phi_{\eta x}x(0) + \Phi_{\eta\eta}\eta(h_1) + \Gamma_{r\eta}y_r \end{aligned} \tag{4.27}$$

The new constraints on velocity, position and control signal are given by

$$\begin{aligned} &\Phi_{cvx}x(0) + \Phi_{cv\eta}\eta(0) - \Gamma_{cv}F_C + \Gamma_{crv}y_r = 0 \\ &\Phi_{cxx}x(0) + \Phi_{cx\eta}\eta(0) - \Gamma_{cx}F_C + \Gamma_{crx}y_r = -x(0) \\ &-L \begin{pmatrix} 0 \\ -x(0) \\ -\eta(0) \end{pmatrix} = -F_S \end{aligned} \tag{4.28}$$

For the reduced problem we have the following result, where e is used to denote $-x(0)$.

THEOREM 4.2
Assume an odd periodic solution exists with period $T = 2(h_1 + h_2)$ and that $I + \Phi_{\eta\eta}\Phi_{c\eta\eta}$ is nonsingular. The following equations then hold:

$$f_1(h_1, h_2, e) = -\Phi_{cvx}e - \Phi_{cv\eta}\alpha - \Gamma_{cv}F_C + \Gamma_{crv}y_r = 0 \tag{4.29}$$

$$f_2(h_1, h_2, e) = -\Phi_{cxx}e - \Phi_{cx\eta}\alpha - \Gamma_{cx}F_C + \Gamma_{crx}y_r - e = 0 \tag{4.30}$$

$$f_3(h_1, h_2, e) = -L\begin{pmatrix} 0 \\ e \\ \alpha \end{pmatrix} = -F_S \tag{4.31}$$

where

$$\alpha = (I + \Phi_{\eta\eta}\Phi_{c\eta\eta})^{-1}\left((\Phi_{\eta x} - \Phi_{\eta\eta}\Phi_{c\eta x})e - \Phi_{\eta\eta}\Gamma_{c\eta}F_C + \Phi_{\eta\eta}\Gamma_{cr\eta}y_r + \Gamma_{r\eta}y_r\right) \tag{4.32}$$

The initial condition is given by

$$\xi(0) = -a = \begin{pmatrix} 0 \\ x(0) \\ \eta(0) \end{pmatrix} = \begin{pmatrix} 0 \\ -e \\ -\alpha \end{pmatrix} \tag{4.33}$$

and the state at $t = h_1$ by

$$\xi(h_1) = b = \begin{pmatrix} 0 \\ -x(0) \\ \eta(h_1) \end{pmatrix} = \begin{pmatrix} 0 \\ e \\ \beta \end{pmatrix} \tag{4.34}$$

where

$$\beta = (I + \Phi_{c\eta\eta}\Phi_{\eta\eta})^{-1}\left((\Phi_{c\eta x} - \Phi_{c\eta\eta}\Phi_{\eta x})e - \Gamma_{c\eta}F_C - \Phi_{c\eta\eta}\Gamma_{r\eta}y_r + \Gamma_{cr\eta}y_r\right) \tag{4.35}$$

Furthermore, it is necessary that

$$v(t) = C_v\xi(t) > 0 \quad \text{for} \quad 0 < t < h_1$$

and
$$|u(t)| = |L\xi(t)| \le F_S \quad \text{for} \quad h_1 \le t < h_1 + h_2$$

where $\xi(t)$ is given in Theorem 4.1.

Proof. Equations (4.29), (4.30) and (4.31) follow directly from (4.28). Equations (4.32) and (4.35) can be obtained by solving (4.27). □

Remark 1. If the position x is not part of the state vector then the following two conditions suffice

$$f_1(h_1, h_2) = -\Phi_{cv\eta}\alpha - \Gamma_{cv}F_C + \Gamma_{crv}y_r = 0 \tag{4.36}$$

$$f_2(h_1, h_2) = -L \begin{pmatrix} 0 \\ \alpha \end{pmatrix} = -F_S \tag{4.37}$$

with α given by (4.32) with $e = 0$.

A procedure for application of the theorem is given later.

Numerical Solutions

It is necessary to have numerical procedures to find the values of h_1, h_2 and e that satisfy (4.29), (4.30), and (4.31). The partial derivatives of these functions with respect to the three variables are useful in this respect. These are given in the following lemma.

LEMMA 4.1
The derivatives of (4.29), (4.30), and (4.31) are given by

$$\frac{\partial f_1}{\partial h_1} = -P^T A_c \Phi_c (Qe + R\alpha) - \Phi_{cv\eta}\frac{\partial \alpha}{\partial h_1} + P^T \Phi_c (B_r y_r - BF_C)$$

$$\frac{\partial f_1}{\partial h_2} = -\Phi_{cv\eta}\frac{\partial \alpha}{\partial h_2}$$

$$\frac{\partial f_1}{\partial e} = -\Phi_{cvx} - \Phi_{cv\eta}\frac{\partial \alpha}{\partial e}$$

$$\frac{\partial f_2}{\partial h_1} = -Q^T A_c \Phi_c (Qe + R\alpha) - \Phi_{cx\eta}\frac{\partial \alpha}{\partial h_1} + Q^T \Phi_c (B_r y_r - BF_C)$$

$$\frac{\partial f_2}{\partial h_2} = -\Phi_{cx\eta}\frac{\partial \alpha}{\partial h_2}$$

$$\frac{\partial f_2}{\partial e} = -\Phi_{cxx} - \Phi_{cx\eta}\frac{\partial \alpha}{\partial e} - 1$$

$$\frac{\partial f_3}{\partial h_1} = -L \begin{pmatrix} 0 & 0 & \partial\alpha/\partial h_1 \end{pmatrix}^T$$

$$\frac{\partial f_3}{\partial h_2} = -L \begin{pmatrix} 0 & 0 & \partial\alpha/\partial h_2 \end{pmatrix}^T$$

$$\frac{\partial f_3}{\partial e} = -L \begin{pmatrix} 0 & 1 & \partial\alpha/\partial e \end{pmatrix}^T$$

where

$$\begin{aligned}\frac{\partial \alpha}{\partial h_1} = &-(I + \Phi_{\eta\eta}\Phi_{c\eta\eta})^{-1}\Phi_{\eta\eta}R^T A_c \Phi_c R(I + \Phi_{\eta\eta}\Phi_{c\eta\eta})^{-1}\cdot \\ &\left(\Phi_{\eta x}e - \Phi_{\eta\eta}(\Phi_{c\eta x}e + \Gamma_{c\eta}F_C - \Gamma_{cr\eta}y_r) + \Gamma_{r\eta}y_r\right) \\ &- (I + \Phi_{\eta\eta}\Phi_{c\eta\eta})^{-1}\Phi_{\eta\eta}R^T\left(A_c\Phi_c Q e + \Phi_c B F_C - \Phi_c B_r y_r\right)\end{aligned}$$

$$\begin{aligned}\frac{\partial \alpha}{\partial h_2} = &-(I + \Phi_{\eta\eta}\Phi_{c\eta\eta})^{-1}R^T A\Phi R\Phi_{c\eta\eta}(I + \Phi_{\eta\eta}\Phi_{c\eta\eta})^{-1}\cdot \\ &(\Phi_{\eta x}e - \Phi_{\eta\eta}(\Phi_{c\eta x}e + \Gamma_{c\eta}F_C - \Gamma_{cr\eta}y_r) + \Gamma_{r\eta}y_r) \\ &+ (I + \Phi_{\eta\eta}\Phi_{c\eta\eta})^{-1}\Big(R^T A\Phi\big((Q - R\Phi_{c\eta x})e \\ &+ R(-\Gamma_{c\eta}F_C + \Gamma_{cr\eta}y_r)\big) + R^T\Phi B_r y_r\Big)\end{aligned}$$

$$\frac{\partial \alpha}{\partial e} = (I + \Phi_{\eta\eta}\Phi_{c\eta\eta})^{-1}(\Phi_{\eta x} - \Phi_{\eta\eta}\Phi_{c\eta x})$$

The matrices P, Q, and R are defined as

$$\begin{aligned}P^T &= \begin{pmatrix} 1 & 0 & \cdots & 0 \end{pmatrix} \\ Q^T &= \begin{pmatrix} 0 & 1 & 0 & \cdots & 0 \end{pmatrix} \\ R^T &= \begin{pmatrix} 0_{(n-2)\times 2} & I_{(n-2)\times(n-2)} \end{pmatrix}\end{aligned}$$

Proof. The derivatives are obtained using

$$\frac{d}{dh}\int_0^h e^{As}ds B = e^{Ah}B = \Phi B$$

and

$$\frac{d}{dh}(M^{-1}) = -M^{-1}\frac{dM}{dh}M^{-1}$$

□

For numerical solutions it is advantageous to have a good initial estimate of the solution. For this reason it is desirable to show the conditions graphically. For pure relay oscillation it is necessary to find the solution to a scalar function $f(h) = 0$. It can simply be plotted for a number of values of h to estimate solutions.

For friction-generated limit cycles we have, in the reduced case, three functions of three variables, namely (4.29), (4.30), and (4.31). These cannot be illustrated easily together. If, however, we plot the zero level curves

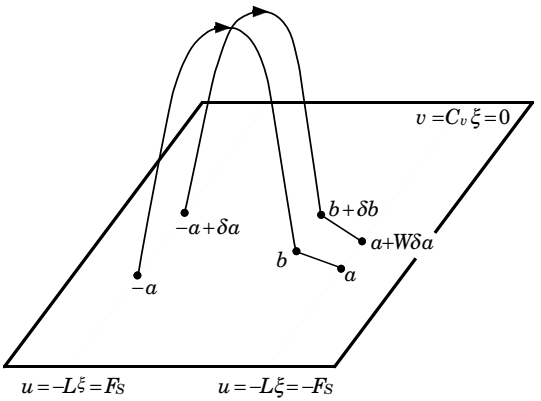

Figure 4.18 The Poincaré map describes how the solution changes between the time instants when it leaves a hyperplane given by $v = C_v\xi = 0$. The two lines are determined by $u = -L\xi = F_S$ and $u = -L\xi = -F_S$. The figure shows the solution when the initial state of the limit cycle is perturbed.

for (4.17) and (4.18) we can get an indication of the values of h_1 and h_2 except in the singular cases. For the case when the position associated with the friction interface is not part of the state vector the conditions (4.37) and (4.36) sufficed. It is then possible to determine approximate values of h_1 and h_2 by plotting the zero level curves of $f_1(h_1, h_2)$ and $f_2(h_1, h_2)$. It is, of course, also possible to find initial estimates by simulating the limit cycle.

Stability of the Limit Cycle

Local stability of the limit cycle can be determined by calculating the Jacobian of a Poincaré map. This map describes how the solution changes between the time instants when it leaves the hyperplane given by $v = C_v\xi = 0$. This occurs when $-L\xi = F_S$ or $-L\xi = -F_S$. The map is shown in Figure 4.18. The symmetry implies that it suffices to study one half of the limit cycle. The Jacobian W of this map thus covers only half a period. For a full period the Jacobian is given by W^2. The following theorem gives the expression for W.

THEOREM 4.3
Assume that an odd periodic solution as described in Theorem 4.1 exists. The Jacobian of the Poincaré map, shown in Figure 4.18, is then given by

$$W = \left(I - \frac{wL}{Lw}\right)\Phi\left(I - \frac{zC_v}{C_v z}\right)\Phi_c \tag{4.38}$$

where $z = A_c b - BF_C + B_r y_r$ and $w = Aa + B_r y_r$. The limit cycle is locally stable if and only if the matrix W has all its eigenvalues inside the unit circle.

Proof. Consider the trajectory resulting from the perturbed initial condition $x(0) = -a + \delta a$, see Figure 4.18. The perturbation is chosen such that it satisfies the conditions

$$C_v(-a + \delta a) = 0$$

and

$$-L(-a + \delta a) = F_S$$

Therefore, it lies on the line $-L\xi = F_S$ in the hyperplane $C_v\xi = 0$. Assume that the corresponding perturbation of h_1 is δh_1 so that

$$C_v\xi(h_1 + \delta h_1) = 0$$

Further,

$$\begin{aligned}\xi(h_1 + \delta h_1) &= e^{A_c(h_1+\delta h_1)}(-a + \delta a) \\ &\quad - \int_0^{h_1+\delta h_1} e^{A_c(h_1+\delta h_1-s)} ds B F_C + \int_0^{h_1+\delta h_1} e^{A_c(h_1+\delta h_1-s)} ds B_r y_r\end{aligned}$$

Making a series expansion in δa and δh_1, we get

$$\begin{aligned}\xi(h_1 + \delta h_1) &= \Phi_c(I + A_c\delta h_1)(-a + \delta a) - (I + A_c\delta h_1)\Gamma_c F_c + \\ &\quad (I + A_c\delta h_1)\Gamma_{cr} y_r - BF_c\delta h_1 + B_r y_r \delta h_1 + O(\delta^2) \\ &= -\Phi_c a - \Gamma_c F_c + \Gamma_{cr} y_r + \Phi_c \delta a + A_c(-\Phi_c a - \Gamma_c F_c \\ &\quad + \Gamma_{cr} y_r)\delta h_1 - BF_c\delta h_1 + B_r y_r \delta h_1 + O(\delta^2) \\ &= b + \Phi_c\delta a + (A_c b - BF_c + B_r y_r)\delta h_1 + O(\delta^2) \qquad (4.39)\end{aligned}$$

Since $C_v b = C_v\xi(h_1 + \delta h_1) = 0$, we get

$$C_v\Phi_c\delta a = -C_v z\delta h_1 + O(\delta^2)$$

It follows from Remark 1 of Theorem 4.1 that $C_v z < 0$, hence

$$\delta h_1 = -\frac{C_v\Phi_c}{C_v z}\delta a + O(\delta^2)$$

Inserting this in (4.39) gives

$$\xi(h_1 + \delta h_1) = b + \left(I - \frac{zC_v}{C_v z}\right)\Phi_c\delta a + O(\delta^2)$$

The perturbation at time $t = h_1 + \delta h_1$ is thus given by

$$\delta b = \left(I - \frac{zC_v}{C_v z} \right) \Phi_c \delta a + O(\delta^2)$$

In the same way we can study how the perturbation δb of b affects the solution at the end of the half period, i.e., at time $h_1 + \delta h_1 + h_2 + \delta h_2$. We get

$$\xi(h_1 + \delta h_1 + h_2 + \delta h_2) = e^{A(h_2+\delta h_2)}(b + \delta b) + \int_0^{h_2+\delta h_2} e^{A(h_2+\delta h_2-s)} ds B_r y_r$$

A series expansion gives

$$\xi(h_1 + \delta h_1 + h_2 + \delta h_2) = a + \Phi \delta b + (Aa + B_r y_r)\delta h_2 + O(\delta^2)$$

Further, it holds that $-La = -L\xi(h_1 + \delta h_1 + h_2 + \delta h_2) = -F_S$ and from Remark 1 of Theorem 4.1 we know that $-Lw < 0$, which gives

$$\delta h_2 = -\frac{L\Phi}{Lw} \delta b + O(\delta^2)$$

Finally,

$$x(h_1 + \delta h_1 + h_2 + \delta h_2) = a + \left(I - \frac{wL}{Lw} \right) \Phi \delta b + O(\delta^2)$$

The Jacobian of the Poincaré map in Figure 4.18 is hence given by (4.38) which proves the theorem □

Remark. The matrix W has two eigenvalues at the origin. One comes from $(I - zC_v/C_v z)\,\Phi_c$ with right eigenvector $\Phi_c^{-1} z$. This removes any perturbation in the velocity at time $h_1 + \delta h_1$ caused by δa. The second zero eigenvalue originates from $(I - wL/Lw)\,\Phi$ with left eigenvector L. It annihilates any remaining perturbation in $\eta(h_1)$, i.e., in the subsystem that is free to move during sticking.

Analysis of a Given System

Tools for analyzing a given system have now been given. The procedure to determine if a system may have an odd stable periodic solution due to friction of the type (4.1) is simply:

Step1: Find h_1, h_2 and e such that $f_1(h_1, h_2, e) = 0$, $f_2(h_1, h_2, e) = 0$ and $f_3(h_1, h_2, e) = -F_S$.

Step2: Compute a, b, z, w, and W and check that $C_v z < 0$, $-Lw < 0$ and $|\lambda(W)| < 1$.

Step 3: Check the conditions $C_v x(t) > 0$ for $0 < t < h_1$ and $|Lx(t)| < F_S$ for $h_1 \leq t < h_1 + h_2$.

Even Limit Cycles

The analysis has to be modified slightly to deal with even periodic solutions, see Figure 4.16. For this case we have

$$\xi(h_1 + h_2) = \xi(0) \quad \text{and} \quad u(h_1 + h_2) = -L\xi(h_1 + h_2) = F_S$$

which causes some sign changes in the conditions for a periodic solution in Theorem 4.1.

COROLLARY 4.1
Consider again the system (4.14) with friction force (4.1). Assume that there exists an even periodic solution with period $T = h_1 + h_2$ and that the matrix $I - \Phi\Phi_c$ is nonsingular. Furthermore, we assume that during the interval $0 < t < h_1$ the motion is unconstrained and for $h_1 \leq t \leq h_1 + h_2$ the friction force keeps the velocity at zero as in Figure 4.16. The following equations then hold.

$$f_1(h_1, h_2) = C_v(I - \Phi_c\Phi)^{-1}(\Phi_c\Gamma_r y_r - \Gamma_c F_C + \Gamma_{cr} y_r) = 0 \tag{4.40}$$

$$f_2(h_1, h_2) = -L(I - \Phi\Phi_c)^{-1}(-\Phi\Gamma_c F_C + \Phi\Gamma_{cr} y_r + \Gamma_r y_r) = F_S \tag{4.41}$$

and

$$v(t) = C_v\xi(t) > 0 \quad \text{for} \quad 0 < t < h_1 \tag{4.42}$$

$$|u(t)| = |L\xi(t)| < F_S \quad \text{for} \quad h_1 \leq t < h_1 + h_2 \tag{4.43}$$

Furthermore, the periodic solution is obtained with the initial condition

$$\xi(0) = a = (I - \Phi\Phi_c)^{-1}(-\Phi\Gamma_c F_C + \Phi\Gamma_{cr} y_r + \Gamma_r y_r) \tag{4.44}$$

and the state at time h_1 is given by

$$\xi(h_1) = b = (I - \Phi_c\Phi)^{-1}(\Phi_c\Gamma_r y_r - \Gamma_c F_C + \Gamma_{cr} y_r) \tag{4.45}$$

Remark. It is of course also possible to reduce velocity and position equations as was done for odd periodic solutions. The derivatives of f_1, f_2, and f_3 then have to be changed accordingly. The Jacobian of the Poincaré map remains the same. □

The results will now be applied to the examples in Section 4.2.

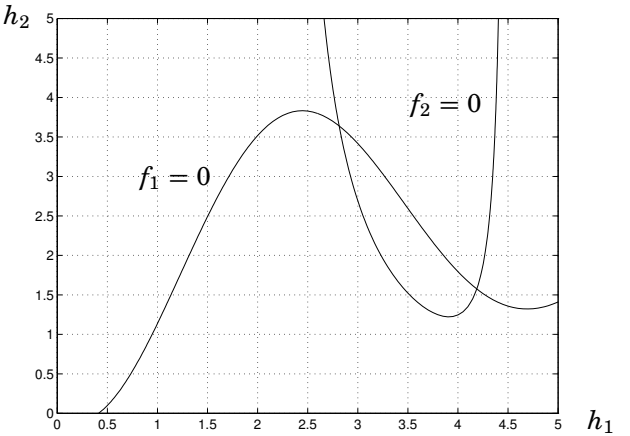

Figure 4.19 Zero levels for the functions f_1 and f_2 in Example 4.1.

4.5 Applications

The tools developed in Section 4.4 have been implemented in Matlab, where the zeros of the functions are found using a Newton-Raphson method. The numerical algorithms are now used to analyze the examples in Section 4.2.

EXAMPLE 4.1—STICK-SLIP MOTION (CONT.)
Consider the stick-slip motion in Example 4.1. The system shows an even limit cycle. The system equations (4.2) with $m = 1$, $k = 2$, $v_{ref} = 0.1$, and with viscous friction $F_v = 0.4$ are equivalent to (4.14) with

$$A = \begin{pmatrix} 0 & 0 \\ 1 & 0 \end{pmatrix} \qquad B = \begin{pmatrix} 1 \\ 0 \end{pmatrix} \qquad B_r = \begin{pmatrix} 0 \\ -1 \end{pmatrix} \qquad C_v = \begin{pmatrix} 1 & 0 \end{pmatrix}$$

and

$$L = \begin{pmatrix} 0.4 & 2 \end{pmatrix}$$

Furthermore, the friction is characterized by $F_S = 1.5$ and $F_C = 1$. The second state of the example is the extension of the spring. Hence, it suffices to reduce the velocity state according to Remark 1 of Theorem 4.2. By plotting the zero level curves of the functions $f_1(h_1, h_2)$ and $f_2(h_1, h_2)$ we can get an initial estimate of feasible solutions h_1 and h_2. The level curves are shown in Figure 4.19. There are two points of intersection between the curves. Numerical solution gives $h_1 = 2.81$, $h_2 = 3.64$, and

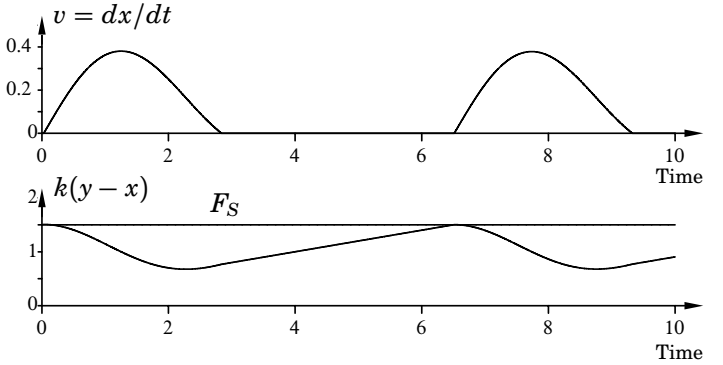

Figure 4.20 Simulation of the first suggested limit cycle of Example 4.1 with $h_1 = 2.81$ and $h_2 = 3.64$, and with the numerically determined initial conditions.

$h_1 = 4.19$, $h_2 = 1.58$, respectively. For the first point we get the states

$$a = \begin{pmatrix} 0 \\ -0.75 \end{pmatrix} \quad b = \begin{pmatrix} 0 \\ -0.386 \end{pmatrix}$$

The derivatives of the velocity at time $t = h_1$ and of the control signal at time $t = h_1 + h_2$ are

$$C_v z = -0.228 \qquad -Lw = 0.2$$

and have the correct sign for an even limit cycle. The Jacobian of the Poincaré map becomes

$$W = \begin{pmatrix} 0 & 0 \\ 0 & 0 \end{pmatrix}$$

This matrix trivially has both eigenvalues at the origin and is thus stable and even assures immediate convergence to the periodic solution. The period of the limit cycle is

$$T = h_1 + h_2 = 6.45$$

Finally, in Figure 4.20 we show a simulation of the limit cycle to check conditions (4.19) and (4.20). As can be seen these conditions are fulfilled.

For the second solution we have $h_1 = 4.19$ and $h_2 = 1.58$. This gives

$$a = \begin{pmatrix} 0 \\ -0.75 \end{pmatrix} \quad b = \begin{pmatrix} 0 \\ -0.592 \end{pmatrix}$$

and

$$C_v z = 0.185 > 0 \qquad -Lw = 0.2$$

The sign of $C_v z$ is wrong and indicates that the velocity has switched sign between $t = 0$ and $t = h_1$. In Figure 4.21 we show a simulation of the suggested limit cycle and, as can be seen, this is not an acceptable solution.

Varying the parameters of the system will, of course, affect a possible periodic solution. We can easily see how h_1 and h_2 changes with varying F_S, since only the function f_1 depends on F_S and in a simple manner. This is shown in Figure 4.22, where F_S is varied from 1 to 2 in steps of 0.1. F_S is approximately 1.277 in the limiting case when the level curves loses their intersection. A simulation for this value of F_S is shown in Figure 4.23. The velocity barely reaches zero velocity so that sticking occurs. □

EXAMPLE 4.2—HUNTING (CONT.)
Next we consider Example 4.2. Simulations in Section 4.2 showed that there is an odd limit cycle. The system is given by (4.3) and the control law by (4.4), which corresponds to

$$A = \begin{pmatrix} 0 & 0 & 0 \\ 1 & 0 & 0 \\ 0 & 1 & 0 \end{pmatrix} \qquad B = \begin{pmatrix} 1 \\ 0 \\ 0 \end{pmatrix} \qquad C_v = \begin{pmatrix} 1 & 0 & 0 \end{pmatrix}$$

with

$$L = \begin{pmatrix} 2 & 2 & 1 \end{pmatrix}$$

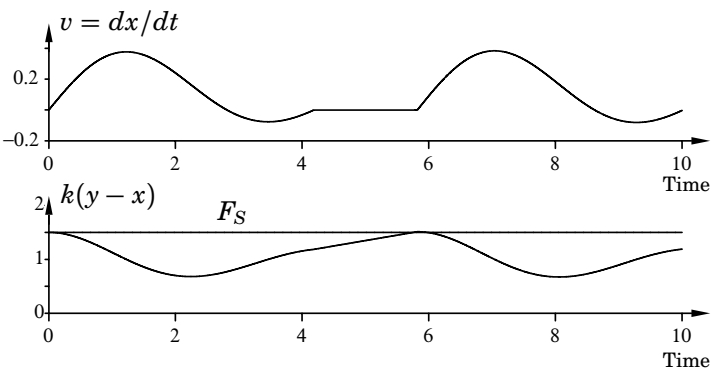

Figure 4.21 Simulation of the second suggested limit cycle of Example 4.1 with $h_1 = 4.19$ and $h_2 = 1.58$, and with the numerically determined initial conditions.

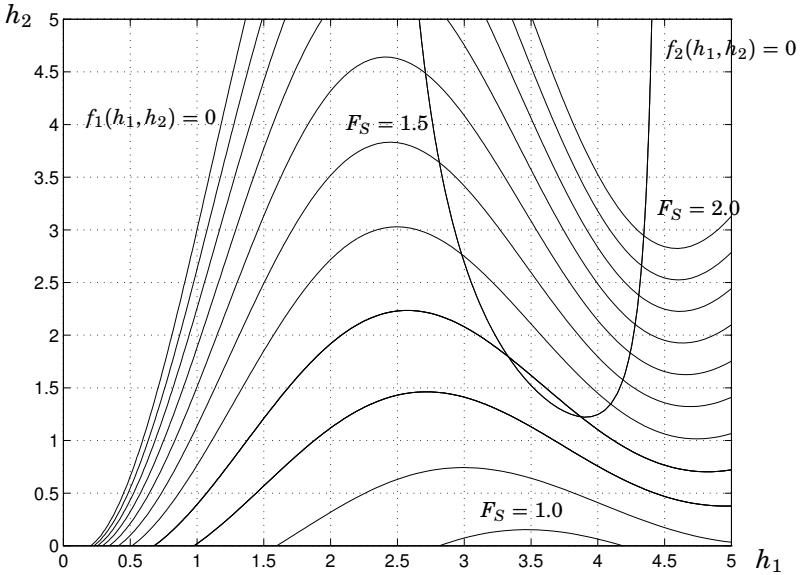

Figure 4.22 Zero level curves of $f_1(h_1,h_2)$ and $f_2(h_1,h_2)$ when the static friction force F_S is varied between 1 and 2. For low static friction there is no intersection and hence no limit cycle.

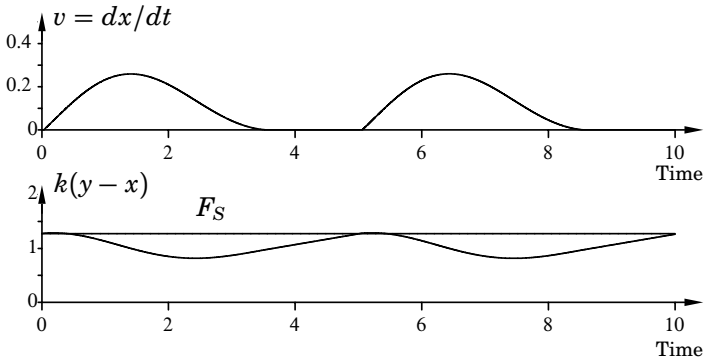

Figure 4.23 When the static friction force is lowered the limit cycle of Example 4.1 finally will disappear. In the limiting case the velocity just barely reaches zero.

and we let $y_r = 0$, $F_S = 1$, and $F_C = 0.5$. The example includes position as a state and the problem can thus be reduced to the solution of three functions of three variables. Numerical solution gives $h_1 = 2.50$, $h_2 = 9.93$,

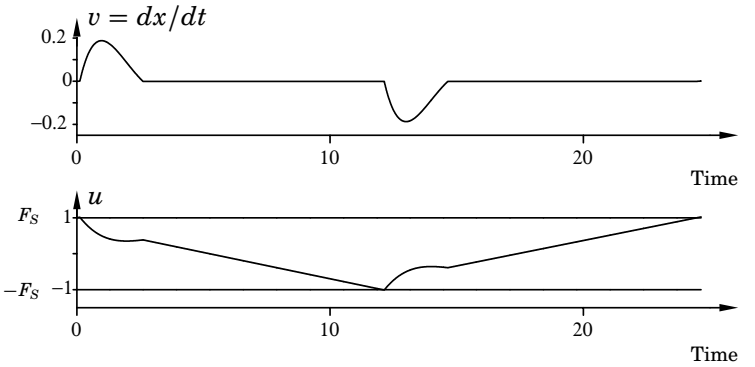

Figure 4.24 Simulation of the periodic solution to Example 4.2. The initial conditions are computed using the numerical algorithms.

and $e = 0.140$. This gives the states

$$a = \begin{pmatrix} 0 \\ 0.140 \\ 0.720 \end{pmatrix} \qquad b = \begin{pmatrix} 0 \\ 0.140 \\ -0.669 \end{pmatrix}$$

and, further,

$$C_v z = -0.110 \qquad -Lw = -0.140$$

which both have the correct sign. The Jacobian becomes

$$W = \begin{pmatrix} 0 & 0 & 0 \\ -0.106 & -0.404 & -0.379 \\ 0.212 & 0.807 & 0.758 \end{pmatrix}$$

This matrix has the eigenvalues 0, 0, and 0.355 and is thus stable. The fast convergence in Figure 4.5 is confirmed. A simulation of the limit cycle using the derived initial condition is shown in Figure 4.24. □

Example 4.3—Inverted Pendulum on a Cart (Cont.)
A simple model of an inverted pendulum on a cart was given by (4.5). This is equivalent to

$$A = \begin{pmatrix} 0 & 0 & 0 & 0 \\ 1 & 0 & 0 & 0 \\ 0 & 0 & 0 & 1 \\ 0 & 0 & 1 & 0 \end{pmatrix} \qquad B = \begin{pmatrix} 1 \\ 0 \\ 1 \\ 0 \end{pmatrix} \qquad C_v = \begin{pmatrix} 1 & 0 & 0 & 0 \end{pmatrix}$$

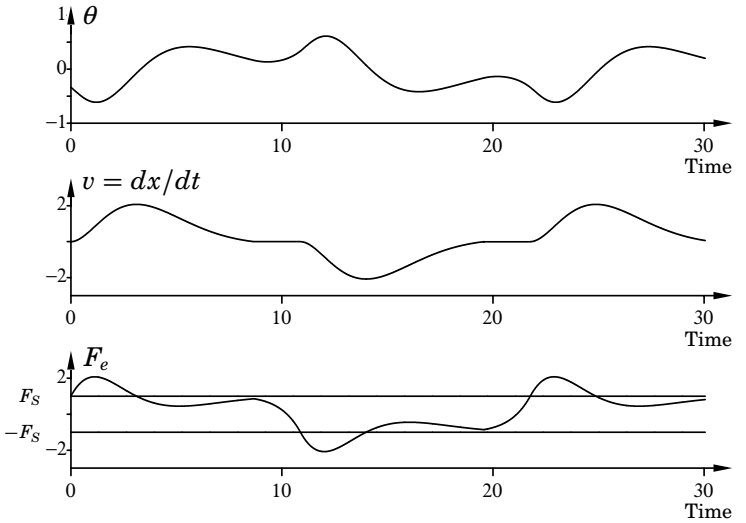

Figure 4.25 A simulation of the periodic solution to Example 4.3.

The control law (4.6) is

$$L = \begin{pmatrix} -1.05 & -0.25 & 3.15 & 3.48 \end{pmatrix}$$

The remaining parameters are $F_S = 1$, $F_C = 1$, and $y_r = 0$. Numerical solution of the equations in Theorem 4.2 gives $h_1 = 8.69$, $h_2 = 2.20$, and $e = 4.54$. We also get

$$a = \begin{pmatrix} 0 \\ 4.545 \\ 0.307 \\ 0.336 \end{pmatrix} \qquad b = \begin{pmatrix} 0 \\ 4.545 \\ -0.0924 \\ 0.163 \end{pmatrix}$$

and

$$C_v z = -0.1413 \qquad -Lw = -2.1269$$

The derivatives of the velocity and the control signal thus have the correct sign. The Jacobian becomes

$$W = \begin{pmatrix} 0 & 0 & 0 & 0 \\ -0.0277 & -0.0640 & -0.0376 & 0.0411 \\ 0.0005 & 0.0010 & 0.0007 & -0.0008 \\ -0.0024 & -0.0055 & -0.0033 & 0.0036 \end{pmatrix}$$

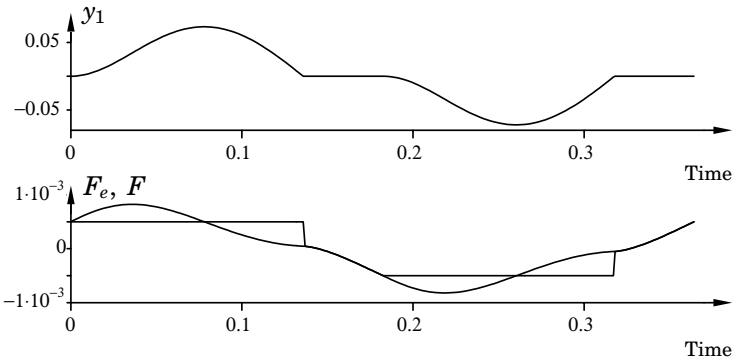

Figure 4.26 Simulation of the periodic solution for the flexible servo when $\rho = 11$. The initial conditions are numerically determined.

with eigenvalues 0, 0, 0.0003, and −0.0600, which assures a very fast convergence to the limit cycle. A simulation of the periodic solution using the computed initial condition is shown in Figure 4.25. □

EXAMPLE 4.4—FLEXIBLE SERVO (CONT.)
The flexible servo in Example 4.4 is given by (4.7). It shows different limit cycles depending on the design parameter ρ.

For $\rho = 10$, the simulation shows no limit cycle. A numerical solution for h_1, h_2, and e could not be found. This confirms the simulations.

An odd limit cycle with sticking occurs when simulating the flexible servo for $\rho = 11$. A numerical solution gives $h_1 = 0.1357$, $h_2 = 0.0465$, and

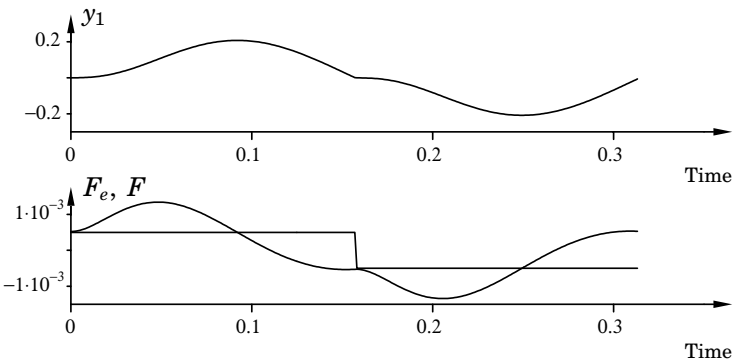

Figure 4.27 Simulation of the periodic solution for the flexible servo when $\rho = 12$. The initial conditions are numerically determined.

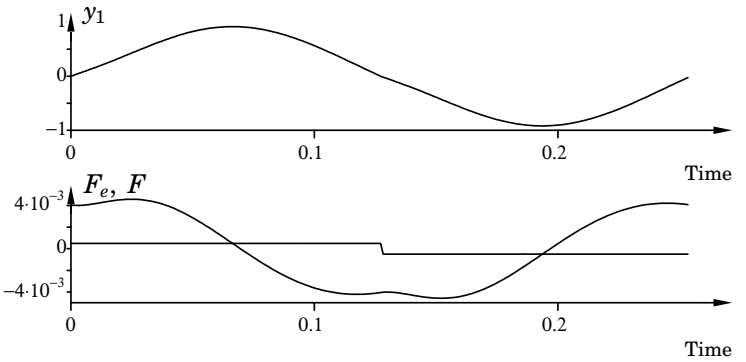

Figure 4.28 Simulation of the periodic solution for the flexible servo when $\rho = 15$. The initial conditions are numerically determined.

$e = -0.00281$. The magnitude of the largest eigenvalue of the Jacobian is 0.618. The limit cycle is thus stable and with moderate convergence. The derivatives of the velocity and the control signal has the correct sign at times $t = h_1$ and $t = h_1 + h_2$, respectively. Figure 4.26 shows a simulated period with initial conditions computed numerically.

The oscillation for $\rho = 12$ is of relay type and can, therefore, be analyzed with the tools in Åström (1995). A numerical solution gives $h = 0.157$, which is half the period. The largest eigenvalue of the Jacobian has magnitude 0.573, which assures stability. A simulation of one period with initial conditions computed numerically is shown in Figure 4.27.

If ρ is increased to 15, the oscillation in the velocity becomes more sinusoidal. Half the period is given by $h = 0.127$ and the largest eigenvalue of the Jacobian has magnitude 0.5054. The convergence to the limit cycle is thus faster with larger values of ρ. Figure 4.28 shows the velocity and the control signal for one period. □

4.6 Describing Function Analysis

The describing function method is widely used. It is an approximate technique to analyze self-sustained oscillations in dynamical systems with nonlinearities. It has been used for a long time for control problems with friction. Tustin (1947) used the technique to study the performance of control loops. At that time the name describing function had not been introduced. Other early papers are Tou and Schultheiss (1953) and Shen (1962). There are some drawbacks with the method and the results are

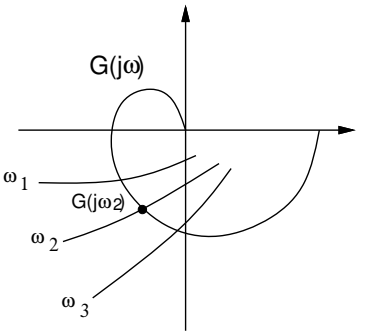

Figure 4.29 Possible limit cycle for a frequency dependent describing function.

not always correct as discussed in Amin and Armstrong-Hélouvry (1994). The cases where a limit cycle can be proved are restricted to special classes of nonlinearities that exclude friction, see Mees and Bergen (1975).

A possible limit cycle is indicated if there exists an amplitude A and a frequency ω such that

$$1 + N(A, \omega)G(j\omega) = 0$$

where $N(A, \omega)G$ is the describing function of the nonlinearity. To graphically illustrate a possible limit cycle, the Nyquist curve of $G(i\omega)$ is plotted together with the negative inverse of the describing function, i.e., $-1/N(A, \omega)$. Any intersection between these curves indicates a candidate limit cycle. From the Nyquist diagram it is easy to see how design changes affect the occurrence of a possible limit cycle by changes in $G(j\omega)$. This has been one of the main advantages of the method. It works well if the describing function is only a function of amplitude. When it also depends on frequency, it is common to plot the describing function for several fixed frequencies and then look for an intersection between such a curve and the Nyquist curve at the particular frequency, see Figure 4.29.

Friction has traditionally been described as a function of velocity. It is, therefore, natural to let the describing function show how the friction nonlinearity responds to sinusoidal velocities. For the simple relay friction $F = F_C \operatorname{sgn}(v)$ the describing function becomes

$$N(A, \omega) = \frac{4F_C}{\pi A}. \tag{4.46}$$

A question that may be raised is that classical models with stiction cannot be described as a function of velocity for zero velocity. For this case it depends on the applied force. However, the events at zero velocity do not

affect the computation of the describing function since they are of measure zero. The describing function does, therefore, not capture the special friction behavior for zero velocity. The friction force has really no possibility to affect the velocity input so that it "sticks" at zero. Therefore, the static model (4.1) also has the describing function given by (4.46).

The linear block for the describing function analysis is the transfer function from F to v of (4.14). This transfer function is given by

$$G(s) = C_v(sI - A + BL)^{-1}B$$

The negative inverse of (4.46) lies on the negative real axis where the origin corresponds to zero amplitude. Knowing the point $G(j\omega_d)$, where the Nyquist curve crosses the negative real axis, we can readily compute the amplitude and the period of the limit cycles suggested by the describing function method as follows:

$$A = -\frac{4F_C G(j\omega_d)}{\pi} \qquad \text{and} \qquad T = \frac{2\pi}{\omega_d}$$

We will now apply describing function analysis to Example 4.4. This particular example has also been analyzed in Wallenborg and Åström (1988). The values obtained from the analysis will be compared to the computed values in Section 4.5.

Example 4.4—Flexible Servo (Cont.)
No limit cycle appeared in the simulation for $\rho = 10$. The Nyquist diagram of $G(j\omega)$ is shown in Figure 4.30. The controller for the servo is stable and, therefore, there is no encirclement of -1 and no intersection between the Nyquist curve and the negative real axis. This means that the describing function method does not predict any limit cycle, which agrees both with simulations and previous computations.

If the design is made slightly faster by increasing ρ to 11, the controller becomes unstable and the Nyquist curve therefore encircles -1, as seen in Figure 4.31. It intersects the negative real axis at -807.1 for $\omega_d = 16.79$. The describing function hence suggests a limit cycle with

$$A = 0.514 \qquad \text{and} \qquad T = 0.374$$

The results in Section 4.5 are a peak amplitude $A = 0.737$ and a period $T = 0.364$. The simulated limit cycle was shown in Figure 4.26. At the time when the velocity becomes zero the external force is not large enough to overcome the friction force. The result is a period during which motion is stopped, which means that the velocity deviates significantly from the sinusoid assumed by the describing function method. The peak

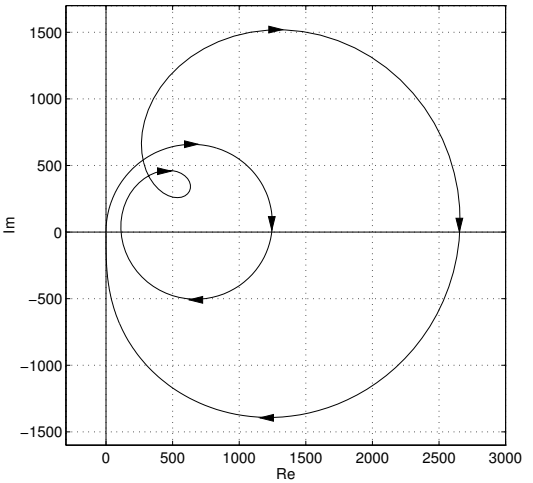

Figure 4.30 Nyquist curve for $G(j\omega)$ when $\rho = 10$. There is no intersection with the negative real axis.

amplitude, therefore, deviates from the amplitude of the fundamental frequency, which the describing function method predicts.

If ρ is increased further to 12 the limit cycle becomes a pure relay oscillation. The Nyquist diagram of $G(j\omega)$ still encircles -1 one time, as seen in Figure 4.32, and intersects the negative real axis at -2846 for $\omega_d = 19.26$. Describing function analysis thus suggests a limit cycle with

$$A = 1.81 \quad \text{and} \quad T = 0.326$$

The computed peak amplitude and period in Section 4.5 are $A = 2.145$ and $T = 0.314$. The simulated limit cycle is shown in Figure 4.27. This time the control force immediately overcomes the friction force at the time when the velocity becomes zero. The result is a pure relay oscillation. The velocity is, therefore, closer to a sinusoidal than for $\rho = 11$, which implies better accuracy for the describing function method.

When ρ is increased to 15 the controller becomes more unstable and the limit cycle is also a pure relay oscillation. The Nyquist diagram is seen in Figure 4.33. The intersection between the Nyquist curve and the negative real axis occurs at -13884 for $\omega_d = 24.45$. This suggests a limit cycle with

$$A = 8.84 \qquad \text{and} \qquad T = 0.257$$

The analysis in Section 4.5 gave a peak amplitude $A = 9.27$ and a period $T = 0.254$. Figure 4.28 shows the simulated limit cycle. As seen the veloc-

ity is almost sinusoidal. The assumptions made by the describing function method therefore holds well, which results in the accurate prediction. □

Discussion

The ability of the describing function analysis to accurately predict friction-generated limit cycles depends on how well the approximation of the method holds. Generally, limit cycles with relatively long periods of sticking will be badly predicted, since they are not sinusoidal as assumed. Limit cycles, which depend on the condition $F_S > F_C$ for their existence, are poorly predicted in particular. This is the case for the limit cycles in Examples 4.1 and 4.2. No limit cycle is predicted by the describing function method for those examples, since there is no intersection between $G(j\omega)$ and the negative real axis (if the closed linear loop is stable). The problem is that the behavior for zero velocity is not captured in the describing function when velocity is considered as the nonlinearity input, see Figure 4.34.

Historically this problem has been overcome in different ways. Tustin (1947) did it by assuming a sinusoidal velocity and then figuring out what input force that was required. In this way he actually determined the describing function for the interconnection of the inertia with friction. By doing so, force was regarded as the input and velocity the resulting output of the nonlinearity. Tou and Schultheiss (1953) replaced the friction

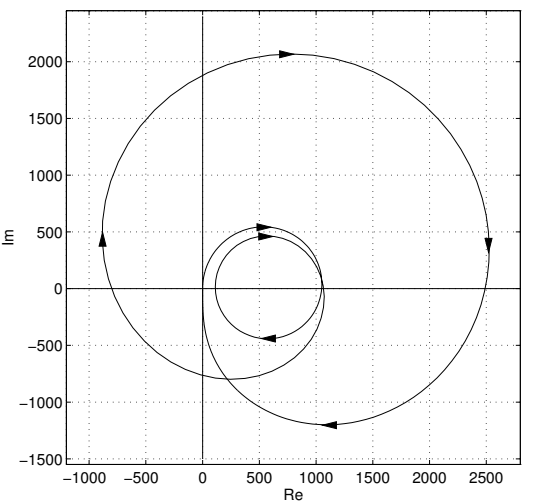

Figure 4.31 Nyquist curve for $\rho = 11$. The curve intersects the negative real axis at -807.1 for $\omega_d = 16.79$.

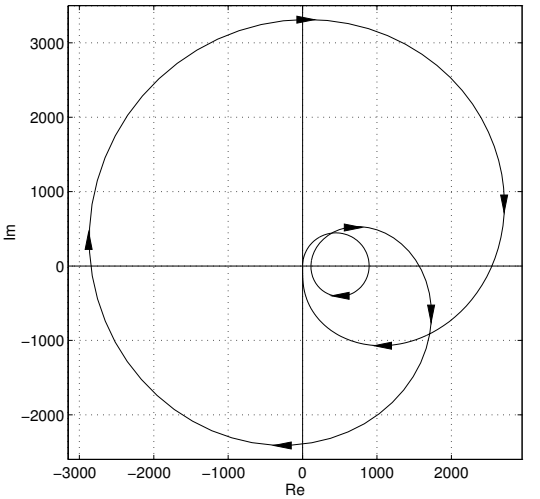

Figure 4.32 Nyquist curve for $\rho = 12$. The curve intersects the negative real axis at -2846 for $\omega_d = 19.26$.

block with a nonlinear block in series with the inertia. The behavior of this new nonlinear block was determined by the expected behavior for a sinusoidal force input to the original interconnection. The replacement is valid only for this type of inputs. Shen (1962) graphically showed the force and resulting velocity for stick-slip motion with a ramp reference. He constructed the describing function from these curves and thus avoided the problem of zero velocity.

The velocity at the friction interface is the result of the external forces and the friction force and may be zero for longer periods. Therefore, it seems more reasonable to regard the external force as the input and velocity as the output. The external force is also more sinusoidal than the velocity; see, for example, Figure 4.26. The nonlinearity then has to be considered as the inertia combined with the friction force in order to have a force as the input as seen in Figure 4.35. This approach is taken in Olsson (1995). The disadvantage is that the nonlinearity includes dynamics. The describing function, therefore, depends both on frequency and amplitude. Furthermore, it makes the computation of the describing function more difficult. The approach makes it possible to predict the limit cycles even for stick-slip motion, see Olsson (1995). A problem associated with this approach may occur for limit cycles with unidirectional, motion where the input to the nonlinearity must include an average force in addition to the sinusoid. This is the case for stick-slip motion. It requires the use of so called dual-input describing function, see Gelb and Vander Velde (1968).

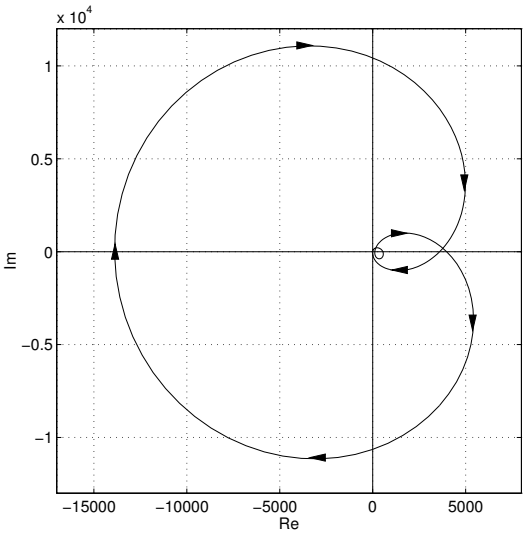

Figure 4.33 Nyquist curve for $\rho = 15$. The curve intersects the negative real axis at -13884 for $\omega_d = 24.45$.

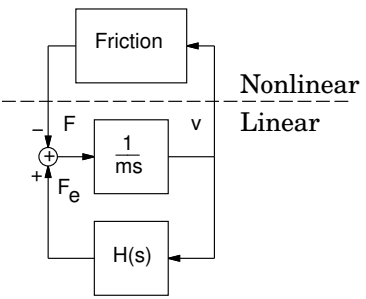

Figure 4.34 Describing function analysis where only friction is considered in the nonlinear block.

The problem is discussed in Olsson (1995).

4.7 Model Dependency

In this section we use the dynamic model of Chapter 3 to investigate how the nature of the limit cycles in the examples in Section 4.2 depend on the friction model. The simplified standard model, described in the previous chapter and with default parameters, is stiff and on the time scales of

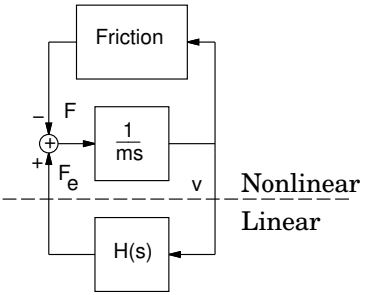

Figure 4.35 Describing function analysis where friction together with the inertia is considered in the nonlinear block.

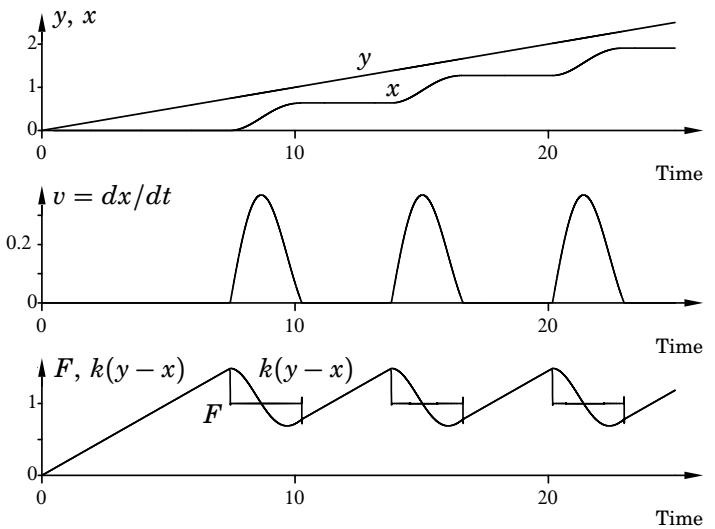

Figure 4.36 Simulation of Example 4.1 with the standard dynamic friction model. Compare with Figure 4.3.

interest in the examples it behaves almost as a static model. Therefore, it can be expected that the results will be similar to those obtained with the static friction model (4.1). This is indeed the case. The simulations using the dynamic model with default parameters are shown in Figures 4.36, 4.37, 4.38, and 4.39, which should be compared with Figures 4.3, 4.5, 4.7, and 4.13, respectively. As seen, the simulations are almost identical.

We will now investigate how changes of the model parameters affect the limit cycles.

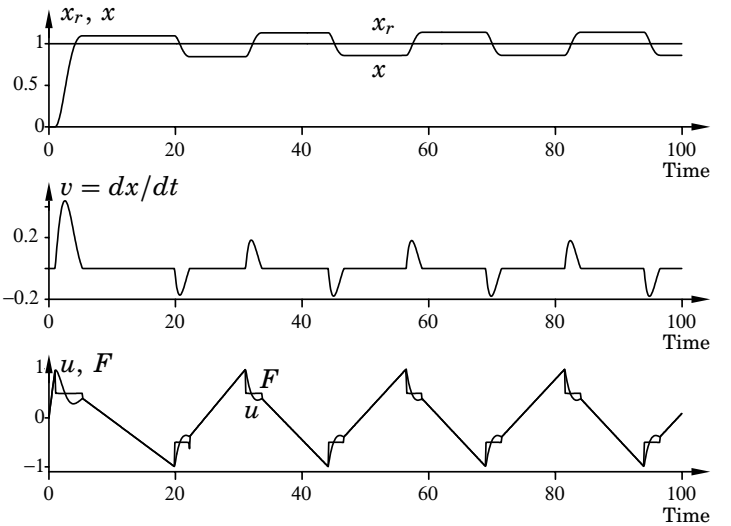

Figure 4.37 Simulation of Example 4.2 with the standard dynamic friction model. Compare with Figure 4.5.

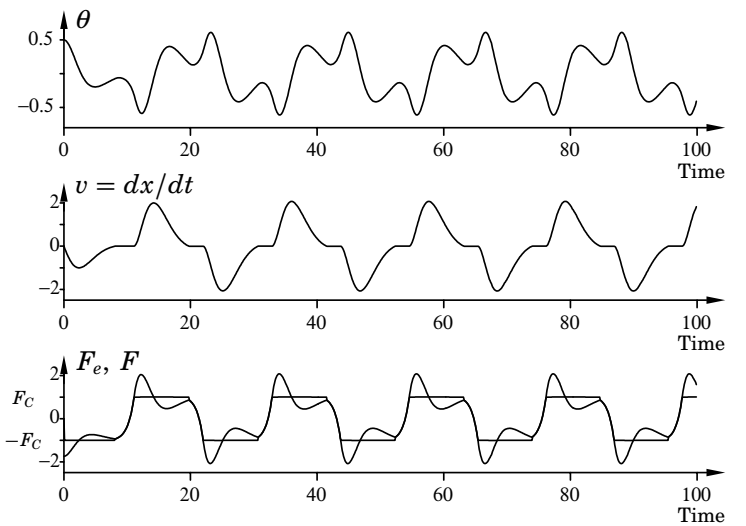

Figure 4.38 Simulation of Example 4.3 with the standard dynamic friction model. Compare with Figure 4.7.

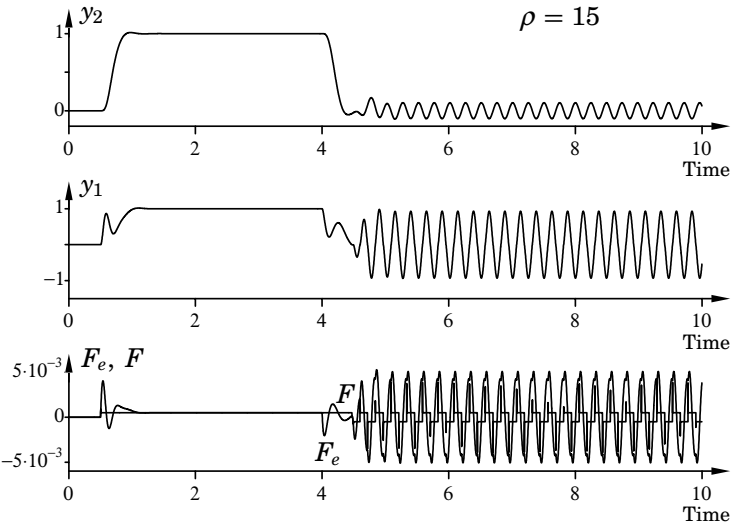

Figure 4.39 Simulation of Example 4.4 for $\rho = 15$ using the standard dynamic friction model. Compare with Figure 4.13.

Stribeck velocity v_S**:** The static friction F_S is higher than the sliding friction F_C for Examples 4.1 and 4.2. For the static model (4.1) the drop from F_S to F_C is instantaneous when the velocity becomes nonzero. This is not the case for the dynamic model, where the parameter v_S determines the velocity range where a gradual drop occurs. The effect of an increasing v_S is that the accelerating force after break-away will be lower than with the static model. For Example 4.1 this results in a longer sliding distance and thus a longer period of the limit cycle. The effect is seen in Figure 4.40, where $v_S = 0.1$. Compare with Figures 4.3 and 4.36.

For Example 4.2 the lower accelerating force has the effect of reducing the size of the "jumps," i.e., the amplitude of the limit cycle. With a smaller position error the integrator needs longer time to overcome the static friction force and, therefore, the period of the periodic solution increases as seen in Figure 4.41, where $v_S = 0.1$. The simulation should be compared with Figures 4.5 and 4.37.

For the inverted pendulum and the flexible servo $F_S = F_C$, and therefore v_s has no influence on those examples.

Stiffness σ_0**:** The parameter σ_0 determines the speed of the model dynamics. The dynamics are also coupled to the damping coefficient. If this is chosen as $\sigma_1 = 2\sqrt{\sigma_0}$ the relative damping of the linearized system when sticking is $\zeta = 1$.

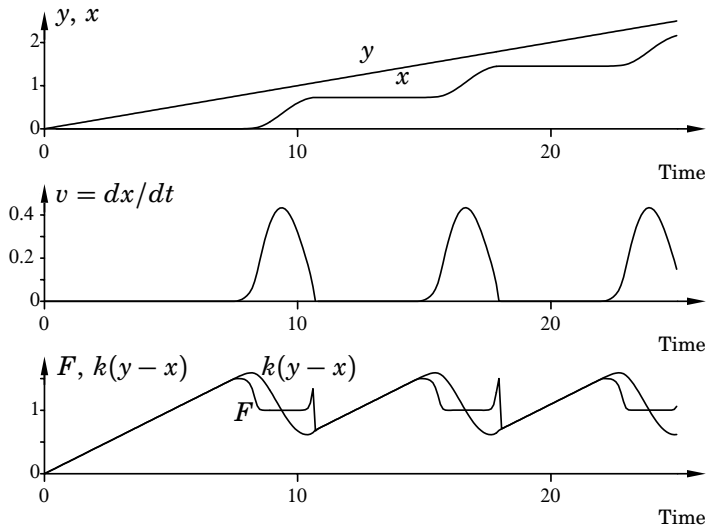

Figure 4.40 Simulation of Example 4.1 using the dynamic friction model with default parameters except $v_S = 0.1$. Compare with Figures 4.3 and 4.36.

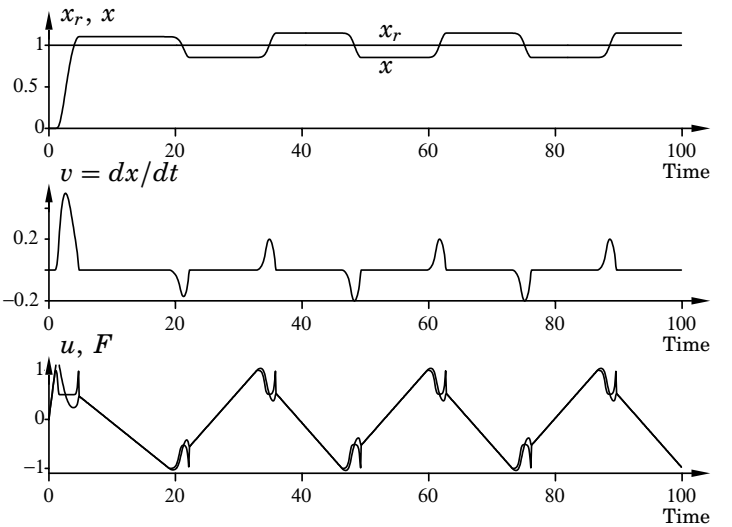

Figure 4.41 Simulation of Example 4.2 using the standard dynamic friction model with default parameters except $v_S = 0.1$. Compare with Figures 4.5 and 4.37.

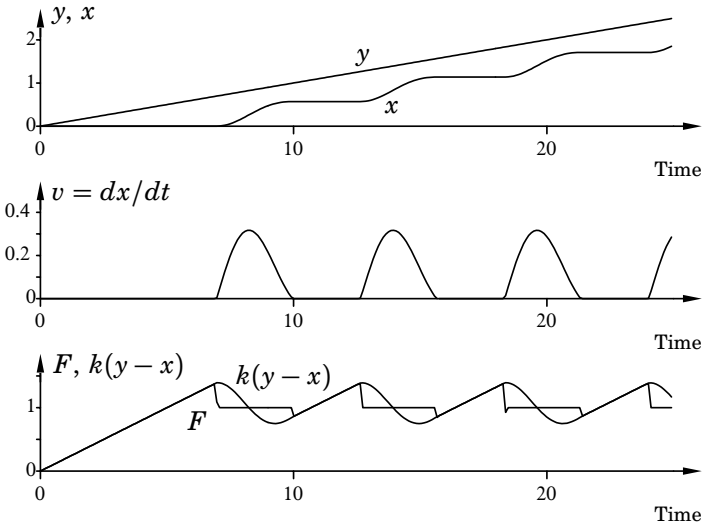

Figure 4.42 Simulation of Example 4.1 using the dynamic friction model with default parameters except $\sigma_0 = 10^4$ and $\sigma_1 = 200$. Compare with Figures 4.3 and 4.36.

In Chapter 3 it was shown that the break-away force decreased when the model dynamics were made slower. The result is similar to what would be achieved with a lower F_S. Figure 4.42 shows a simulation of Example 4.1 when $\sigma_0 = 10^4$ and $\sigma_1 = 200$. The period of the limit cycle is shortened, as would be the result if F_S was lowered to approximately 1.3. If the dynamics are slowed down further, the limit cycle will disappear, since the friction force is never built up significantly above F_C.

For Example 4.2 the slower dynamics causes the size of the "jump" to decrease in the same way as if F_S in the static model was made smaller. This leads to a smaller amplitude and a longer period of the oscillation. The case where $\sigma_0 = 1000$ and $\sigma_1 = 2\sqrt{1000}$ is shown in Figure 4.43. The limit cycle disappears when the dynamics are even slower.

The dynamics can be said to govern not only how fast the friction force can shift between the static and kinetic levels but also how fast it can respond to changes in the direction of the motion. The limit cycles in the stick-slip motion example and the hunting example depend critically on the difference between the static friction level and the sliding friction. In the other examples the static and dynamic friction levels are the same, and the limit cycles are, therefore, caused by the change in friction force for different directions of motion. This switch is not as sensitive to the speed of the model dynamics.

For Example 4.3 a number of simulations have been performed to in-

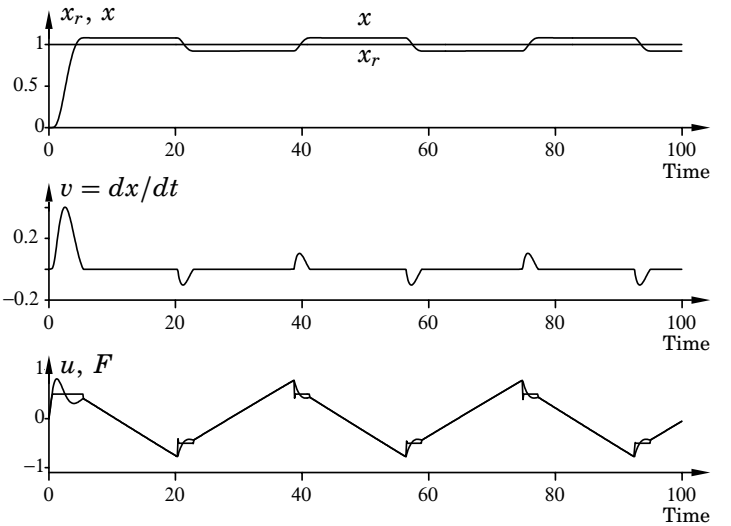

Figure 4.43 Simulation of Example 4.2 using the dynamic friction model with default parameters except $\sigma_0 = 1000$ and $\sigma_1 = 2\sqrt{1000}$. Compare with Figures 4.5 and 4.37.

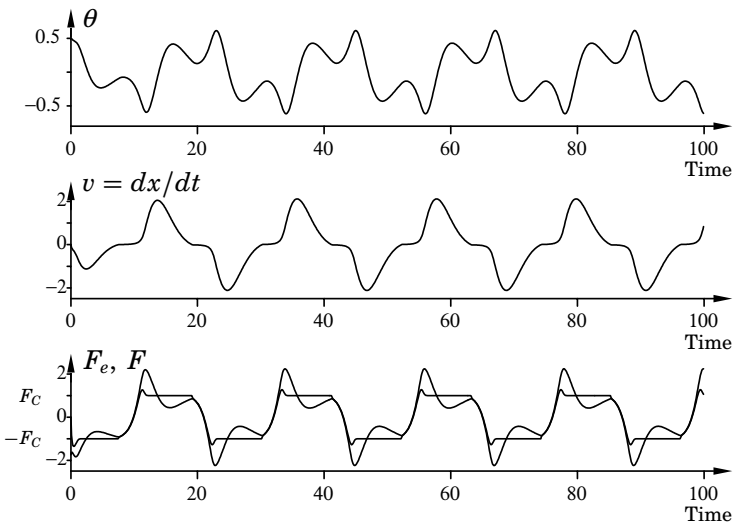

Figure 4.44 Simulation of Example 4.3 using the dynamic friction model with default parameters except $\sigma_0 = 10$ and $\sigma_1 = 2\sqrt{10}$. Compare with Figures 4.7 and 4.38.

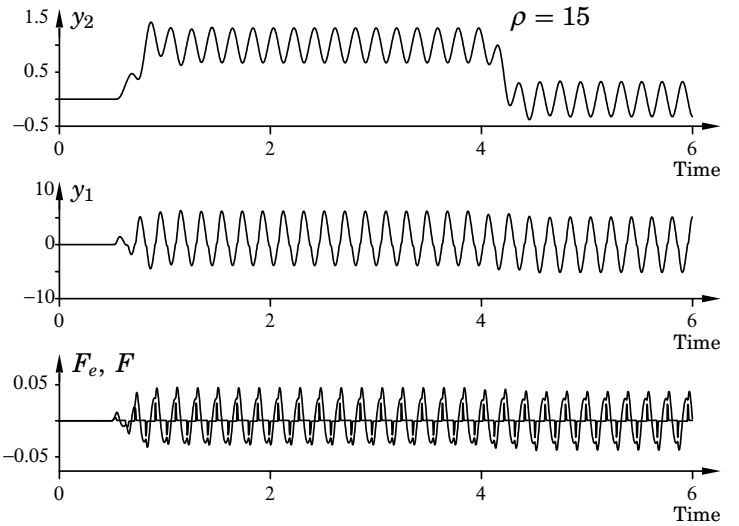

Figure 4.45 Simulation of Example 4.4 for $\rho = 15$ using the dynamic friction model with $\sigma_0 = 100$ and $\sigma_1 = 20$. Compare with Figures 4.13 and 4.39.

vestigate the influence of the speed of the model dynamics. The stiffness was varied between $\sigma_0 = 10$ and 10^5. The simulations showed that it only affected the limit cycles marginally. The simulation with $\sigma_0 = 10$ and $\sigma_1 = 2\sqrt{10}$ is shown in Figure 4.44, which should be compared with Figures 4.7 and 4.38. A new limit cycle arises in Example 4.4 if the dynamics of the friction model are made significantly slower. The system is of order eight, which makes it hard to explain. There are large peaks in the friction force at the zero velocity crossings, which probably induces the oscillations. The amplitude of the limit cycle is larger and the frequency is about 50% higher than for the limit cycle obtained with the static model. Figure 4.45 shows the simulation when $\sigma_0 = 100$ and $\sigma_1 = 20$. It should be noted that the limit cycle is present even prior to $t = 4$, which was not the case for the limit cycle in Figures 4.13 and 4.39.

4.8 Summary

We have in this chapter discussed limit cycles generated by friction. A number of examples have demonstrated where oscillations may occur and also different natures of the limit cycles. The oscillations have been characterized. It is necessary to distinguish between limit cycles with and without periods of sticking. If sticking does not occur, the limit cycles are

equivalent to pure relay oscillations and can be analyzed as such. The tools available for relay oscillations have then been extended to limit cycles with sticking. The tools are suitable for numerical determination of possible limit cycles. The examples have been analyzed using the derived numerical methods. The results are compared with describing function analysis. The describing function analysis works poorly for limit cycles with long periods of sticking and especially for limit cycles, which require that the static friction is higher than the sliding friction. Finally, the limit cycles are compared with the results obtained using the dynamic friction model introduced in Chapter 3.

5

Control of Systems with Friction

5.1 Introduction

Friction limits the performance of motion control systems. Recently there has been substantial interest in control strategies that can reduce the effects of friction. There are many ways to do this, see Armstrong-Hélouvry *et al.* (1994) for a survey. In early systems it was common to use a mechanical vibrator. Such a simple device gave improvements particularly for systems with a large amount of stiction. A similar approach is to superimpose a high frequency dither signal on the control signal. Other approaches uses detailed knowledge of the friction. To design such strategies it is necessary to have mathematical models that capture the behavior of friction. The models must be sufficiently simple so that they can be used to design safe control strategies. Most of the proposed schemes use classical friction models, such as Coulomb and viscous friction. These work reasonably well for velocity control, where the system typically spends only a small time in regions where the velocity is zero, see for example Canudas de Wit *et al.* (1987). The methods based on the simple models do, however, not work so well in applications such as high-precision positioning. The reason is that the simple models do not capture the behavior of friction well in regions with low velocity.

A new dynamic friction model was introduced in Chapter 3. It captures most of the experimentally observed friction properties. In this chapter we use this model to design friction compensators. Conditions for asymptotically stable velocity and position control are given. These conditions are less conservative than those given in Canudas de Wit *et al.* (1995) and allow a wider range of design considerations. The results are applied to a

velocity control problem for which the friction compensation is thoroughly explored. The sensitivity to model errors and disturbances is also investigated and the nature of the resulting control error is examined.

5.2 Friction Compensation

Electromechanical systems for motion control typically have a cascade structure with a current loop, a velocity loop and a position loop as shown in Figure 5.1. It would be advantageous to introduce friction compensation into the current loop. This is difficult to do with conventional systems because the current loop is not easily accessible. Most friction compensation schemes are therefore implemented in the velocity loop. To obtain an effective friction compensation it is necessary that the velocity is measured or estimated with good resolution and small time delay. The sensor problem can be considerable with a shaft encoder because of a variable delay in the estimation of the velocity. Friction compensation is also more difficult if there are considerable dynamics between the control signal and the point where the friction force enters the system. Typical examples are hydraulic and pneumatic actuators, where the control signal normally determines the flow into the actuator cylinder and not the pressure in it. There is then an integrator between the control signal and the force exerted by the pressure in the actuator.

Model-based friction compensation schemes use mathematical models of friction. If the dynamics between control signal and exerted force are fast, then the force applied is essentially proportional to the control signal. A straightforward way to reduce the friction is then to use the control law

$$u(t) = u_{lin}(t) + \hat{F}(t) \tag{5.1}$$

where $\hat{F}$ is an estimate of the friction force. With a Coulomb friction model

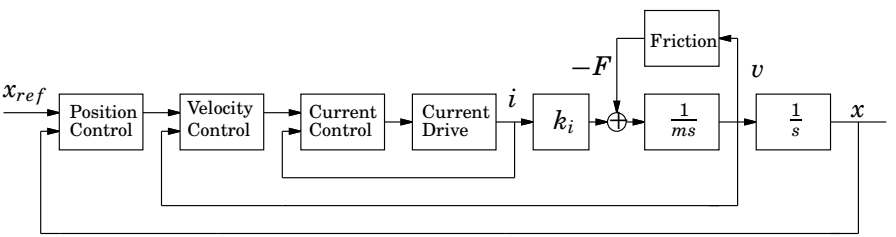

Figure 5.1 Cascade control structure for position control. The loop includes an inner current loop, a velocity loop and an outer position loop.

we have

$$\hat{F}(t) = F_C \operatorname{sgn}(v)$$

With more elaborate friction models $\hat{F}$ is instead given by a dynamical system, see Friedland and Mentzelopoulou (1993). The method requires that the control signal is proportional to the force applied at the friction interface or at least that the dynamics between the control signal and the applied force are known and invertible.

In a simple motion control problem, the control law (5.1) gives the following closed-loop system:

$$m\frac{d^2x}{dt^2} = u - F = u_{lin} + \hat{F} - F = u_{lin} - \tilde{F}$$

With a perfect estimate of the friction force, $\tilde{F} = F - \hat{F} = 0$ and the resulting system is therefore linear and control laws can be obtained with well established design methods for linear systems. It is thus possible to view friction compensation as a task that is isolated from the normal control design.

In reality the friction force is not perfectly known and it may also vary due to a number of factors such as temperature, wear, etc. The estimation error $\tilde{F}$ will therefore in practice not become zero. It is of great practical interest to study how sensitive the control strategy, including the friction estimate, is with respect to uncertainties in the friction model.

This chapter treats friction compensation based on the model introduced in Chapter 3. Different schemes for friction compensation are given and explored.

5.3 A Friction Force Observer

The friction model introduced in Chapter 3 is given by

$$\begin{aligned} \frac{dz}{dt} &= v - \frac{|v|}{g(v)}z \\ F &= \sigma_0 z + \sigma_1(v)\frac{dz}{dt} + F_v v \end{aligned} \tag{5.2}$$

where the details are given in Section 3.2. In order to use (5.2) for model-based friction compensation it is necessary to have an observer for the unknown state z. The estimate $\hat{z}$ can then be used to determine the estimate of the friction force $\hat{F}$ in the control law (5.1). The following observer

was suggested in Canudas de Wit *et al.* (1995) under the assumption that all parameters of the friction model are known.

$$\begin{aligned} \frac{d\hat{z}}{dt} &= v - \frac{|v|}{g(v)}\hat{z} - ke, \quad k > 0 \\ \hat{F} &= \sigma_0\hat{z} + \sigma_1(v)\frac{d\hat{z}}{dt} + F_v v \end{aligned} \tag{5.3}$$

The observer consists of a replica of the friction model but is in addition driven by the term ke. To agree with linear observers it is desirable that e is a function of the estimation error $\tilde{z}$. There is, however, no direct measurement available which is a function of the estimation error. Other options that will guarantee stability are therefore considered. The choice of e may depend on the control task.

The model (5.2) describes a dissipative map between v and z and also between v and F if

$$\sigma_1(v) \leq \frac{4\sigma_0 g(v)}{|v|} \tag{5.4}$$

This was shown in Section 3.5. The condition (5.4) on the velocity dependent damping coefficient agrees with empirical observations on how the damping should be chosen so as to give good model behavior. We will make use of some properties of the friction force observer that are similar to the dissipativity of the friction model. These are stated next.

PROPERTY 5.1
The map between e and $\tilde{z} = z - \hat{z}$ defined by the friction model (5.2) and the observer (5.3) is dissipative with respect to the function $V(t) = \tilde{z}^2(t)/2k$.

Proof. The error equation for $\tilde{z}$ becomes

$$\frac{d\tilde{z}}{dt} = -\frac{|v|}{g(v)}\tilde{z} + ke$$

We then have

$$\tilde{z}e = \frac{1}{k}\left(\frac{d\tilde{z}}{dt}\tilde{z} + \frac{|v|}{g(v)}\tilde{z}^2\right) \geq \frac{1}{k}\frac{d\tilde{z}}{dt}\tilde{z}$$

which implies

$$\int_0^t \tilde{z}e\,d\tau \geq \int_0^t \frac{1}{k}\frac{d\tilde{z}}{dt}\tilde{z}\,d\tau = \frac{1}{2k}\left(\tilde{z}^2(t) - \tilde{z}^2(0)\right)$$

□

Note that this is equivalent to Property 3.4. Next we show a property of the observer that is equivalent to Property 3.3, i.e., that the friction model is dissipative from v to F under condition (5.4).

PROPERTY 5.2
The map between e and $\tilde{F} = F - \hat{F}$ as defined by the friction model (5.2) and the friction force observer (5.3) is dissipative with respect to $V(t) = \sigma_0 \tilde{z}^2(t)/2k$ if $\sigma_1(v) \leq 4\sigma_0 g(v)/|v|$.

Proof. The equations governing the observer error are

$$\begin{aligned} \frac{d\tilde{z}}{dt} &= -\frac{|v|}{g(v)}\tilde{z} + ke \\ \tilde{F} &= \sigma_0 \tilde{z} + \sigma_1(v)\frac{d\tilde{z}}{dt} \end{aligned} \tag{5.5}$$

and, therefore,

$$\begin{aligned} \tilde{F}e &= \frac{1}{k}\left(\sigma_0\tilde{z} + \sigma_1(v)\frac{d\tilde{z}}{dt}\right)\left(\frac{d\tilde{z}}{dt} + \frac{|v|}{g(v)}\tilde{z}\right) \\ &= \frac{1}{k}\sigma_0\frac{d\tilde{z}}{dt}\tilde{z} + \sigma_1(v)\left(\left(\frac{d\tilde{z}}{dt} + \frac{|v|\tilde{z}}{2g(v)}\right)^2 + \frac{|v|}{g(v)}\left(\frac{\sigma_0}{\sigma_1(v)} - \frac{|v|}{4g(v)}\right)\tilde{z}^2\right) \\ &\geq \frac{\sigma_0}{k}\frac{d\tilde{z}}{dt}\tilde{z} \end{aligned} \tag{5.6}$$

since $\sigma_1(v) \leq 4\sigma_0 g(v)/|v|$. Hence,

$$\int_0^t \tilde{F}e\,d\tau \geq \frac{\sigma_0}{2k}\left(\tilde{z}^2(t) - \tilde{z}^2(0)\right) \tag{5.7}$$

and the property is established. □

We will make implicit use of these properties as control laws for velocity control are investigated.

5.4 Observer-Based Velocity Control

We now consider velocity control with model-based friction compensation using the introduced friction force observer. A prime objective is to assure stability of the control system so that convergence of the control error to zero is obtained. We consider the simple case when the equation of motion is given by

$$m\frac{d^2x}{dt^2} = m\frac{dv}{dt} = u - F \tag{5.8}$$

The friction force observer can be used for velocity control in the following way. Let

$$U(s) = H(s)E_v(s) + msV_{ref}(s) + \hat{F}(s) \tag{5.9}$$

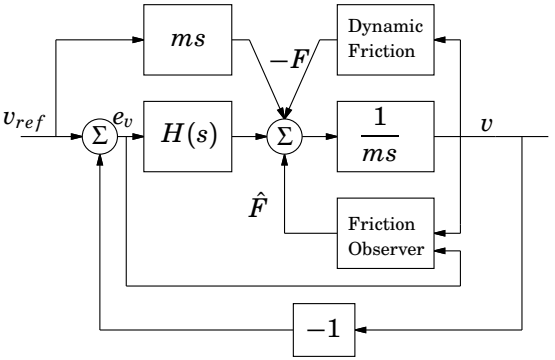

Figure 5.2 Block diagram for velocity control using a friction force observer.

where v_{ref} is the velocity reference, which is assumed to be differentiable, and $e_v = v_{ref} - v$ is the velocity error. The closed-loop system is represented by the block diagram in Figure 5.2. The control error e_v is used as the input e in (5.3). The control law results in the following equation for the control error when inserting (5.9) into (5.8).

$$E_v(s) = \frac{1}{ms + H(s)}(-\tilde{F}(s)) = -G(s)\tilde{F}(s) \tag{5.10}$$

Thus, the transfer function $G(s)$ relates the observer error and the control error. Using e_v as the input to the observer thus provides information about the observer error. By an appropriate choice of $H(s)$ and by utilizing the dissipativity of the observer we can give conditions for the convergence of the control error e_v to zero. In the proofs we use the following variant of the Kalman-Yakubovitch lemma.

LEMMA 5.1
Let A, B, C and D be a minimal realization of the transfer function $G(s)$, i.e.,

$$G(s) = C(sI - A)^{-1}B + D$$

If $G(s)$ is positive real and has no poles on the imaginary axis, then there exist matrices $P^T = P > 0$, L, and W such that

$$\begin{aligned} A^T P + PA &= -L^T L \\ PB &= C^T - L^T W \\ W^T W &= D + D^T \end{aligned}$$

Proof. The proof follows from the proof of Lemma 5.1 in Khalil (1992) by letting $\varepsilon = 0$. □

For the general case when the damping $\sigma_1(v)$ is velocity dependent but satisfies (5.4) we can now show the following theorem.

THEOREM 5.1
Consider the system (5.8) with friction (5.2), friction observer (5.3), and control law (5.9). The damping is assumed to satisfy (5.4). If $H(s)$ is chosen such that $G(s)$ is positive real, has no poles on the imaginary axis, and $\mathrm{Re}[G(i\omega)] > 0$ for $\omega > 0$, then the system is globally asymptotically stable in the sense that $e_v \to 0$ and all other states remain bounded. Furthermore, if $v_{ref} \neq 0$ then $\tilde{F} \to 0$.

Proof. Since $G(s)$ is PR and has no poles on the imaginary axis, there exist matrices $P > 0$ and L such that

$$\begin{aligned} \frac{d\xi}{dt} &= A\xi + B(-\tilde{F}) \\ e_v &= C\xi \end{aligned}$$

is a state-space realization of $G(s)$ and, further,

$$\begin{aligned} A^T P + PA &= -L^T L \\ PB &= C^T \end{aligned}$$

There is no D-matrix since $G(s)$ in (5.10) always has relative degree one if $H(s)$ is a proper transfer function. Now introduce the Lyapunov function

$$V(t) = \xi^T P \xi + \frac{\sigma_0}{k}\tilde{z}^2$$

This function is radially unbounded in the states ξ and $\tilde{z}$. Evaluating the

derivative of the Lyapunov function along the system trajectories, we find

$$\begin{aligned}
\frac{dV}{dt} &= \xi^T(A^TP + PA)\xi - 2\xi^T PB\tilde{F} + \frac{2\sigma_0}{k}\tilde{z}\frac{d\tilde{z}}{dt} \\
&= -\xi^T L^T L\xi - 2\xi^T C^T\tilde{F} + \frac{2\sigma_0}{k}\tilde{z}\frac{d\tilde{z}}{dt} \\
&= -\xi^T L^T L\xi - 2e_v\left(\sigma_0\tilde{z} + \sigma_1(v)\frac{d\tilde{z}}{dt}\right) + \frac{2\sigma_0}{k}\tilde{z}\frac{d\tilde{z}}{dt} \\
&= -\xi^T L^T L\xi - \frac{2}{k}\left(\frac{d\tilde{z}}{dt} + \frac{|v|}{g(v)}\tilde{z}\right)\left(\sigma_0\tilde{z} + \sigma_1(v)\frac{d\tilde{z}}{dt}\right) + \frac{2\sigma_0}{k}\tilde{z}\frac{d\tilde{z}}{dt} \\
&= -\xi^T L^T L\xi - \frac{2}{k}\left(\sigma_1(v)\frac{d\tilde{z}}{dt}^2 + \sigma_0\frac{|v|}{g(v)}\tilde{z}^2 + \sigma_1(v)\frac{|v|}{g(v)}\tilde{z}\frac{d\tilde{z}}{dt}\right) \\
&= -\xi^T L^T L\xi - \frac{2}{k}\left(\sigma_1(v)\left(\frac{d\tilde{z}}{dt} + \frac{|v|}{2g(v)}\tilde{z}\right)^2 + \frac{|v|}{g(v)}\tilde{z}^2\left(\sigma_0 - \frac{\sigma_1(v)|v|}{4g(v)}\right)\right) \\
&\leq 0
\end{aligned}$$

since $\sigma_1(v) \leq 4\sigma_0 g(v)/|v|$. This implies that the Lyapunov function is non-increasing and, since it is radially unbounded, it guarantees that all states are bounded. In order to apply La Salle's theorem we need to study the system solution on the subspace where $dV/dt = 0$, see Khalil (1992). We must then have $L\xi = 0$,

$$\sigma_1(v)\left(\frac{d\tilde{z}}{dt} + \frac{|v|\tilde{z}}{2g(v)}\right)^2 = 0 \tag{5.11}$$

and

$$\frac{|v|}{g(v)}\tilde{z}^2\left(\sigma_0 - \frac{\sigma_1(v)|v|}{4g(v)}\right) = 0 \tag{5.12}$$

The condition (5.12) is fulfilled if either $v = 0$ or $\tilde{z} = 0$. We investigate these conditions separately.

When $\tilde{z} = 0$ it follows that $\tilde{F} = 0$ and hence $e_v \to 0$ since $G(s)$ is asymptotically stable, see (5.10). Thus, both the control error and the estimation error goes to zero.

When $v = 0$ it follows from (5.5) that

$$\frac{d\tilde{z}}{dt} = ke_v$$

Since condition (5.11) must be fulfilled, it follows that $e_v \to 0$ unless

$\sigma_1(0) = 0$. If $\sigma_1(0) = 0$ the system is given by

$$\frac{d\xi}{dt} = A\xi + B(-\sigma_0\tilde{z})$$
$$\frac{d\tilde{z}}{dt} = kC\xi$$

This is an interconnection (negative feedback) of $\sigma_0 G(s)/k$ with an integrator, since $d\tilde{z}/dt$ is the output and $-\tilde{z}$ the input. We require that $\mathrm{Re}[G(i\omega)] > 0$ for $\omega > 0$ so this system is asymptotically stable. This follows from a simple argument. The total phase shift of the loop gain can be at most $-\pi$ and only for $\omega = 0$, which implies that $\tilde{z}$ would grow indefinitely if $d\tilde{z}/dt \neq 0$. The control error e_v must therefore tend to zero. We can, however, not guarantee that $\tilde{F} \to 0$ if $e_v = 0$. There is then no excitation of the observer.

From La Salle's theorem it now follows that $e_v \to 0$ and, further, if $v_{ref} \neq 0$ then also $\tilde{F} \to 0$. The only case where the observer error will not converge is when both the velocity and the reference velocity are zero. □

Remark 1. The required condition on $G(s)$ implies that we can handle integral action in $H(s)$. An integrator gives a zero at the origin in $G(s)$, which we allow with the special requirements on $G(s)$.

Remark 2. It is possible to guarantee that also $\tilde{F} \to 0$ by requiring that $G(s)$ is strictly positive real. Integral action can then not be included in $H(s)$. If $G(s)$ is strictly positive real then its static gain is different from zero so that $\tilde{F} \neq 0$ would imply that $e_v \neq 0$.

We will next treat the case when σ_1 is considered constant. This was also done in Canudas de Wit *et al.* (1995). However, the conditions for stability are here relaxed.

THEOREM 5.2
Consider the system (5.8) together with the friction model (5.2), the friction observer (5.3), and the observer-based control law (5.9). Assume that the damping is constant, i.e., $\sigma_1(v) = \sigma_1$. If $H(s)$ is chosen such that

$$G(s) = \frac{\sigma_1 s + \sigma_0}{ms + H(s)}$$

is positive real, with no poles on the imaginary axis, and $\mathrm{Re}[G(i\omega)] > 0$ for $\omega > 0$, then the velocity error will asymptotically go to zero and the other states will be bounded. Further, if $v_{ref} \neq 0$ then also $\tilde{F} \to 0$.

Proof. Since $G(s)$ is positive real and has no poles on the imaginary axis, there exist matrices $P > 0$, L, and W such that

$$\begin{aligned} \frac{d\xi}{dt} &= A\xi + B(-\tilde{z}) \\ e_v &= C\xi + D(-\tilde{z}) \end{aligned}$$

is a state-space realization of $G(s)$ and

$$\begin{aligned} A^T P + PA &= -L^T L \\ PB &= C^T - L^T W \\ W^T W &= D + D^T \end{aligned}$$

This follows from the Kalman-Yakubovich lemma. The relative degree of $G(s)$ is zero and, therefore, the state space description includes a D-matrix as opposed to the previous theorem. Introduce the radially unbounded Lyapunov function

$$V = \xi^T P \xi + \frac{\tilde{z}^2}{k}$$

Evaluating the derivative of the Lyapunov function along the system solution we get

$$\begin{aligned} \frac{dV}{dt} &= \xi^T (A^T P + PA)\xi - 2\xi^T PB\tilde{z} + \frac{2}{k}\tilde{z}\frac{d\tilde{z}}{dt} \\ &= -\xi^T (L^T L)\xi - 2\xi^T (C^T - L^T W)\tilde{z} + \frac{2}{k}\tilde{z}\left(-\frac{|v|}{g(v)}\tilde{z} + ke\right) \\ &= -\xi^T L^T L\xi - 2(e^T + D^T\tilde{z}^T)\tilde{z} + 2\xi^T L^T W\tilde{z} - \frac{2}{k}\frac{|v|}{g(v)}\tilde{z}^2 - 2e\tilde{z} \\ &= -(\xi^T L^T - \tilde{z}^T W^T)(L\xi - W\tilde{z}) - \frac{2}{k}\frac{|v|}{g(v)}\tilde{z}^2 \leq 0 \end{aligned}$$

The derivative is non-positive and hence the states ξ and $\tilde{z}$ are bounded. Stability can now be proved in the same manner as in Theorem 5.1 by considering the solutions on the subspace, where $dV/dt = 0$, and then by applying La Salle's Theorem.

The derivative dV/dt is zero if $L\xi = W\tilde{z}$ and if either $v = 0$ or $\tilde{z} = 0$. We investigate these conditions separately.

When $\tilde{z} = 0$ it follows, since $G(s)$ is asymptotically stable, that $\xi \to 0$ and in particular $e_v \to 0$.

When $v = 0$ it holds that $d\tilde{z}/dt = ke_v$ and the system is then given by

$$\frac{d\xi}{dt} = A\xi + B(-\tilde{z})$$
$$\frac{d\tilde{z}}{dt} = k(C\xi + D(-\tilde{z}))$$

This is an interconnection (negative feedback) of $G(s)/k$ with an integrator since $d\tilde{z}/dt$ is the output and $-\tilde{z}$ the input. We require that $\mathrm{Re}[G(i\omega)] > 0$ for $\omega > 0$ so this system is asymptotically stable. The total phase shift of the loop gain can be at most $-\pi$ and only for $\omega = 0$, which implies that $\tilde{z}$ would grow indefinitely if $d\tilde{z}/dt \neq 0$. The control error e_v must therefore tend to zero. If $e_v = 0$ we cannot assure that $\tilde{z} \to 0$. We have thus shown that $e_v \to 0$ and further that $\tilde{z} \to 0$ if $v_{ref} \neq 0$. □

Remark 1. The conditions on $G(s)$ are relaxed compared with Canudas de Wit *et al.* (1995), where it was required that $G(s)$ is strictly positive real. This implies that we allow $H(s)$ to include a pure integrator such as for a PI-controller. The integrator gives a zero at the origin in $G(s)$. This could not be included in the results in Canudas de Wit *et al.* (1995).

Remark 2. If $G(s)$ is strictly positive real, it is also possible to guarantee that $\tilde{z} \to 0$. The static gain of $G(s)$ is then zero and $e_v = 0$ then requires that $\tilde{z} = 0$.

Although both theorems have already been proved using Lyapunov techniques, we can gain better insight by considering the error equations (5.5) and (5.10). When introducing the observer we get a dissipative map from e_v to either $\tilde{F}$ or $\tilde{z}$. Adding the friction estimate to the control signal means

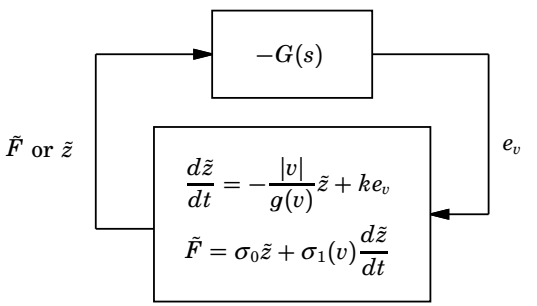

Figure 5.3 The block diagram in Figure (5.2) redrawn with e_v and $\tilde{z}$ as outputs of a linear and a nonlinear block respectively.

that the control error will be the output of a linear system operating on either $\tilde{F}$ or $\tilde{z}$. The closed loop consists of a linear system interconnected with a nonlinear dissipative system as seen in Figure 5.3. Such a system cannot be guaranteed to be asymptotically stable if we only require that $G(s)$ is positive real. By utilizing the extra terms that show up for the Lyapunov technique it was, however, possible to show convergence of the control error. If instead $G(s)$ is strictly positive real, stability follows directly from the passivity theorem.

5.5 Observer-Based Position Control

For position control it is natural to have an inner velocity control loop with friction compensation and an outer position control loop as shown in Figure 5.1. It is, however, also possible to have a single position-control loop that also performs the friction compensation. For the simple system (5.8) it is possible to prove a theorem similar to Theorem 5.2 if the damping σ_1 is assumed constant. The driving term ke in the friction observer (5.3) is then given by ke_p where $e_p = x_{ref} - x$, i.e., the position error. The desired reference x_{ref} is assumed to be twice differentiable. Now let

$$U(s) = H(s)E_p(s) + \hat{F} + ms^2X_{ref}(s) \tag{5.13}$$

The closed-loop system is represented by the block diagram in Figure 5.4. With the observer-based friction compensation, we achieve position tracking as shown in the following theorem.

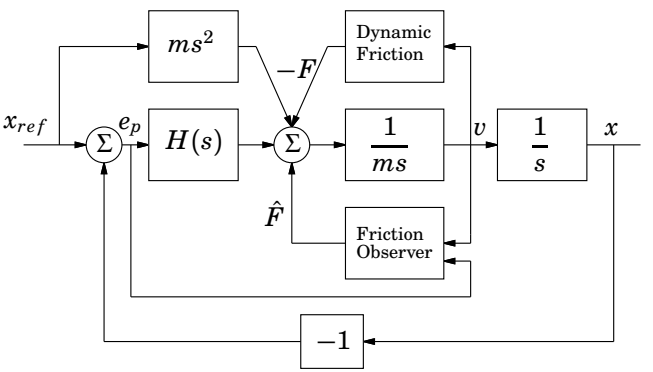

Figure 5.4 Block diagram for position control using a friction observer.

THEOREM 5.3
Consider the system (5.8) together with the friction model (5.2), the friction observer (5.3), and the control law (5.13). Assume that the damping is constant, i.e., $\sigma_1(v) = \sigma_1$. If $H(s)$ is chosen such that

$$G(s) = \frac{\sigma_1 s + \sigma_0}{ms^2 + H(s)}$$

is strictly positive real, then the observer error, $\tilde{F} = F - \hat{F}$, and the position error, e_p, will asymptotically go to zero.

Proof. The control law yields the following equations:

$$E_p(s) = \frac{1}{ms^2 + H(s)}\left(-\tilde{F}(s)\right) = \frac{\sigma_1 s + \sigma_0}{ms^2 + H(s)}\left(-\tilde{z}(s)\right) = -G(s)\tilde{z}(s)$$

$$\frac{d\tilde{z}}{dt} = -\frac{|v|}{g(v)}\tilde{z} + ke_p$$

Now introduce

$$V = \xi^T P \xi + \frac{\tilde{z}^2}{k}$$

as a Lyapunov function. Since $G(s)$ is strictly positive real, there exist matrices $P = P^T > 0$ and $Q = Q^T > 0$ such that

$$\frac{d\xi}{dt} = A\xi + B(-\tilde{z})$$
$$e_p = C\xi$$

is a state space representation of $G(s)$ that has relative degree one for a proper $H(s)$. Further,

$$A^T P + PA = -Q$$
$$PB = C^T$$

Now

$$\frac{dV}{dt} = -\xi^T Q \xi - 2\xi^T PB\tilde{z} + \frac{2}{k}\tilde{z}\frac{d\tilde{z}}{dt} = -\xi^T Q \xi - 2e\tilde{z} + \frac{2}{k}\tilde{z}\left(-\frac{|v|}{g(v)}\tilde{z} + ke\right)$$

$$= -\xi^T Q \xi - \frac{2}{k}\frac{|v|}{g(v)}\tilde{z}^2 \leq -\xi^T Q \xi$$

The radial unboundedness of V together with the semi-definiteness of dV/dt implies that the states are bounded. The derivative dV/dt is zero when $\xi = 0$. This implies that $e_p = 0$. Since $G(s)$ is strictly positive real, we also have $\tilde{z} \to 0$. We can now apply La Salle's theorem, which concludes the proof. □

Remark 1. It is possible to relax the strictly positive real condition on $G(s)$ in the same way as in Theorem 5.2.

Remark 2. Note that the theorem can only be proved if $\sigma_1(v)$ is constant. If $G(s)$ instead describes the map between $\tilde{F}$ and e_p, the relative degree becomes two for a proper $H(s)$. The transfer function $G(s)$ can then not be strictly positive real.

5.6 Control Design

The conditions we have given so far guarantee stability of the closed-loop system. In, for example, Theorem 5.1 the requirement is that the transfer function $H(s)$ should be chosen such that

$$G(s) = \frac{1}{ms + H(s)}$$

is positive real with no poles on the imaginary axis and, further, such that $\mathrm{Re}[G(i\omega)] > 0$ for $\omega > 0$. In an actual design there are, of course, other factors than stability that have to be considered. There is, however, considerable freedom in the choice of $H(s)$. For example, the PI controller $H(s) = K(1 + 1/sT_i)$ gives

$$G(s) = \frac{s}{ms^2 + Ks + k/T_i}$$

which fulfills the condition for all $K > 0$ and $T_i > 0$. A PID controller gives

$$G(s) = \frac{s}{(m + T_d)s^2 + Ks + K/T_i}$$

which also satifies the condition for all positive controller parameters. The requirements for stability thus allows a wide range of design considerations.

The model-based friction compensation with a friction-force observer for velocity control will now be investigated in an example.

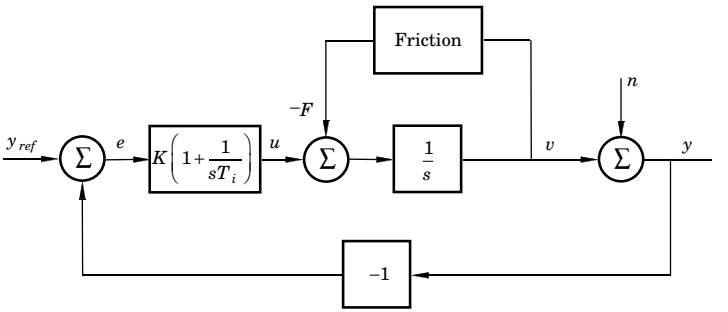

Figure 5.5 A block diagram showing the example of velocity control.

5.7 An Example

Consider the velocity control problem shown in Figure 5.5. The system is subjected to a velocity disturbance n and is described by

$$\frac{dv}{dt} = u - F \tag{5.14}$$
$$y = v + n$$

It can, for instance, describe a telescope where the disturbances are vibrations in the foundation. This problem is treated in the classical paper Gilbart and Winston (1974), which uses a similar model. The variable v is the relative velocity between the foundation and the telescope and thus the velocity associated with the friction interface.

Disturbance: The disturbance is a perturbation in the velocity. The aim of the control loop is to keep y at zero (assuming $y_{ref} = 0$). Most difficulties occur when the velocity disturbance fluctuates around zero where the friction force changes substantially. Therefore, to test the ability of the control system it is desirable that the disturbance n crosses zero relatively often during the test period. The DC component is, therefore, removed so that the realization will not drift away from zero. This is done by the filter

$$H_n(s) = 250\,\frac{s^2}{(s+0.2)^4}$$

which also gives high frequency roll-off. The input to the filter is white noise with unit variance. The disturbance $n(t)$ has a power spectrum with a peek at 0.2 rad/s as seen in Figure 5.6. For comparison, the same realization of the disturbance will be used in all simulations. For the test period $t = 0$ to 100 it is shown in Figure 5.7. The distribution of the disturbance sampled every 0.1 s is shown in Figure 5.8.

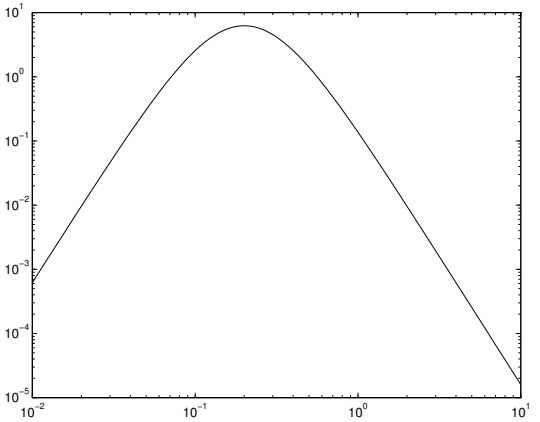

Figure 5.6 The power spectrum of the disturbance $n(t)$ in the velocity control example.

Linear Controller: A PI-controller normally suffices for a velocity servo. This controller structure is a reasonable choice. The integral action can, for example, handle load disturbances. Note that it is not the optimal controller for the particular disturbance in the sense that it does not achieve minimum variance of the control error. We let the control signal by given by

$$u_{PI}(t) = K\left(e(t) + \frac{1}{T_i}\int^{t} e(\tau)d\tau\right)$$
$$e(t) = y_{ref} - y$$

where the controller parameters are $K = 4$ and $T_i = 0.25$. This gives the closed-loop characteristic polynomial $s^2 + 4s + 16$. The sensitivity function of the closed loop is shown in Figure 5.9. The peek value is $|S|_{\max} = 1.13$. It has appropriate damping at the frequency range of the disturbance n and should therefore reject the disturbance well. The reference y_{ref} will be zero in all the simulations and therefore $e = -y$.

Friction Model and Friction Observer: The friction force in (5.14) is

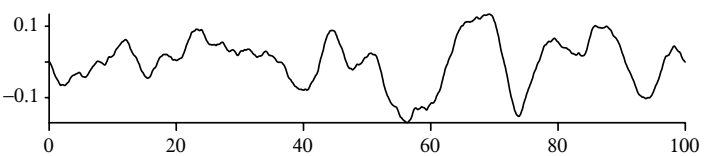

Figure 5.7 The disturbance realization n used in all simulations of the example.

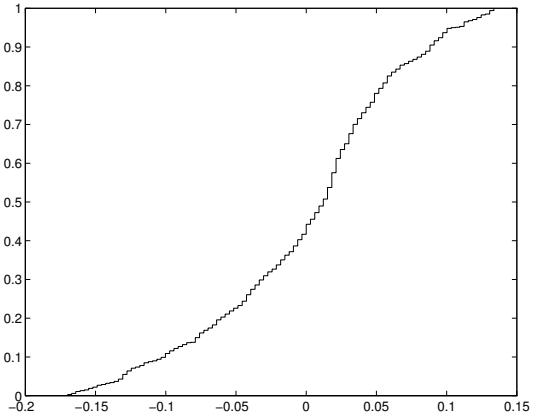

Figure 5.8 The velocity distribution of the disturbance n. For approximately 10% of the time the disturbance is within the interval defined by $\pm v_S = \pm 0.01$.

given by the simplified standard model (3.11) with parameters $\sigma_0 = 1000$, $\sigma_1 = 2 \cdot \sqrt{1000}$, $F_v = 0$, and $g(v) = F_C + (F_S - F_C)e^{-(v/v_S)^2}$ with $F_S = 0.4$, $F_C = 0.2$, and $v_S = 0.01$. These are default parameters in this chapter and are used unless otherwise specified. The Stribeck velocity of the friction is given by $v_S = 0.01$ and, hence, the disturbance is within the most problematic region approximately 10% of the time, see Figure 5.8. The friction observer is given by (5.3). It uses the same parameters as the friction model unless explicitly stated. The default value of the gain is $k = 0.2$. With the PI controller the total control signal becomes

$$u(t) = u_{PI}(t) + \hat{F}(t) = K\left(e(t) + \frac{1}{T_i}\int^t e(\tau)d\tau\right) + \hat{F}(t) \tag{5.15}$$

To determine stability of the closed loop we investigate the transfer function $G(s)$ in Theorem 5.2 relating the estimation error $\tilde{z}$ to the control error e_v. This becomes

$$G(s) = \frac{s(\sigma_1 s + \sigma_0)}{ms^2 + Ks + K/T_i} \tag{5.16}$$

which has a zero at the origin. If $K > 0$, $T_i > 0$ and $\sigma_0/\sigma_1 > 1/T_i$ the system satisfies the conditions of Theorem 5.2. With the nominal values this is fulfilled. Asymptotic convergence of the control error is thus assured in the disturbance free case if the parameters of the friction model are known. Using the example we will investigate how the observer-based

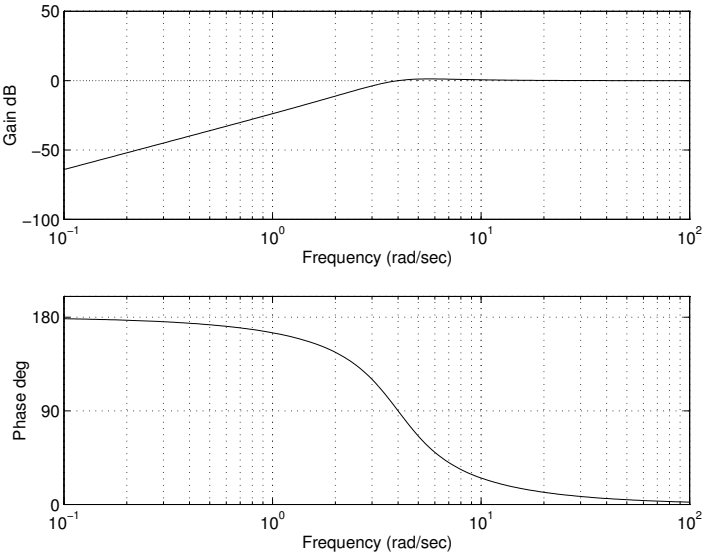

Figure 5.9 The sensitivity function of the closed linear loop.

friction compensation behaves for disturbances, different observer gains, model errors, etc.

The reference velocity in the example is zero which means that the feed-forward term mdv_{ref}/dt in the control law (5.9) is zero. The disturbance $n(t)$, however, causes a motion that must be compensated. The problem is equivalent to tracking a reference without using the feed-forward term. The control error and observer error can, therefore, not be guaranteed to converge.

Performance Criteria: Different criteria are used to evaluate the control performance and in particular the friction compensation. A common measure in the literature is the root-mean-square error of the control performance given by

$$e_{rms} = \sqrt{\frac{1}{T}\int_0^T e^2(\tau)d\tau}$$

or the largest control error

$$e_{max} = \max_t |e(t)|$$

In addition to these criteria we also study the distribution of the control error. It is therefore sampled every 0.1 s giving the error sequence $\{e(k)$,

$k = 1, 2, \ldots, 1000\}$. The distribution is determined by examining the sampled error. The result is plotted as a histogram with 100 equally spaced bins between the largest positive and negative errors. The accumulated distribution of the error is shown in a separate diagram. For comparison, we also show the normal distribution given by both the empirical variance of the error, i.e., with

$$\mu_{data} = \frac{1}{N} \sum_{k=1}^{N} e(k)$$

$$\sigma_{data} = \frac{1}{N-1} \sum_{k=1}^{N} (e(k) - \mu_{data})^2$$

and by a normal distribution fitted to the distribution of the errors around zero. This can be done by determining the center slope of the accumulated distribution which gives the standard deviation σ_{center}. With these two normal distributions it is possible to judge how close the error is to being normally distributed. The information revealed by the distribution will be clear when effects of friction are considered. The error magnitudes for the 90th, 95th, and 97.5th percentiles are also given. For a normal distribution these magnitudes are 1.3σ, 1.65σ, and 1.96σ, respectively. This information is shown in Table 5.1, which summarizes the results at the end of the section.

Nominal Cases

When investigating the merits of the observer-based friction compensation we compare the results with two nominal cases without friction compensation.

Without Friction: The first case is the friction free case which is shown in Figure 5.10. As can be seen the disturbance is effectively rejected by the control system. The control error is of high frequency compared to the closed loop bandwidth. Figure 5.11 shows the histogram and accumulated distribution of the control errors. The error is approximately in the range $(-0.01, 0.01)$. The error distribution agrees very well with a normal distribution with $\mu = 0$ and $\sigma = 0.00312$ as is expected.

With Friction: If friction is added without any friction compensation, the performance deteriorates. In particular, we notice large control errors at the times when v passes zero, see Figure 5.12. These glitches in the error are typical. They have also been observed experimentally;, see, for example, Tung *et al.* (1991) and Baril (1993). Figure 5.13 shows the error

distribution. The errors are in the range $(-0.06, 0.05)$ but about 70% of them are in the range $(-0.01, 0.01)$, which was the range for the friction free case. The distribution is characterized by long tails, which makes it deviate substantially from a normal distribution. Approximately 60% of the data agree with the normal distribution determined by the center slope of the distribution. Most of the friction is compensated by the integral action but this fails as the velocity approaches and crosses zero.

We will now explore how the control performance changes with the observer based friction compensation method. We start with the case when the parameters of the friction model are known.

Perfect Model Knowledge

Figure 5.14 shows the observer-based friction compensation with the observer gain $k = 0.2$. The observer tracks the friction force quite accurately despite the disturbance and the resulting compensation, therefore, resembles the friction-free case. This is confirmed by the distribution of the error, shown in Figure 5.15, which agrees with Figure 5.11. The performance is in fact improved slightly compared with the friction-free case, since the observer also compensates for some of the disturbance. The extra compensation is done through the friction observer by the term ke_v. This is even more apparent if the gain is increased to $k = 2$. The results are shown in Figures 5.16 and 5.17. For the higher gain the friction observer interprets some of the disturbance as friction and therefore has a more irregular friction estimate. In this manner part of the disturbance is compensated by the nonlinear friction observer. Remember that the PI controller was not optimal for the particular disturbance. The feedback through the observer implies that the closed loop, however, exhibits a nonlinear behavior, which is seen clearly in the error distributions.

Model Errors

Since friction depends on so many factors, it is unrealistic to assume that the friction model and parameters are perfectly known. It is vital that the friction compensation scheme works well even for errors in the model. It is also useful to consider adaptation of the parameters in the friction model.

Stiffness σ_0***:*** We first consider errors in the stiffness of the observer model. This implies that the dynamics of the friction estimate will not agree with the true friction. The speed of the dynamics affects the friction behavior to a large extent when approaching and crossing zero velocity, i.e., for the Stribeck effect as well as the response speed of the friction force to a change in motion direction. If σ_0 of the observer is decreased

from 1000 to 10 and σ_1 from $2\sqrt{1000}$ to $2\sqrt{10}$, we get the results shown in Figure 5.18. These values also violates the stability conditions of Theorem 5.2. The observer does not follow the friction force when the direction of motion changes. This causes a large control error. There is also a backlash in the error after the zero crossing, which is even larger than the error at the crossing. This is discussed further in Section 5.8. The distribution in Figure 5.19 shows very long and flat tails. Approximately 60% of the data agree with a normal distribution having the center slope. It should also be pointed out that the performance has deteriorated compared to the case with no friction compensation shown in figures 5.12 and 5.13. A higher gain in the observer improves the performance.

Stribeck Velocity v_S***:*** Figures 5.20 and 5.21 show the results when there is a mismatch in the Stribeck effect. This is achieved by letting the Stribeck velocity of the observer be $v_S = 0.0001$ instead of 0.01. It implies that the friction force will be underestimated for small nonzero velocities. The static friction F_S is, however, correctly estimated. The result is a slightly increased error at the times close to the zero crossings of the velocity. The error distribution, therefore, gets longer tails but the distribution is still almost normal and the performance is acceptable. It is important that the friction estimate at the zero crossing is correct and for very low velocities the observer and the true friction agrees.

Friction Levels F_S ***and*** F_C***:*** We next consider the case when the steady-state levels of the friction force are mismatched. This is done by scaling the parameters F_S and F_C.

Figures 5.22 and 5.23 show the result when the observer levels are increased by 50% compared to the true friction, i.e., $F_S = 0.6$ and $F_C = 0.3$. The gain of the observer is $k = 0.2$. The integral action of the PI controller compensates for the error in the friction-force estimate during longer periods with unidirectional motion. However, when the direction of motion changes, the mismatch results in an over-compensation of the friction force until the integral action has responded. This leads to a large control error occuring mainly after the zero crossing. Note that the control error has the opposite sign compared to the error in the case of no friction compensation shown in Figure 5.12.

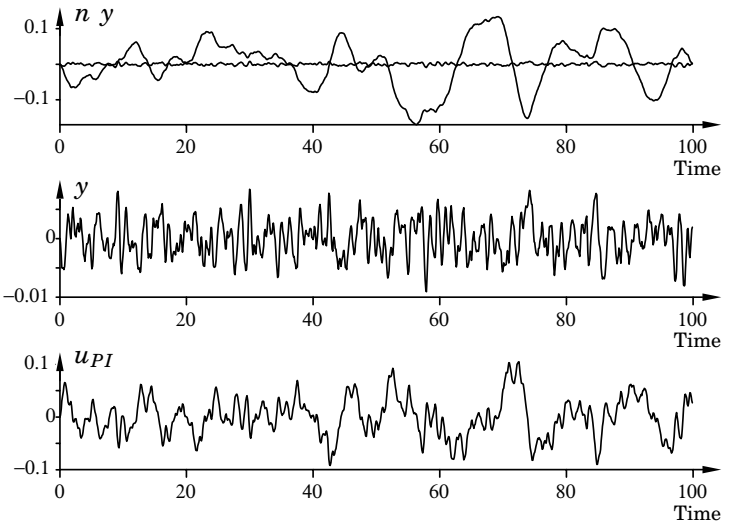

Figure 5.10 Simulation of the velocity control example without friction. The disturbance is well rejected by the PI controller.

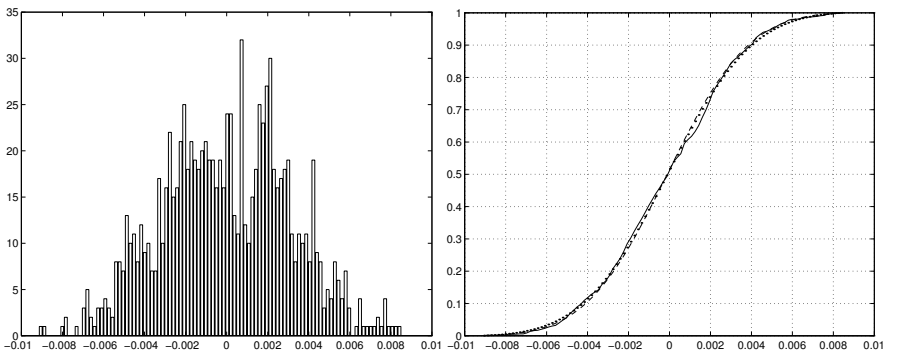

Figure 5.11 Histogram over the error distribution and the accumulated distribution of the error. The solid line shows the distribution of the error. The dashed line shows the normal distribution based on the empirical mean and standard deviation. The dotted line shows the normal distribution, which corresponds to the center-most errors. It is thus fitted to the slope of the solid line at zero error.

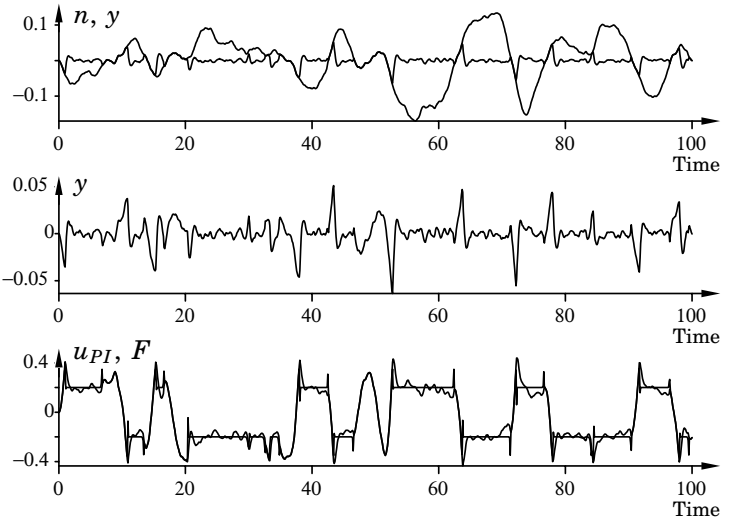

Figure 5.12 The performance deteriorates if friction is present. The main problem is the large control errors that the friction causes as the direction of motion changes. During the longer periods of unidirectional motion the error is no larger than in the friction free case. Compare with Figure 5.10 which shows the results without friction.

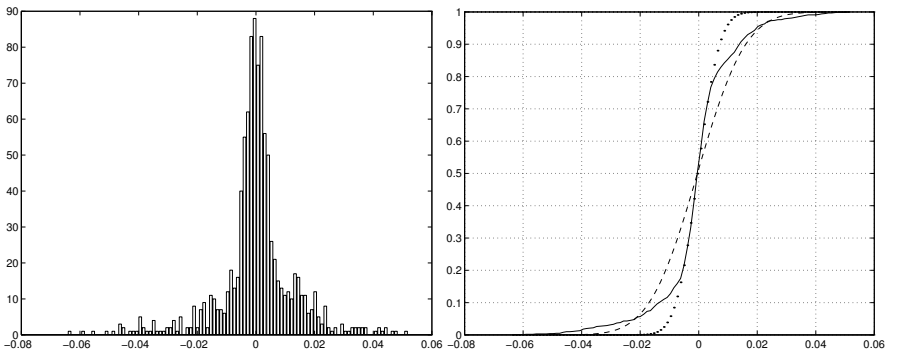

Figure 5.13 Histogram over the error distribution when friction is present. Also shown is the accumulated distribution of the error. For comparison, normal distributions based on both the experimental variance (dashed) and the slope of the distribution for small errors (dotted) are shown. The accumulated distribution deviates significantly from a normal distribution due to its long tails. These errors are due to the friction when changing direction of motion.

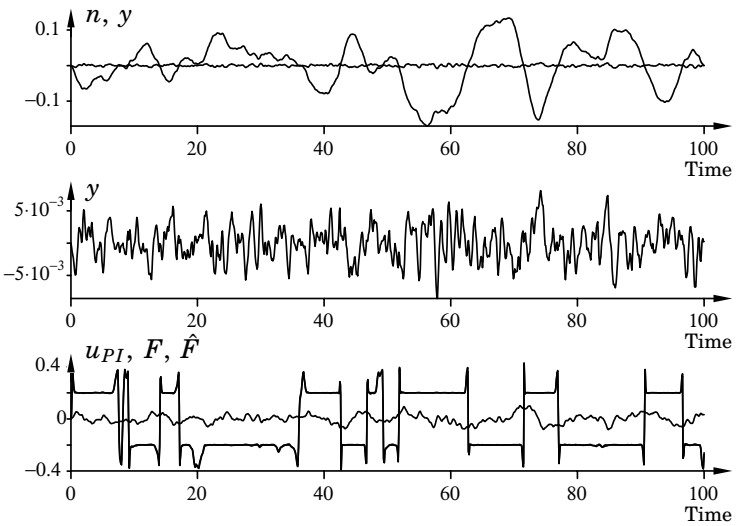

Figure 5.14 Friction compensation using the observer. The observer gain has been $k = 0.2$ and the observer parameters agrees with the true friction. The friction compensation is successful and cancels the friction force leading to an error which is behaving as in the friction free case.

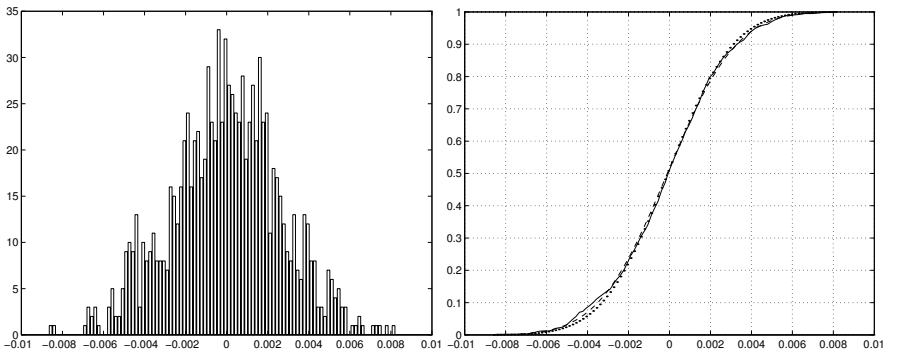

Figure 5.15 Distribution for the error when compensating friction with the observer. The observer parameters agrees with the true friction and the gain is $k = 0.2$. The accumulated distribution is shown together with normal distributions based on both the experimental standard deviation (dashed) and the slope of the experimental distribution for small errors (dotted). The distribution agrees well with a normal distribution as was the case when no friction was present.

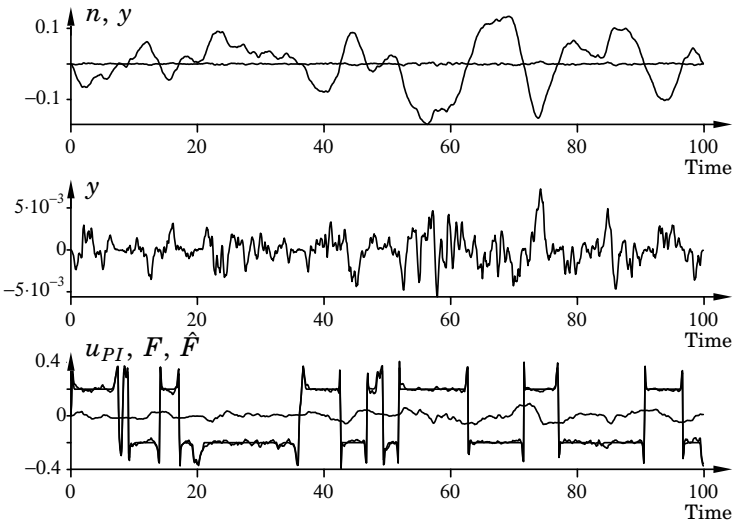

Figure 5.16 Friction compensation using the observer with a higher gain $k = 2$. The parameters agree with the true friction. The friction estimate is more irregular in this case but this actually leads to a compensation of the disturbance.

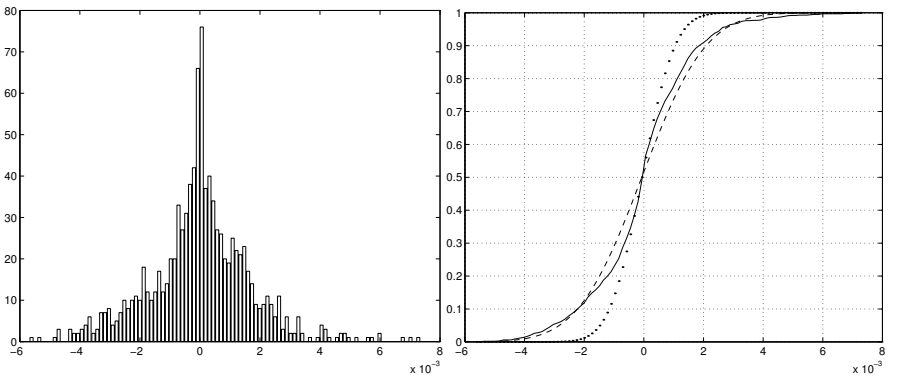

Figure 5.17 Distribution of the control error in Figure 5.16. Normal distributions based on the experimental standard deviation (dashed) and slope of the error distribution for small errors (dotted) are also shown. The distribution deviates from a normal distribution due to the high nonlinear feedback obtained through the observer.

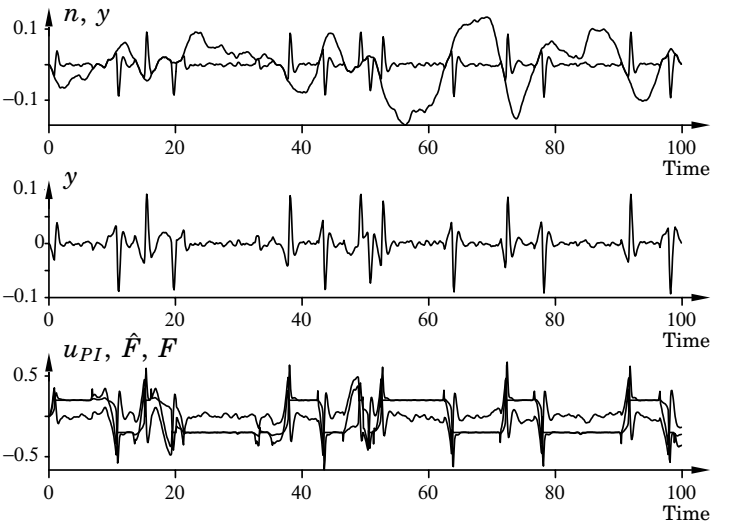

Figure 5.18 Friction compensation based on an observer with mismatched stiffness. In this case the stiffness is $\sigma_0 = 10$, which should be compared with 1000 which is the stiffness of the true friction. The damping is $\sigma_1 = 2\sqrt{10}$. The observer gain is $k = 0.2$. The static levels of the friction force agrees with the true friction but the dynamics are much slower. This gets manifested when the motion changes direction. For those intervals the friction estimate deviates significantly from the true friction.

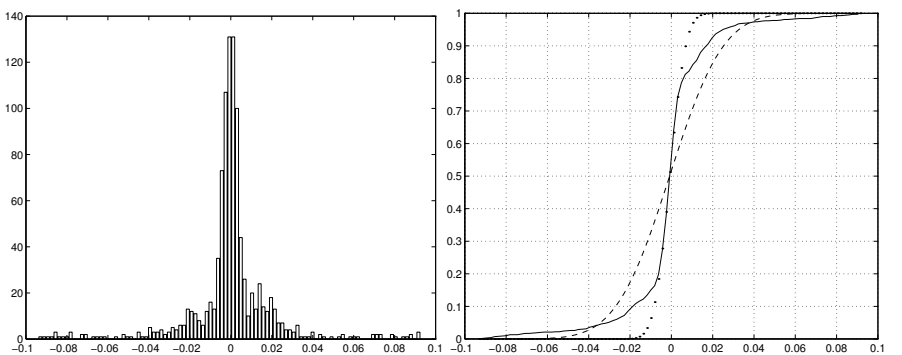

Figure 5.19 The distribution of the error in Figure 5.18. The distribution has very long tails due to the errors in the friction estimate.

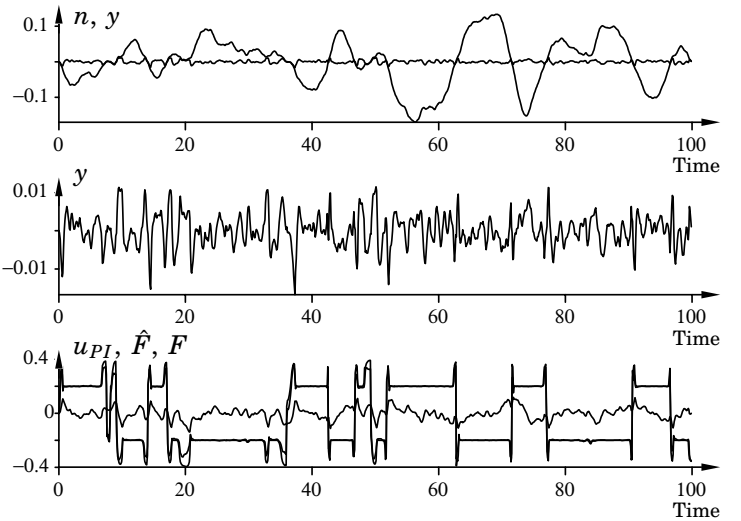

Figure 5.20 Observer-based friction compensation when the Stribeck is mismatched. This is done by letting $v_s = 0.0001$ compared to 0.01 for the friction. It implies that the true friction starts to increase earlier when zero velocity is approached. The friction is, however, correctly modeled for extremely low velocities.

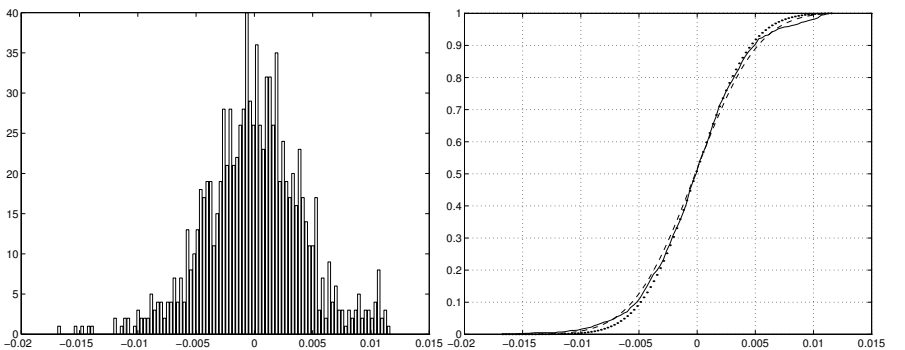

Figure 5.21 The error distribution associated with the simulation in Figure 5.20.

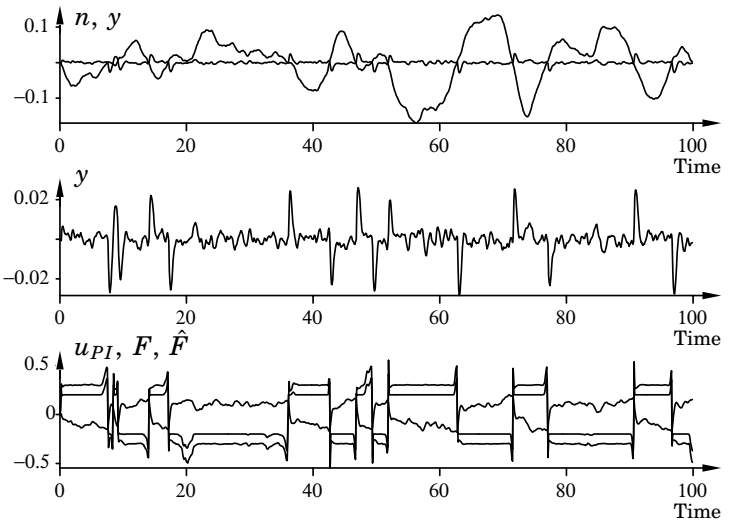

Figure 5.22 Observer based friction compensation when the steady state friction force of the observer is 50% higher than the true friction. The gain has been $k = 0.2$. The over-compensation causes large control errors after a zero velocity crossing has occurred.

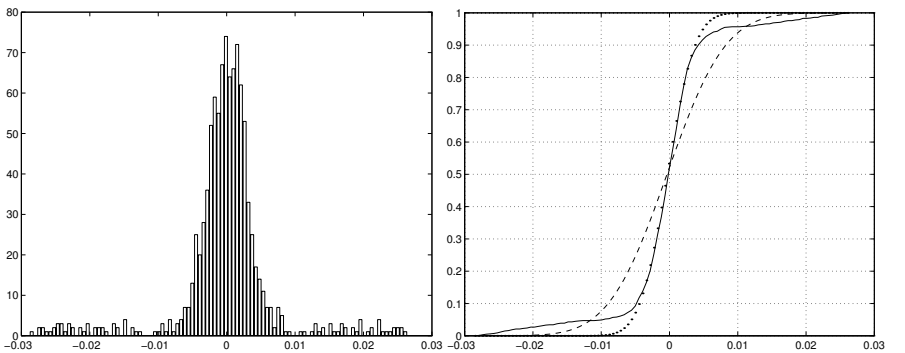

Figure 5.23 The error distribution corresponding to the simulation in Figure 5.22. The distribution is very flat for errors larger than 0.01 in magnitude.

Approximately 80% of the errors agree with the normal distribution. The errors can be reduced by increasing the gain k of the observer.

If instead the steady-state friction is underestimated by 50%, as when $F_S = 0.2$ and $F_C = 0.1$ in the observer, we get the results shown in Figures 5.24 and 5.25. This resembles the case without friction compensation but with a better performance. The errors primarily occurs after the zero crossings, since some of the Stribeck friction is still compensated for. The sign of the errors agrees with those achieved without friction compensation, since the friction force is underestimated.

Compensation Using a Coulomb model

For comparison, we also show the results when using a Coulomb friction model for the compensation, i.e., $\hat{F} = F_C \operatorname{sgn}(v)$. This is the most common form of friction compensation. The results in Figures 5.26 and 5.27 are similar to those without friction compensation. The performance is, however, improved since we get an immediate switch in the control signal from the friction estimate when the velocity changes sign. The inability to predict the stiction force has the effect that sticking still occurs during the zero crossing. The control error is therefore quite substantial. Note that if the friction model with stiction (2.6) is used as the basis for friction compensation, then it must be possible to exactly detect zero velocity. This leads to large practical problems. A friction estimate based on (2.6) is therefore hard to use. A remedy is to have logic that detects if sticking occurs and increases the friction estimate to $\pm F_S$ if motion is commanded.

It is interesting to note that even with large model errors the closed loop is well behaved and stable. With a high observer gain the friction estimate becomes more sensitive to disturbances, whereas for low gains a smoother estimate is obtained. The observer then puts most of the emphasis on the built-in model. The results of the different cases are summarized in Table 5.1.

5.8 The Error Signal

In the previous section we draw conclusions from the statistics of the control error. We only considered the distribution of the sampled error. More information is, however, available in the error signal. We, therefore, study the control error for a time interval where the velocity at the friction interface crosses zero. This happens for example in the interval $70 \leq t \leq 80$, see Figure 5.7. We discuss the behavior of control error, velocity, friction, and friction estimate in detail.

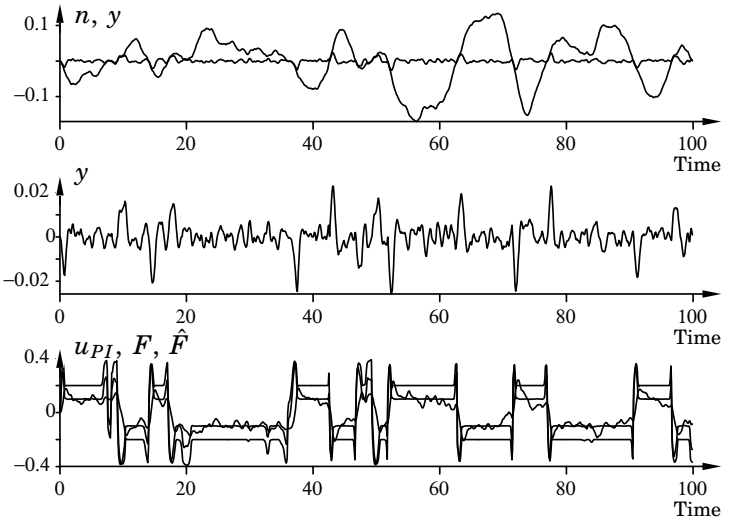

Figure 5.24 Observer-based friction compensation when the steady-state friction force of the observer is 50% lower than the true friction. The gain has been $k = 0.2$. The under-compensation results in a control error, which resembles the error when no compensation is done. The errors are, however, reduced by approximately a factor two.

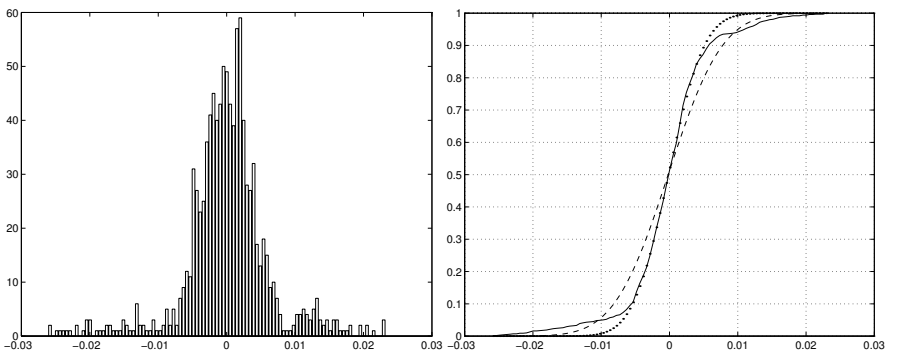

Figure 5.25 The error distribution corresponding to the simulation in Figure 5.24. The 10% largest errors deviates from the normal distribution. This corresponds to the errors larger than 0.006 in magnitude.

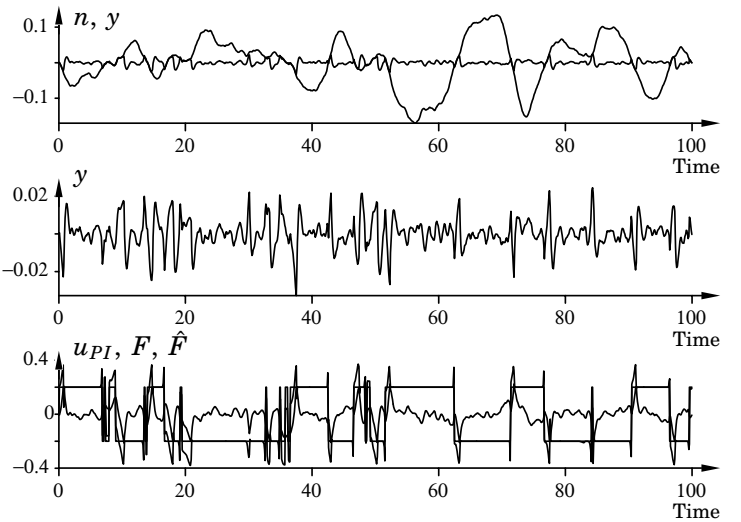

Figure 5.26 Friction compensation using a Coulomb friction model. Note that the observer (5.3) is not used in this case. The result is similar to the under-compensation in Figure 5.24.

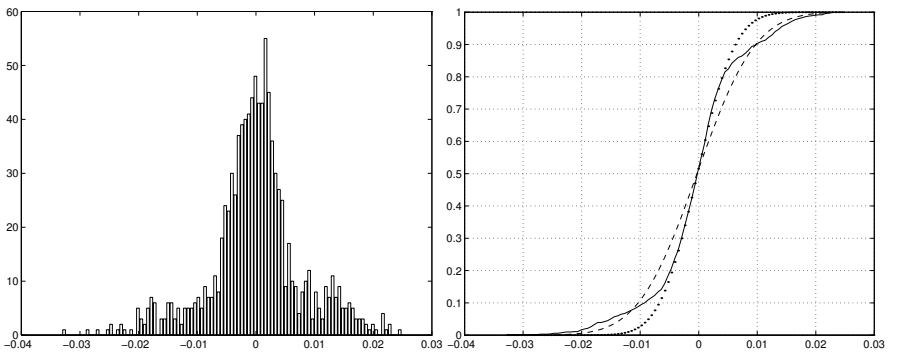

Figure 5.27 Error distribution for friction compensation using a Coulomb model. The distribution has longer tails than a normal distribution. This is caused by the friction-induced errors at the zero crossings of the velocity.

	σ_{center}	σ_{data}	% Gaussian	90th percentile (1.3σ)	95th percentile (1.65σ)	97.5th percentile (1.96σ)
Case 1	0.00326	0.00312	100	0.0041	0.0050	0.0058
Case 2	0.00638	0.01290	60	0.0144	0.0202	0.0301
Case 3	0.00251	0.00265	100	0.0035	0.0045	0.0051
Case 4	0.00086	0.00169	30	0.0021	0.0029	0.0037
Case 5	0.00597	0.02040	60	0.0165	0.0272	0.0451
Case 6	0.00371	0.00425	80	0.0050	0.0069	0.0090
Case 7	0.00318	0.00673	80	0.0045	0.0083	0.0190
Case 8	0.00410	0.00622	80	0.0057	0.0108	0.0148
Case 9	0.00508	0.00785	70	0.0099	0.0142	0.0177

Table 5.1 Summary of the results for the various cases of friction compensation. Case 1) Without friction; Case 2) With friction; Case 3) Ideal observer with $k = 0.2$; Case 4) Ideal observer with $k = 2$; Case 5) Slow observer dynamics, $\sigma_0 = 10$, $\sigma_1 = 2\sqrt{10}$; Case 6) Mismatched Stribeck effect, $v_S = 0.0001$; Case 7) Over-compensation, $F_S = 0.6$ and $F_C = 0.3$; Case 8) Under-compensation, $F_S = 0.2$ and $F_C = 0.1$; Case 9) Compensation using Coulomb model

Friction is not a big problem for unidirectional motion with relatively large velocities. The friction force will vary slowly with time. It essentially acts as a constant load disturbance and can therefore be handled by integral action. When the velocity comes closer to zero, and particularly when it crosses zero, friction changes rapidly with time. An accurate friction model can then be very useful.

The control algorithm cancels all effects of friction for ideal friction compensation. Since there will always be model errors, parameter drift and other conditions that change, any error in the friction estimate give an accelerating or decelerating force that causes a control error. By studying the control error during the velocity crossing it is possible to detect errors in the friction model. This is also useful for adaptive control.

Nominal Cases

We first consider the nominal cases without friction compensation.

Without Friction: For the nominal case with no friction, the error is Gaussian and there is no correlation with the zero crossings as seen in Figure 5.28. The top diagram shows the disturbance, the output y, and the velocity at the friction interface. The mid diagram shows the control error, and the bottom diagram shows the control signal from the PI controller, the friction force, and the friction force estimate.

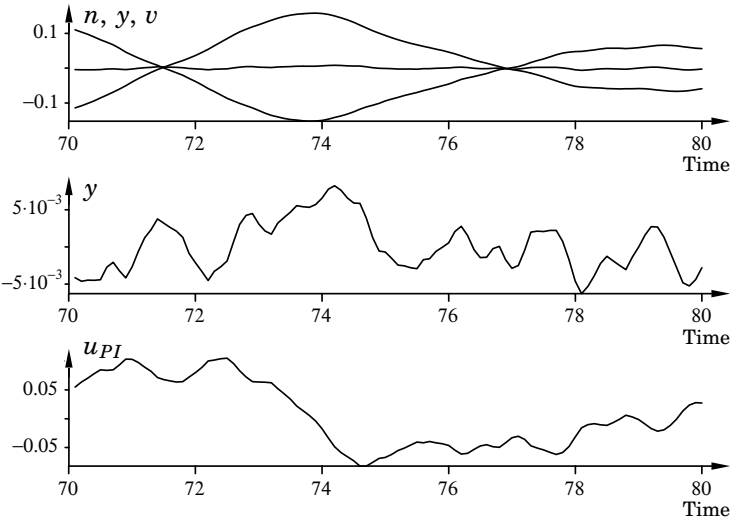

Figure 5.28 The simulation between $t = 70$ and $t = 80$ of the system when no friction is present. No correlation between the error and the velocity crossings can be seen.

With Friction: If friction is included, we get the typical characteristics shown in Figure 5.29. The error is small during the unidirectional motion, where it is compensated by the integral action. As the velocity approaches zero the Stribeck effect leads to an increased friction force and hence an increased control error. This takes place before zero velocity is reached. Sticking normally occurs as the velocity reaches zero. A large control force is necessary in order to initiate motion again. This has to be generated by the linear controller either by a large control error or by the integral action. This takes some time and we therefore have sticking for a period during which the control error may become large. If the velocity should go from negative to positive, the error $e = -y$ will be large and positive for a time after the zero crossing.

Observer-Based Friction Compensation

We now study the control error in detail for the observer-based friction compensation.

Perfect Model Knowledge: We start by looking at the control error for the case when the true model is used in the observer with gain $k = 0.2$. Figure 5.30 shows the results. In this case the error is small and there is no correlation between the error signal and the zero crossings. This

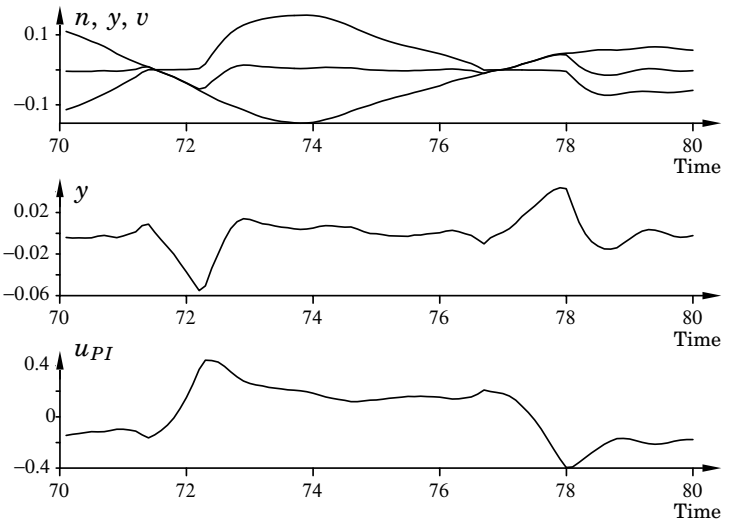

Figure 5.29 When the system includes friction without compensation, the error behavior around the zero-velocity crossing is clear. The error appears shortly before the crossing due to the Stribeck effect but becomes even larger as the motion should change direction.

is as expected since the true model is used. The error agrees with the friction-free case.

Friction Levels F_S and F_C: Next we look at the results when the friction levels F_S and F_C of the observer are incorrect. If friction is over-compensated as when $F_S = 0.6$ and $F_C = 0.3$, we get the results shown in Figure 5.31. Integral action will take care of the error in the friction estimate up to the time of the zero crossing. The friction force estimate then changes rapidly as the velocity changes sign. This leads to an extra accelerating torque and a control error. Note that in this case the control error $e = -y$ is negative after a zero crossing from negative to positive velocities.

For the case of under-compensation with $F_S = 0.2$ and $F_C = 0.1$ the result is the opposite as seen in Figure 5.32. A large positive error $e = -y$ occurs when the velocity goes from negative to positive. It thus resembles the case without friction compensation. Note, however, that the control error is small up to the time of the zero crossing since the Stribeck effect is still mostly compensated by the change in the friction estimate in the observer.

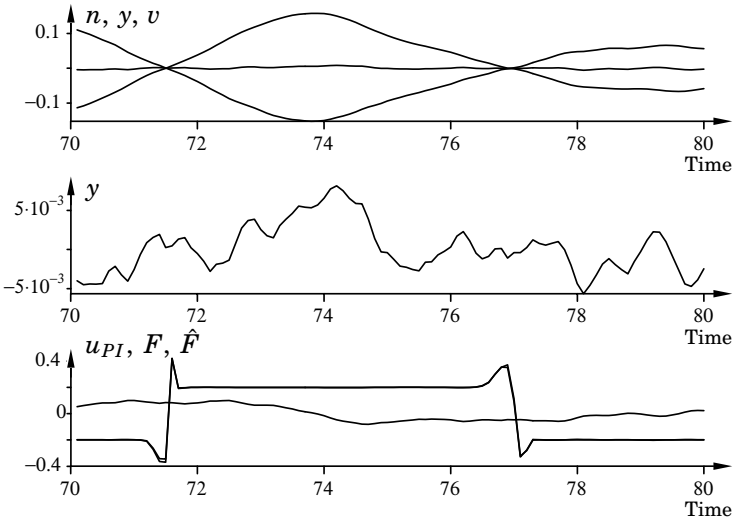

Figure 5.30 When observer-based friction compensation is done with the correct model parameters, the error shows no correlation with the zero-velocity crossings.

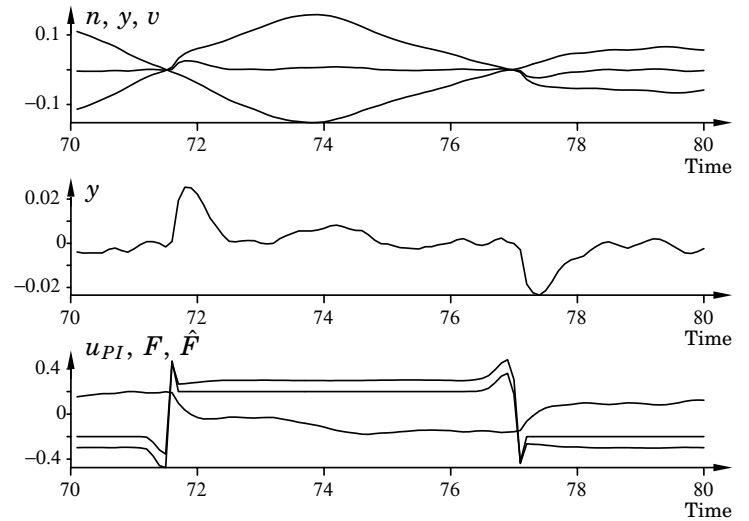

Figure 5.31 Over-compensating the friction force results in an accelerating force as zero velocity is passed. This results in a typical error that has the opposite sign compared to the case without friction compensation.

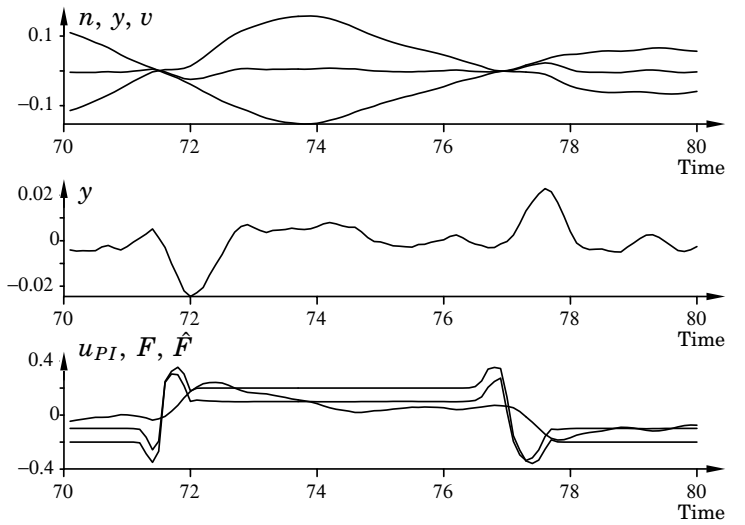

Figure 5.32 Under-compensating the friction force results in an error that resembles the case without compensation, although the size of the error is reduced by approximately a factor two.

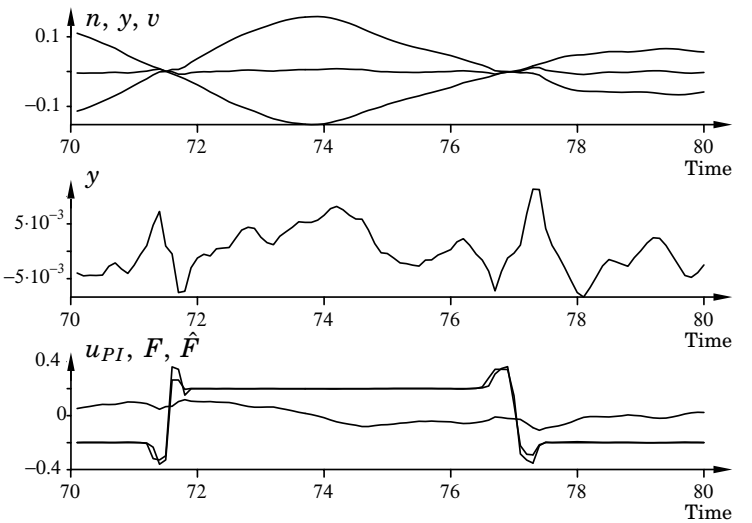

Figure 5.33 If the Stribeck effect is under-estimated this results in a control error, which is almost antisymmetric with respect to the zero crossing. Note that the friction force at and immediately around the zero crossing is correctly estimated.

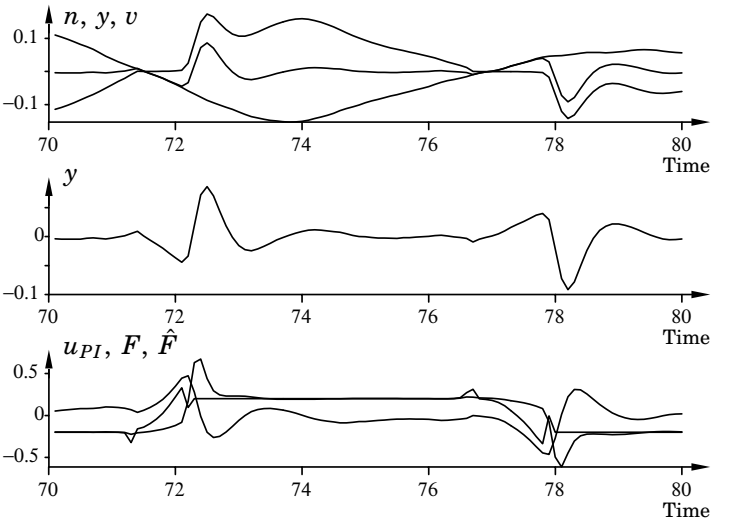

Figure 5.34 If the stiffness of the observer disagrees with the true friction, we get large observer errors in particular after a zero crossing when motion starts again. This leads to a large backlash in the control error, which is worse than the error caused by friction without compensation. A higher observer gain will improve the situation significantly.

Stribeck Velocity v_S**:** We now look at the case where the observer has the correct friction levels F_S and F_C but where the Stribeck effect is underestimated. This occurs when $v_S = 0.0001$ in the observer model. For the true friction $v_S = 0.01$. The observer model predicts that the Stribeck effect starts at much lower velocities. This is shown in Figure 5.33. The control error is small since a long period of sticking does not occur. The error is almost antisymmetric with respect to the zero crossing. Note that there is an error in the friction estimate only for velocities slightly lower and slightly larger than zero.

Stiffness σ_0**:** The rate at which the friction force estimate changes during the zero crossing is important. We may get large control errors around the zero velocity crossing if the dynamics of the observer do not match the dynamics of the true friction. This is seen in Figure 5.34 where $\sigma_0 = 10$ in the observer instead of 1000 and $\sigma_1 = 2\sqrt{10}$ instead of $2\sqrt{1000}$. The error before time $t = 72$ resembles that without friction compensation. However, after the sticking terminates the friction estimation error becomes very large. This leads to a back-lash in the error that is even larger than the error caused by the friction.

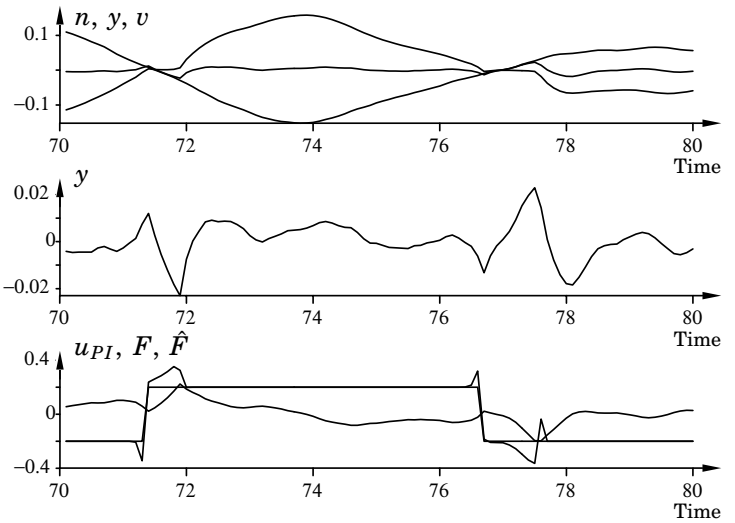

Figure 5.35 The error behavior when compensating using a Coulomb model resembles the case without friction compensation. The error magnitude is, however, smaller.

Compensation Using a Coulomb Model: Finally, we look at the case when friction compensation is based on a Coulomb model. The results are shown in Figure 5.35. The error is similar to the case without friction compensation except that the problems after zero velocity have been alleviated. The control force from the friction compensation switches immediately at the zero crossing, which reduces the error. In the case without friction compensation this was handled by the integral action which, of course, has a much longer response time.

Next we summarize the behavior of the control error at zero crossings. The conclusions give guidelines to how the friction compensation should be changed in order to better compensate for the true friction. It also gives guidelines for design of adaptive friction compensation.

Discussion

Figure 5.36 shows different error types that are discussed. The error is considered when the desired velocity v_d goes from negative to positive.

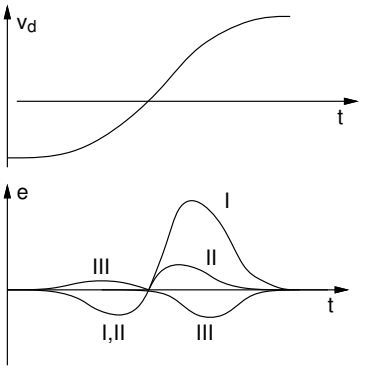

Figure 5.36 Some of the typical error characteristics for a system with friction. The velocity v_d is the desired velocity. The actual velocity at the friction interface may be zero for a period of time due to sticking. This causes the large control error indicated by I in the figure.

The most typical error associated with friction is when sticking occurs as a change of direction of motion is desired. This is manifested by a relatively large positive control error after the crossing. The accuracy of the friction model determines how long sticking occurs and, thus, also the size of the control error. Typically, compensation using a Coulomb friction model leads to this type of error. The performance depends essentially on the difference between F_S and F_C. This is error type I in Figure 5.36. If no sticking occurs but there is a pronounced control error when approaching zero velocity there may be an error in the model of the Stribeck effect. If the Stribeck velocity is too low we typically get an error of type II as seen in Figure 5.36. The error is also asymmetric. Over-compensation of the friction leads to errors of the opposite sign, i.e., that are negative before the zero crossing and positive afterwards. This is indicated by III in Figure 5.36.

5.9 Summary

This chapter has investigated compensation using a friction-force observer first suggested in Canudas de Wit *et al.* (1995). Properties of the friction observer have been explored and stability conditions for velocity and position control have been given. The new conditions are less conservative than those in Canudas de Wit *et al.* (1995) and imply that the controller may include a pure integrator. The requirements allow a wide range of design alternatives. The observer-based friction compensation has been

applied to an example of velocity control. The performance of the observer with respect to model errors and disturbances have been investigated. The observer behaves well despite large model errors and disturbances, although the control performance deteriorates.

The control error is studied extensively, which gives new information about the effects of friction and the friction observer. For friction-caused control errors the distribution of the error is not Gaussian. The statistical information provides knowledge to which extent nonlinear effects such as friction is the reason for the control error. More information is also available when studying the temporal behavior of the error as a zero velocity crossing occurs. It is common in the literature on friction compensation only to specify the performance in terms of mean square error or maximum error. It would be desirable to also provide other information to better be able to evaluate the benefits of the friction compensation.

6

Conclusions

This thesis has discussed friction related problems from a control engineering point of view. Three main themes have been investigated.

Modeling: Friction is a very complex phenomenon. Experimental observations of the dynamical behavior shows many different features. A new dynamic model of friction has been described in this work. The model is relatively simple with a reasonable number of parameters yet captures most of the complex behavior of friction. The model is investigated in simulations which show good agreement with experimental observations. Identification of the model parameters has been done in Canudas de Wit and Lischinsky (1996).

Analysis: It is important to have tools which are well-suited to analyze the effects of friction in control loops. Simulations have traditionally been used extensively. The describing function method has also been widely used, although it is unreliable since it may not predict all limit cycles. The thesis has presented tools for the exact computation of the shape and stability of frictional limit cycles in control systems. The tools have been implemented in software for numerical computations. Their usefulness has been demonstrated by applying the algorithms for a wide range of examples. The analysis tools are extensions of methods for analysis of systems with relay feedback, see Åström (1995).

Compensation: The new friction model is well adapted to control design. Friction compensation can be performed using a friction force observer which can be combined with traditional linear compensators. Stability of the closed loop has been proved for a large class of linear controllers which will give good performance. The requirements for high performance control is a good estimate of the velocity. This requires a high sampling rate and good sensors and actuators. Because of emerging tech-

nologies based on micro-mechanics it may be possible to use accelerometers which could give drastically better velocity estimates.

A number of simulations show how friction compensation with the friction force observer performs for a velocity control problem with a simple linear controller design. There are indeed substantial differences between the results using our model compared with a simple model of Coulomb type. The behavior of the control error is discussed in detail. It is shown that much information can be deduced from its behavior when the velocity changes sign. This is important if the control demands are high. It also gives an understanding of how model parameters should be changed. In addition knowledge can be obtained from a statistical analysis of the control error. It is thus possible to qualitatively judge the success of the friction compensation. When comparing the benefits of different friction compensation algorithms it is important to provide this information.

Future Work

There are many interesting research problems which can extend the work in this thesis.

Implementation issues are important. In order for the friction compensation to be efficient there must be an as short time lag as possible between the velocity measurement and the time when the control signal results in an applied force. It is therefore desirable to incorporate the friction compensation within the current loop in electromechanical motion-control systems. This is a long term goal. In the short term friction compensation has to be performed in the velocity loop.

It is natural to include adaptation in the friction compensation algorithm. The friction force varies with many factors such as temperature, load and wear and it is thus advantageous to have a continuous tuning of the model parameters.

7

Bibliography

AMIN, B. AND B. ARMSTRONG-HÉLOUVRY (1994): "PID control in the presence of static friction Part II: The reliability of describing function predictions." Technical Report, Dept. of Electrical Engineering and Computer Science, University of Wisconsin.

AMONTONS, G. (1699): "On the resistance originating in machines." In *Proc. of the French Royal Academy of Sciences*, pp. 206–22.

ANDERSSON, S. (1993): Seminar at The Department of Automatic Control, Lund Institute of Technology, Lund, Sweden.

ARMSTRONG, B. (1995): "Challenges to Systematically Engineered Friction Compensation." In *Proceedings of IFAC Workshop on Motion Control, Munich, Germany*, pp. 21–30.

ARMSTRONG-HÉLOUVRY, B. (1991): *Control of Machines with Friction*. Kluwer Academic Publishers, Boston, Ma.

ARMSTRONG-HÉLOUVRY, B., P. DUPONT, AND C. CANUDAS DE WIT (1994): "A Survey of Models, Analysis Tools and Compensation Methods for the Control of Machines with Friction." *Automatica*, **30:7**, pp. 1083–1138.

ÅSTRÖM, K. J. (1995): "Oscillations in Systems with Relay Feedback." In ÅSTRÖM *et al.*, (Eds.), *Adaptive Control, Filtering and Signal Processing*. Springer-Verlag.

BAKKER, E., L. NYBORG, AND H. PACEJKA (1987): "Tyre Modelling for Use in Vehicle Dynamics Studies." Technical Report 870421, Society of Automotive Engineers, Inc.

BARIL, C. B. (1993): *Control of Mechanical Systems Affected by Friction and Other Nondifferentiable Nonlinearities*. PhD thesis, Technion, Israel Institute of Technology, Haifa, Israel.

BERSEKERSKII, V. A. (1947): "Applying vibrators to eliminate nonlinearities in automatic regulators." *Avtomat. i Telemekh.*, **No 8**, pp. 411–17.

Bialkowski, W. L. (1993): "Dreams versus reality: A view from both sides of the gap." *Pulp and Paper Canada*, **94:11**.

Bliman, P.-A. (1992): "Mathematical Study of the Dahl's Friction Model." *European Journal of Mechanics. A/Solids*, **11:6**, pp. 835–848.

Bliman, P. A., T. Bonald, and M. Sorine (1995): "Hysteresis Operators and Tyre Friction Models. Application to Vehicle Dynamic Simulation." In *Proceedings of ICIAM 95, Hamburg, Germany*.

Bliman, P.-A. and M. Sorine (1991): "Friction Modelling by Hysteresis Operators. Application to Dahl, Sticktion and Stribeck Effects." In *Proceedings of the Conference "Models of Hysteresis"*, Trento, Italy.

Bliman, P.-A. and M. Sorine (1993): "A System-Theoretic Approach of Systems with Hysteresis. Application to Friction Modelling and Compensation." In *Proceedings of the second European Control Conference*, pp. 1844–49, Groningen, The Netherlands.

Bliman, P.-A. and M. Sorine (1995): "Easy-to-use Realistic Dry Friction Models for Automatic Control." In *Proceedings of 3rd European Control Conference, Rome, Italy*, pp. 3788–3794.

Bo, L. C. and D. Pavelescu (1982): "The friction–speed relation and its influence on the critical velocity of the stick-slip motion." *Wear*, **82:3**, pp. 277–89.

Bowden, F. P. and D. Tabor (1973): *Friction — An Introduction to Tribology*. Anchor Press/Doubleday, New York.

Brandenburg, G. and U. Schäfer (1991): "Influence and Compensation of Coulomb Friction in Industrial Pointing and Tracking Systems." In *1991 IEEE Industry Application Society Annual Meeting.*, pp. 1407–1413.

Canudas de Wit, C. (1993): "Robust Control for Servo-Mechanisms under Inexact Friction Compensation." *Automatica*, **29:3**, pp. 757–761.

Canudas de Wit, C., K. J. Åström, and K. Braun (1987): "Adaptive Friction Compensation in DC Motor Drives." *IEEE Journal of Robotics and Automation*, **RA-3:6**, pp. 681–685.

Canudas de Wit, C. and P. Lischinsky (1996): "Adaptive friction compensation with partially known dynamic friction model." *Int. J. of Adaptive Control and Signal Processing*, **10:2**.

Canudas de Wit, C., H. Olsson, K. J. Åström, and P. Lischinsky (1993): "Dynamic friction models and control design." In *Proceedings of the 1993 American Control Conference, San Fransisco, California*, pp. 1920–26.

CANUDAS DE WIT, C., H. OLSSON, K. J. ÅSTRÖM, AND P. LISCHINSKY (1995): "A new model for control of systems with friction." *IEEE Trans. Automatic Control*, **40:3**, pp. 419–25.

CODDINGTON, E. A. AND N. LEVINSON (1955): *Theory of Ordinary Differential Equations*. McGraw-Hill, New York.

COULOMB, C. A. (1785): "Théorie des machines simples, en ayant égard au frottement de leurs parties, et la roideur des cordages." In *Mém. Math. Phys.*, volume X, pp. 161–342.

COURTNEY-PRATT, J. AND E. EISNER (1957): "The Effect of a Tangential Force on the Contact of Metallic Bodies." In *Proceedings of the Royal Society*, volume A238, pp. 529–550.

CUBALCHINI, R. (1996): Personal communication. Hughes, El Segundo, California.

DAHL, P. (1968): "A Solid Friction Model." Technical Report TOR-0158(3107–18)-1, The Aerospace Corporation, El Segundo, CA.

DAHL, P. (1975): "Solid Friction Damping of Spacecraft Oscillations." AIAA Paper No.75-1104 presented at the AIAA Guidance and Control Conference, Boston Mass.

DAHL, P. (1977): "Measurement of solid friction parameters of ball bearings." In *Proc. of the 6th Annual Symposium on Incremental Motion, Control Systems and Devices*. University of Illinois.

DAHL, P. R. (1976): "Solid Friction Damping of Mechanical Vibrations." *AIAA Journal*, **14:12**, pp. 1675–82.

DIETERICH, J. H. (1972): "Time-dependent friction in rocks." *Journal of Geophysical Research*, **77**, pp. 3690–97.

DUPONT, P. (1994): "Avoiding Stick-Slip Through PD Control." *IEEE Transactions on Automatic Control*, **39**, pp. 1094–1097.

EBORN, J. AND H. OLSSON (1995): "Modelling and simulation of an industrial control loop with friction." In *Proceedings of the 4th IEEE Conference on Control Applications, Albany, New York*, pp. 316–322.

EHRICH LEONARD, N. AND P. KRISHNAPRASAD (1992): "Adaptive Friction Compensation for Bi-Directional Low-Velocity Position Tracking." In *Proc. of the 31st Conference on Decision and Control*, pp. 267–273.

FRIEDLAND, B. AND S. E. MENTZELOPOULOU (1993): "On estimation of dynamic friction." In *Proceedings of the 32nd Conference on Decision and Control, San Antonio, Texas*.

FRIEDLAND, B. AND Y.-J. PARK (1991): "On Adaptive Friction Compensation." In *Proceedings of the IEEE Conference on Decision and Control*, volume 3, pp. 2899–2902, Piscataway, NJ, USA. IEEE Service Center. IEEE cat n 91CH3076-7.

FUTAMI, S., A. FURUTANI, AND S. YOSHIDA (1990): "Nanometer Positioning and Its Micro-Dynamics." *Nanotechnology*, **No 1**, pp. 31–37.

GELB, A. AND W. E. VANDER VELDE (1968): *Multiple-input describing functions and nonlinear system design*. McGraw-Hill.

GILBART, J. AND G. WINSTON (1974): "Adaptive Compensation for an Optical Tracking Telescope." *Automatica*, **10**, pp. 125–131.

HAESSIG, D. AND B. FRIEDLAND (1990): "On the Modeling and Simulation of Friction." In *Proceedings of the 1990 American Control Conference,San Diego*, pp. 1256–1261. IEEE Cat n 90CH2896-9.

HAESSIG, D. A. AND B. FRIEDLAND (1991): "On the Modelling and Simulation of Friction." *J Dyn Syst Meas Control Trans ASME*, **113:3**, pp. 354–362.

HAIRER, E., S. P. NØRSETT, AND G. WANNER (1987): *Solving Ordinary Differential Equations I: Nonstiff Problems*. Springer Verlag, Berlin, Germany.

HARNOY, A. AND B. FRIEDLAND (1993): "Dynamic Friction Model of Lubricated Surfaces for Precise Motion Control." Number Preprint No. 93-TC-1D-2. Society of Tribologists and Lubrication Engineers.

HARNOY, A. AND B. FRIEDLAND (1994): "Modeling and Simulation of Elastic and Friction Forces in Lubricated Bearings for Precise Motion Control." *Wear*, **172**, pp. 155–165.

HESS, D. P. AND A. SOOM (1990): "Friction at a Lubricated Line Contact Operating at Oscillating Sliding Velocities." *Journal of Tribology*, **112**, pp. 147–152.

HILL, D. J. AND P. MOYLAN (1977): "Stability Results for Nonlinear Feedback Systems." *Automatica*, **13**, pp. 377–382.

JOHANNES, V. I., M. A. GREEN, AND C. A. BROCKLEY (1973): "The Role of the Rate of Application of the Tangential Force in Determining the Static Friction Coefficient." *Wear*, **24:381–385**.

KARNOPP, D. (1985): "Computer Simulation of Slip-Stick Friction in Mechanical Dynamic Systems." *Journal of Dynamic Systems, Measurement, and Control*, **107:1**, pp. 100–103.

KHALIL, H. K. (1992): *Nonlinear Systems*. Macmillan, New York.

MEES, A. AND A. BERGEN (1975): "Describing functions revisited." *IEEE Transactions on Automatic Control*, **20:4**, pp. 473–478.

MENTZELOPOULOU, S. E. AND B. FRIEDLAND (1994): "Experimental evaluation of friction estimation and compensation techniques." In *Proceedings of the 1994 American Control Conference, Baltimore, Maryland*.

MORIN, A. (1833): "New friction experiments carried out at metz in 1831–1833." In *Proceedings of the French Royal Academy of Sciences*, volume 4, pp. 1–128.

NEWTON, G., L. GOULD, AND J. KAISER (1957): *Analytical Design of Linear Feedback Controls*. John Wiley & Sons.

ODEN, J. T. AND J. MARTINS (1985): "Models and Computational Methods for Dynamic Friction Phenomena." *Computer Methods in Applied Mechanics and Engineering*, **52**, pp. 527–634.

OLSSON, H. (1995): "On describing function analysis of systems with friction." In *Proceedings of the 4th IEEE Conference on Control Applications, Albany, New York*, pp. 310–15.

OPPELT, W. (1976): "A historical review of autopilot development, research, and theory in germany." *Journal of Dynamic Systems, Measurements, and Control*, September, pp. 215–23.

PACEJKA, H. B., (Ed.) (1991): *1st International Colloquium on Tyre Models for Vehicle Dynamics Analysis, Delft, The Netherlands*.

POPOVIĆ, M. R., D. M. GORINEVSKY, AND A. A. GOLDENBERG (1995): "A study of responses to short torque pulses and fuzzy control of positioning for devices with stick-slip friction." In *Proceedings of the 4th IEEE Conference on Control Applications, Albany, New York*.

RABINOWICZ, E. (1951): "The Nature of the Static and Kinetic Coefficients of Friction." *Journal of Applied Physics*, **22:11**, pp. 1373–79.

RABINOWICZ, E. (1958): "The intrinsic variables affecting the stick-slip process." In *Proc. Physical Society of London*, volume 71, pp. 668–675.

RAMBERG, W. AND W. R. OSGOOD (1943): "Description of Stress-Strain Curves by Three Parameters." Tech. Note 902, National Advisory Committee for Aeronautics, Washington.

REYNOLDS, O. (1886): "On the Theory of Lubrication and Its Application to Mr. Beauchamp Tower's Experiments, Including an Experimental Determination of the Viscosity of Olive Oil." *Phil. Trans. Royal Soc.*, **177**, pp. 157–234.

RICHARDSON, R. S. H. AND H. NOLLE (1976): "Surface Friction under Time-Dependent Loads." *Wear*, **37:1**, pp. 87–101.

RUINA, A. L. (1983): "Slip Instability and State Variable Friction Laws." *J Geophys Res*, **88:B12**, pp. 10359–10370.

SARGIN, M. (1971): "Stress-Strain Relationship for Concrete and the Analysis of Structural Concrete Sections." SM Study 4, Solid Mechanics Division, University of Waterloo, Canada.

SHEN, C. N. (1962): "Synthesis of High Order Nonlinear Control Systems with Ramp Input." *IRE Trans. on Automatic Control*, **AC-7:2**, pp. 22–37.

SKF (1970): *General Catalogue*.

STRAUCH, H. (1996): Personal communication. Daimler-Benz Aerospace, Bremen, Germany.

STRIBECK, R. (1902): "Die Wesentlichen Eigenschaften der Gleit- und Rollenlager – The Key Qualities of Sliding and Roller Bearings." *Zeitschrift des Vereines Seutscher Ingenieure*, **46:38,39**, pp. 1342–48,1432–37.

TOU, J. AND P. M. SCHULTHEISS (1953): "Static and sliding friction in feedback systems." *Journal of applied physics*, **24:9**, pp. 1210–17.

TUNG, E., G. ANWAR, AND M. TOMIZUKA (1991): "Low Velocity Friction Compensation and Feedforward Solution Based on Repetitive Control." In *Proc. of the 1991 American Control Conference.*, pp. 2615–20, Green Valley, AZ, USA. American Control Council. IEEE Cat n 91CH2939-7.

TUSTIN, A. (1947): "The Effects of Backlash and of Speed-dependent Friction on the Stability of Closed-cycle Control Systems." *Journal of the Institution of Electrical Engineers Part 1 General*, **94 Part IIA**, pp. 143–151.

WALLENBORG, A. AND K. J. ÅSTRÖM (1988): "Limit cycle oscillations in high performance robot drives." In *Preprints Control '88*, UK. University of Oxford.

WALRATH, C. (1984): "Adaptive Bearing Friction Compensation Based on Recent Knowledge of Dynamic Friction." *Automatica*, **20:6**, pp. 717–727.

WILLEMS, J. (1972): "Dissipative Dynamical Systems Part I: General Theory." *Arch. Rational Mech. Anal.*, **45**, pp. 321–51.